4-20-2015 12:00 AM

# The Effect of Cutting Blade Geometry and Material on Carbon Fiber Severing as Used in High-Volume Production of Composites

Michael Francis Anthony Adamovsky
*The University of Western Ontario*

Supervisor
Dr. Jeffrey T. Wood
*The University of Western Ontario* Joint Supervisor
Dr. Remus Tutunea-Fatan
*The University of Western Ontario*

Graduate Program in Mechanical and Materials Engineering
A thesis submitted in partial fulfillment of the requirements for the degree in Master of Engineering Science

# The Effect of Cutting Blade Geometry and Material on Carbon Fiber Severing as Used in High-Volume Production of Composites

Monograph

by

Michael Francis Anthony Adamovsky

Graduate Program in Mechanical Engineering

A thesis submitted in partial fulfillment
of the requirements for the degree of
Master of Engineering Science

The School of Graduate and Postdoctoral Studies
The University of Western Ontario
London, Ontario, Canada

# Abstract

Automotive manufacturers have started to actively look into weight savings options for mass production of vehicles that meet new government regulations. Falling prices of carbon fibers have made carbon fiber composites a promising material to be used. The study has focused on the fiber-severing unit incorporated in a high-volume composite production line in an attempt to better define the impact of blade geometry and material on the wear as experienced while cutting carbon fiber. A method to quantify the effect of usage on the cutting ability of a blade has been developed, as well as methods to measure blade wear. Results show that wear rates of blades are decreased as blade hardness is increased from 560 $H_v$ to 1300 $H_v$ and the root cause of the chopping unit's failure to cut can be due to height loss of the blade as well as an increase in tip radius of curvature.



Keywords: fiber chopper, carbon fiber, sheet molding compound, SMC, long fiber thermoset, composite material, knife blade wear, critical radius

# Acknowledgments

I would like to sincerely thank my two supervisors Dr. Jeffery Wood, and Dr. Remus Tutunea-Fatan for their generous support throughout my research. Their dedication to education and the understanding of nature was inspirational. I would like to thank my colleague Ryan Alexander for being an excellent research partner. I would like to thank the kind staff at the university including Clayton Cook, Dan Sweiger, Chris VanDellar from the University Machining Services, Eugen Porter, Dave Lunn, Ross Davidson, and Marc Biesinger. I extend my gratitude to Louis Kaptur, Diefenbacher, and the Ontario Center of Excellence. Lastly I would like to thank Allison, my friends and my family; thank you for all the support, love, and patience.

# Table of Contents

# List of Tables

# List of Figures

# List of Appendices

# Chapter 1

# 1 Introduction

## 1.1 Motivation

To remain competitive in the large automotive market, companies are investigating new technologies to entice new customers. As the price and demand of gasoline and fossil fuels rise it is particularly important to reduce the amount of fuel consumption of road vehicles such that the lifetime cost of ownership and operation are kept as low as possible[1]. It has been estimated that a 10% weight reduction would translate to a 7% reduction in fuel consumption[2]. There are a number of potential avenues that can be taken to offset increasing fuel costs. These avenues include increasing the thermodynamic efficiency of the power plant, increasing driveline efficiency, increasing aerodynamic efficiency, and reduction of mass which act to reduce the effect of the four driving resistances of air, rolling, inertia, and gravitational[3]. The reduction of mass will decrease the amount of energy required to bring a vehicle up to a given speed. Mass reduction can be achieved through numerous ways including advancements in analysis techniques which allow for removal of unnecessary material, advancements in manufacturing techniques which enable more efficient use of materials, and the use of higher performance materials[4, 5]. The research relates to use of high performance materials, specifically lightweight sheet molding compound (SMC) panels, for use on class A automotive body panels.

SMC panels have typically been produced using a mixture of chopped glass fibers, polyester resin, calcium carbonate filler, and other compounds including solvents,

thickeners, and mold release agents[6]. Research has been undertaken to transfer over to lighter strength to weight ratio materials through the use of carbon fibers as opposed to glass fibers[7], hollow glass microspheres as opposed to calcium carbonate fillers, and through the use of polyurethane and epoxy resin systems to replace polyester resins[8]. The research presented in this thesis focuses on the transition from glass reinforcement to carbon fiber reinforcement with respect to the chopping of the continuous carbon fiber rovings into discrete lengths. As the mechanical properties and filament diameter of carbon fibers differ from glass fibers, challenges may arise when transitioning from glass to carbon fibers while using the chopping device designed for glass. As continuous production is required by manufacturers to meet high volume demands, lengthy repeated maintenance operations must be avoided to ensure that production rates are met and costs are kept low. The cost of maintenance operations includes the cost of the blades, as well as labour, and as such frequent replacement of knife blades may translate to high cost.

## 1.2 Objective

The objective of this study is to optimize the performance of the direct-sheet molding compound (D-SMC) chopping unit with respect to maximizing time in between maintenance intervals, increasing reliability and repeatability. The paper will also attempt to gain an understanding of the chopping mechanism to help provide insight into why problems arise with extended use, machine malfunction, and/or non-ideal machine set up.

## 1.3 Hypothesis

The research presented within this thesis hypothesizes that knife blade geometry and material have a significant effect on the cutting blade life cycle of the D-SMC chopper.

## 1.4 Contributions

Contributions of the research presented are a number of methods for measurement of thin edge blade wear for blades used in chopping brittle fiber reinforcements for composite materials, the design and fabrication of two testing apparatus that are able to simulate industrial scale machinery and to obtain force and displacement curves for the chopping action. Quantitative and qualitative data has been presented on a number of knife blade options, and a simulation of long scale usage has been done.

## 1.5 Outline

Chapter 2 outlines background information related to this study. An overview presents: the properties of carbon fiber and glass fibers; the existing cutting methods typically used to cut fibers; a description of loop tests which are of particular interest as the mode of failure thought to be utilized by the mechanism in this study is a flexural failure of the fiber; a description of common materials used in chopping machines, and a brief overview of load and measurement techniques. Chapter 3 focuses on describing the experimental procedures that were undertaken, as well as a description of the testing apparatus that have been designed and fabricated. Chapter 4 presents the results of the experiments and Chapter 5 summarizes conclusions and proposed future work in the area.

# Chapter 2

# 2 Background

This chapter focuses on describing the various terminologies, techniques, and state of the art related to reinforcement fiber chopping.

## 2.1 Carbon Fiber Properties vs. Glass

As the transition from glass fibers to carbon fibers is the focus of this study, an investigation of the physical and mechanical properties of glass and carbon fibers may provide insight in to the differences that the two fiber types have with regards to cutting behavior.

Physical dimensions: The typical physical dimensions of glass fibers versus carbon fibers differ slightly. In general, glass fibers have diameters of ~8-15 μm[9] whereas PAN precursor carbon fibers that are commercially available range 5-8 μm[10].

Anisotropy: Carbon fibers comprise of graphite planes that are aligned with the axis of the fiber with a range of misalignment[11]. The directionally ordered nature of the graphite planes, along with the drastic difference in strength in plane vs. out of plane means that the carbon fibers will exhibit a higher degree of anisotropy than glass fibers[9, 11-13], which have been considered to be isotropic[9].

Mechanical properties: The mechanical properties of carbon fibers differ from those of glass fibers. Although not always the case, typically modern carbon fibers are stronger than E glass fibers, and have a higher elastic modulus as summarized in Table 2-1.

**Table 2-1 Properties of E-glass [14, 15] and carbon fibers (Toray T700S data sheet).**

| | E Glass Fiber | T700S Carbon Fiber |
|---|---|---|
| Density (kg/m3) | 2.58 | 1.8 |
| Elastic Modulus (GPa) | 75-80 | 230 |
| Tensile Strength (Gpa) | 2-3.8 | 4.9 |
| Filament Diameter (μm) | 13.5 | 7 |

## 2.2 Existing Cutting Methods

Various methods are employed to cut continuous rovings of brittle fibers into discrete lengths. Figure 2-1 shows diagrams of popular methods of cutting fibers.

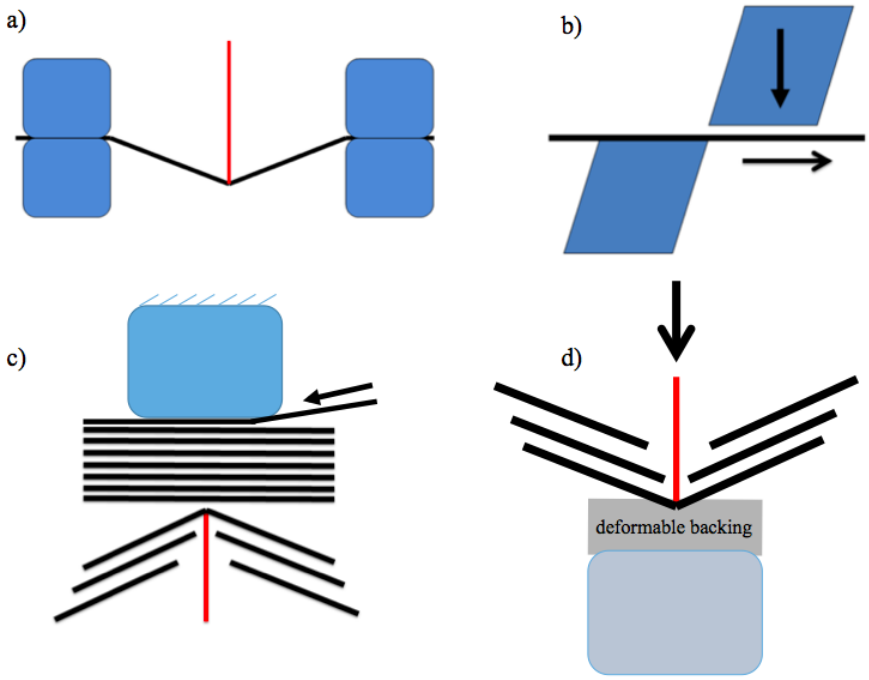


**Figure 2-1 Cutting Methods: a) End supported un-backed cutting b) Shearing c) Fiber build up cutting d) Deformable backing cutting**

In end supported un-backed cutting, Figure 2-1 a, the fiber ends are clamped while a sharp knife is plunged between the supports. The combination of the tensile stresses and bending at the knife tip cause the brittle fibers to fail at the knife tip. After the fibers are severed, the clamps are released, and the chopped roving is allowed to fall. This mechanism is employed in the Chopcot® cutters[16, 17]. The Chopcot® cutter is a continuous roving cutter that utilizes a knife roll and a backing roll.

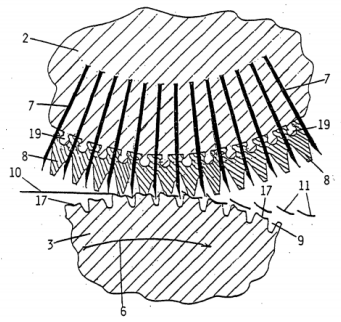


**Figure 2-2 The backingless cutting mechanism of the Chopcot® cutter [16].**

The Chopcot® uses deformable press pads in between the knife blades that grip the incoming fibers. The knives plunge through the fibers into the empty spaces in the backing roll during the cutting process.

In the shearing mechanism, Figure 2-1 b, which is the mechanism that can be used manually with a pair of scissors, the roving of fibers is sheared with two sharp edged surfaces[18]. The combination of contact stresses and shear stresses cause failure of the fibers. One industrial implementation of the shearing mechanism with regards to fiber chopping for an SMC process is the Mag Ias Gmbh developed Fibercut chopping unit[19]. This device uses a rotating blade holder to shear fibers that are passed through the rotating blades and static blades. The rotating and static blades must maintain close

tolerances in order to cut the fibers as the diameter of the fibers may be as small as 5 μm in the case of carbon fibers.

In fiber build up cutting, Figure 2-1 c, fibers are introduced between a knife and backing that remain at a constant separation distance. The continual build up of fibers between the two elements cause the fibers to generate pressure against the knife and the backing. As the pressure rises to a critical level the fibers sever at the knife edge. Two implementations of this cutting mechanism are industrially utilized, generally in the staple fiber (non brittle fibers such as polyester, cotton) industry. The fiber is forced between a knife reel and either a cam or a press roll until the force on the knife edge is sufficiently high to cut the fibers. This method works on both brittle and ductile fibers [20-25].

In deformable backing cutting, Figure 2-1 d, the fiber roving rests against a compliant backing and a sharp knife is plunged into the backing. As the knife plunges into the backing, the fibers conform to the knife edge curvature and break as the fibers reach their critical radius of curvature [26].

## 2.3 Critical Radius

Brittle fibers such as glass and carbon fibers have been shown to possess a critical radius of curvature [12, 27-29]. As the fiber is bent, stresses are generated through the cross section and can be approximated by the following equation for isotropic brittle materials:

$$r_{min} = \frac{Ed}{2\sigma^*} \text{ [9]} \qquad (2.1)$$

The equation is derived from Euler-Bernoulli beam theory for a circular cross section beam in which shear deformation is neglected. As a beam is subjected to a pure bending moment, a curvature is generated in the beam and is inversely proportional to the modulus and diameter. A neutral surface exists at which the strain is equal to zero. The equation relating curvature to applied bending moment and stiffness of the beam is:

$$1/\rho = \frac{M}{EI} \tag{2.2}$$

The equation relating stress in a circular cross section beam to the applied bending moment is (where d is diameter):

$$\sigma = \frac{Md}{2I} \tag{2.3}$$

Using Equation 2.3, solving for M, substituting M it into Equation 2.2 and solving for the radius of curvature yields Equation 2.1.

As a fiber is bent and a curvature is generated, the stress rises until it reaches the ultimate stress of the fiber, at which point, a brittle fiber will fail spontaneously. If the fiber is ductile in flexure, as is the case with aramid fibers, it may not exhibit a repeatable critical radius of curvature as permanent deformation in the form of kink bands will allow far greater curvature in the fiber[9, 30, 31]. The failure of fibers such as aramid is progressive in nature. Carbon fibers do possess a certain degree of ductility as compared to glass fibers, as irreversible deformation has been observed following flexure testing. The degree of ductility is lower than that of fibers like aramid or polyethylene. A

correlation has been found with the degree of anisotropy and non-linear behavior of the carbon fibers during loop tests [32].

## 2.4 Fiber Loop Test

Tests have been developed to observe the critical radius of brittle fibers. Typically a fiber loop or knot is viewed between glass slides in an optical microscope, while the loop or knot is tightened until the point of failure[27]. Load may be recorded in order to estimate the elastic modulus of the fiber. The shape of the fiber loop has been described as the elastica (latin for thin strip of elastic material), which is a characteristic shape that a brittle fiber takes when formed into a loop as seen in Figure 2-3. The mathematical study of the shapes of curved objects dates back to the 13$^{th}$ century; many great mathematical minds have studied it including Galileo, James and Daniel Bernoulli, and Euler[33].


**Figure 2-3 Single fiber in loop form creating the elsastica.**

## 2.5 Cutting Blades

Cutting blades are available in many different geometry options, but in general consist of a thin, flat piece of material that has been sharpened on one end. The thickness of the base material may vary, along with the geometry of the sharpened region. The sharpened region may consist of a number of surfaces in a variety of configurations.

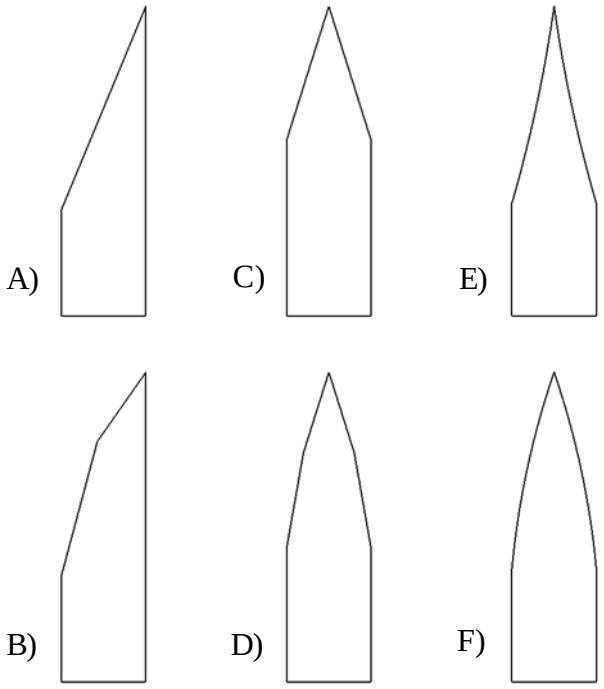


**Figure 2-4 Common blade edge geometry: A) Single bevel or chisel B) Compound single bevel or chisel C) Double bevel D) Compound double bevel E) Concave F) Convex**

There are many other geometrical options for cutting blades; however the blades featured in Figure 2-4 A) – D) are generally used in composite reinforcement cutting. Blade sharpness and characteristics of blades cutting into soft backings has been extensively studied [34], however the characteristics of thin edge blades cutting brittle fibers has not.

Lau et al [35] has studied the wear characteristics and proposed a correlation of blade geometry and wear rate, although they did not carry out experiments to quantify the

correlation. In a grass-sand mixture cutting study, wear was observed to have 2 stages: Initially a first stage of rapid wear followed by a second stage of steady. The high wear rate stage was rationalized by the stress intensity caused by the delicate geometry of the virgin blade and interaction with the stationary blade. As the new blade had a fine edge with thickness in the order of 0.06 mm, with a given load applied to the edge, would generate higher stress than a thicker, dulled blade. As the blade wears from its initial state, the thickness is proportional to the wedge angle of the blade tip, and the distance that the tip has moved from its initial position. Similar wear rates were found with blades of varying carbon content and hardness. It has been proposed by Lau et al that the presence of carbide particles in higher hardness blade material may reduce resistance to wear in the long term in the cutting of grass but initially enhances wear resistance[35].

Cutting blades of appropriate geometry for use in fiber cutting machines come in a wide range of materials including carbon steels, alloy steels, stainless steels, ceramics, and cemented carbides. These blades are available with or without coating though only uncoated blades will be in the scope of this research. The hardness and toughness of these materials varies greatly, but it is the harder varieties that are typically used for fiber cutting as the high strength of the fibers being cut translates to high rates of wear in the cutting knives.

## 2.6 Backing Material

Backing materials used in deformable backing cutting are typically elastomers allowing a high degree of strain and possessing high strength capable of surviving many knife plunges. Polyurethane of 65 shore A Durometer has been chosen by an industry partner as the backing material for the D-SMC fiber chopper. The low modulus of the material

generates a bending moment in fibers as a knife blade is plunged into them while the backing complies as shown in Figure 2-5.

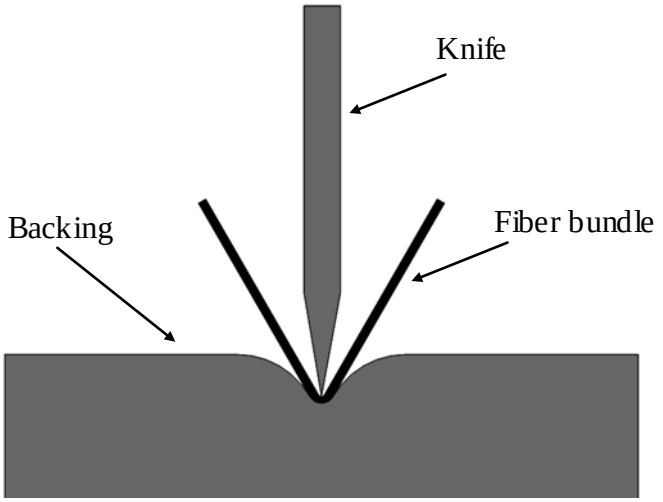


**Figure 2-5 Bending of fiber bundle between knife and backing**

## 2.7 Load and Displacement Measurement Techniques

A variety of load measurement sensors exist for electronic data acquisition. A load cell measures load via calibrated strain gauges mounted on a load carrying structural element. The strain gauge is able to sense strain in the material that it is mounted on, and as such can be calibrated against known loads. As strain may be caused by temperature variations, care must be taken in the design of the load cell in order to sense external loads only and not strains due to variation in temperature. A full or half wheatstone bridge circuit is typically employed for temperature compensation[36]. Of the many ways to measure linear displacement, linear variable differential transformers (LVDT) and linear potentiometers are among the most popular. Other examples of linear displacement measurement techniques are laser time of flight measurement, and video

capture. LVDT sensors have a number of advantages including high misalignment tolerance, high accuracy and repeatability, moderate cost, and wide displacement range.

## 2.8 Signal Processing

Signals that are acquired directly from sensors are typically noisy and as such are not ideal for data analysis and presentation. However, care must be taken when processing raw signals as to not hide any information that is not noise. A moving average filter is appropriate for smoothing noise in a time domain signal such as a signal from a load cell or LVDT. A signal which has a moving average filter applied to it is shifted in the time domain and the amount of data points in the filtered data is reduced by the amount equal to the filtering window. The signal is not scaled in that the number of data points for a given period of time in the filtered signal remains the same as the raw signal. A variation on the moving average filter, the multiple pass moving average filter, alters the filter kernel from a rectangular shape to the shape of a Gaussian distribution as more passes are performed. As the shape of the filter kernel is not rectangular, samples in the input signal that are further away have less of an effect than the samples that are close by. The effect of the Gaussian shaped kernel is that the step response is a smooth S shape as opposed to a straight line[37].

# Chapter 3

# 3 Experimental Procedures

This section describes the experimental procedures undertook during the duration of the research activities. It also describes the equipment that has been developed to carry out the experiments.

## 3.1 Loop Test

Single fiber loop tests were performed with the goal of measuring the critical radius of the carbon fibers used at the FPC. A metallographic optical microscope was used to view the fiber at 500x magnification. The procedure for performing the loop test is as follows:

1. Set up video capture for the microscope digital camera. This can be done either directly through the microscope software or indirectly via capturing video of the computer desktop display as the test is being observed by the microscope software.

2. Isolate a single filament from a roving. This can be accomplished in many ways, and can be aided with the use of a magnifying glass as the fibers are very small in diameter (~5-7 μm). Rolling the roving between the fingers and the use of a utility blade to divide the roving into smaller and smaller number of filaments is recommended.

3. Use masking tape to fixture one end of the isolated filament to the end of a glass slide used in sample preparation for optical microscopes.

4. With the free end of the fiber, rotate the filament until a single loop is formed by the fiber.

5. Gently place a glass slide on top of the fiber loop, with the taped end of the fiber not being placed underneath the glass slide as it tends to offset the slide from the surface of the fibers. This will mean that the fiber loop will not be adequately constrained during the loop test. Glycerin may be used as a lubricant as suggested by Sinclair[27] although the effect of the lubricant on the properties of the carbon fiber are not known.

6. Carefully position the slides with fiber loop on the microscope stage and bring into focus at low magnification. After the tip of the loop has been found, transfer to higher and higher magnification.

7. Begin the loop test by gently pulling on the free end of the fiber in a controlled fashion. This may be accomplished by pressing the free end of the fiber against the microscope stage with a finger while slowly rotating the finger.

8. Keep the field of view of the microscope on the loop as the fiber is pulled as the loop tends to translate during this stage. The focus may also need to be adjusted as the loop is being pulled.

9. Pull on the fiber end until the fiber fractures

10. Isolate the video frame prior to fiber fracture.

11. Import the isolated frame into CAD software and use the scale bar present on the frame as well as a curve drawn over the loop tip to determine the critical radius of curvature of the fiber.

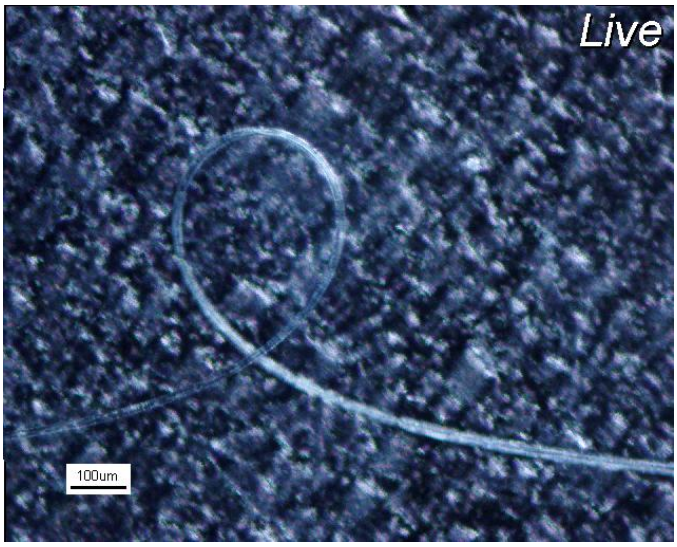


**Figure 3-1 Example of the final frame prior to fracture of an E glass fiber.**

Some sources of error can be considered with the proposed testing scheme and if any anomalous data is recorded, they can potentially explain it. The fiber may have been damaged during isolation from the roving, and if that is the case, it may alter the critical radius achieved by the fiber. The likelihood of the flaw being present at the tip of the loop during the final portion of the test is much lower than if the flaw were to be present in a test such as a tensile test where the volume of the fiber that is at maximum stress is the volume of the fiber between the clamps. In the loop test, the volume of the fiber at maximum stress is limited to the tip of the loop, with the top and bottom surface of the fiber at maximum tensile and compressive stress, respectively. As the fiber is essentially fixed at one end and pulled manually at the other end torsional stresses may be induced in

the fiber. This will increase the stress field throughout the fiber, and cause premature failure, and a larger critical radius measurement. As the length of the fiber is far longer than its diameter, the torsional stresses due to 1-2 rotations of the fiber do not significantly alter the stress field and as such will be neglected. Care must be taken by the operator to not induce excessive torsion in the fiber during the test. The glass slide may be resting on the tip of the fiber loop during the test and may alter the stress field. However, this is an unlikely as the overlap of the fibers at the base of the loop will be double the thickness of the fiber at the loop, and the other supporting end of the glass slide that is resting on the base glass slide is sufficiently far enough to not be in contact with the tip of the loop as seen in Figure 3-2.

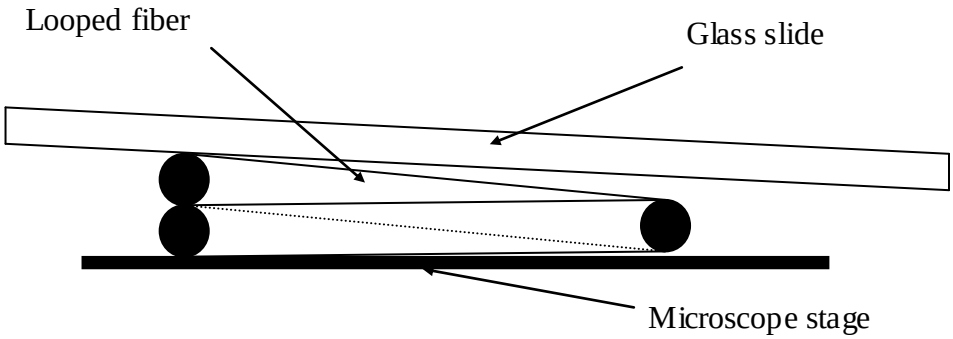


**Figure 3-2 Glass slide resting on fiber loop; angle of glass slide is exaggerated.**

As there will generally be a gap between the fiber loop tip and the glass slide, the fiber loop tip may be angled off of the plane of the microscope stage and as such a slightly smaller critical radius may be observed than what is actually present in the fiber loop. Measuring the width of the loop and the diameter of the filament has provided an estimation of the error associated with the viewing angle being out of plane with the loop using the angle found by Equation 3.1:

$$View\ Angle = \tan(\frac{\text{FiberDiameter}}{\text{Loop Width}}) \quad (3.1)$$

The effect of viewing angle on measured critical radius was assumed to be sinusoidal with the measured value being diminished by the difference in viewing angle. The error associated with the difference in angle was calculated to be -5%.

As the video capture of the loop pulling and fracture is set at a finite frame rate, which is limited by the microscope camera, as well as the computer hardware and video capture software, the exact moment before failure of the loop will not be captured. As such, the true value of the critical radius cannot be measured. As a result, the measured critical radius will always be larger than the true value, but may be minimized by slower tightening of the fiber loop. A measurement of the critical radius of the fiber that was taken from the second last frame prior to fracture was compared to the measurement of critical radius taken from the final frame prior to fracture. The difference in measurements was used to estimate the error due to not capturing the final moment of loop stability. The error estimated was a 5% increase in critical radius measurement. Summing the two errors together, the measured critical radius has an estimated +- 5% error.

## 3.2 Various Cutting Methods Tests

The effect on the end condition of cutting carbon fibers was observed through SEM images. Rovings were severed via the following techniques:

Tensile failure: The roving was divided such that a minimum number of fibers needed to be failed in tension were pulled manually until failure. The severed end was taped off and recorded such that the correct end was imaged;

Scissor cut: A roving was cut with a conventional pair of scissors, and the end taped off and recorded as with the tensile failure roving;

Crush cut: A roving was severed by placing it on a steel backing plate and pressing a knife-edge on the roving until all the fibers were severed;

Bend cut: A roving was folded over the edge of a sharp knife with minimal force input until the roving severed;

Slice cut: A roving was placed on a steel backing and sliced with a blade;

Laser cut: A roving was cut via a 10 W pulsed laser.

## 3.3 Carbon Fibers Used in Experiments

The carbon fibers used in the experiments in this thesis are fibers that have been suggested for use in the D-SMC chopper by the fiber supplier Toray. The fiber suggested is 12k T700S with F0E sizing. The properties of these fibers are summarized in Table 2-1.

## 3.4 Blades Used in Experiments

A variety of blades were acquired for comparison. The characteristics of the blades to be compared were the blade material and blade geometry. The materials that have been compared in this study are M2 tool steel, martensitic stainless steel, high carbon spring

steel, and tungsten carbide-cobalt metal matrix composite. The geometric properties that have been varied are the overall thickness of the blade, the grind angle, the hone angle and the edge configuration. The majority of the blades are compound double bevel blades except for one that was chosen to be a compound single bevel blade. The blade that is currently implemented in the Fraunhofer Project Center (FPC) industrial research partner's chopping machine was used and is named the FPC blade. The rest of the blades that were used in wear testing experiments were sourced from a company named Cadence Inc., a specialty blade manufacturer in the U.S.A. The characteristics of the blades used in the wear testing experiments are outlined in Table 3-1. Vickers hardness measurements were obtained in a micro hardness tester with 1kg of mass and 15s hold time used as the parameters. As the FPC blade was in short supply, a blade close to its geometry and material properties was needed for an extended wear trial, which is the source of the "baseline" name. The other blades are named according to their material or their geometry. The thick blade features a wider base and a broader hone angle. The stainless steel thin blade is both a softer material with an acute grind and hone angle. The chisel blade is a compound single bevel edge blade that has included hone angle similar to the thick blade. The tungsten carbide blade is a harder material than the steel blades with geometry close to the thick blade. A set of wire EDM blades were produced to simulate wear at various stages. The target radii of curvature for the blades were 20, 40, 60, 80, and 100 μm. The blades were mounted in Bakelite and the radius of curvature of the tip was measured using the procedure outlined in Section 3.8. The results of the tip radius of curvature measurements are outlined in Table 3-2.

**Table 3-1 Properties of knife blades**

| Blade name | Baseline | FPC | Thick | Stainless steel thin | Chisel | Tungsten carbide |
|---|---|---|---|---|---|---|
| Material | M2 steel | 1085 steel | M2 steel | 440A stainless steel | M2 steel | 12% cobalt, sub micron carbide |
| Base thickness | 0.25 | 0.30 | 0.89 | 0.25 | 0.89 | 0.89 |
| Grind angle as measured | 9.5 | 9.0 | 9.0 | 6.0 | 29.7 | 8.4 |
| Hone angle as measured | 15.2 | 12.4 | 17.5 | 12.0 | 35.5 | 17.8 |
| Vickers hardness as measured | 745 | 780 | 757 | 558 | 764 | 1301 |

**Table 3-2 EDM blade target vs. measured tip radius of curvature**

| Target radius of curvature (μm) | Measured radius of curvature (μm) |
|---|---|
| 20 | 6 |
| 40 | 2 |
| 60 | 11 |
| 80 | 13 |
| 100 | 34 |

The blades intended for use in wear testing experiments were mounted in Bakelite, ground, polished and etched to observe the microstructure under an optical microscope at 500x magnification and were compared to samples in the ASM handbook volume 9[38]. Images of the material microstructure are presented in Figure 3-3. The FPC blade, being 1085 steel hardened to $R_c63$ shows a martensitic microstructure. The M2 tool steel blades (baseline, chisel, and thick) show very similar microstructure of martensite and undissolved carbides. The tungsten carbide blade shows a very fine grain sized microstructure with small amounts of cobalt binder. The stainless steel thin blade, being composed of 440A and having a carbon content of 0.60-0.75% with a chromium content of 16-18%, shows a fine microstructure with a chromium carbide phase.

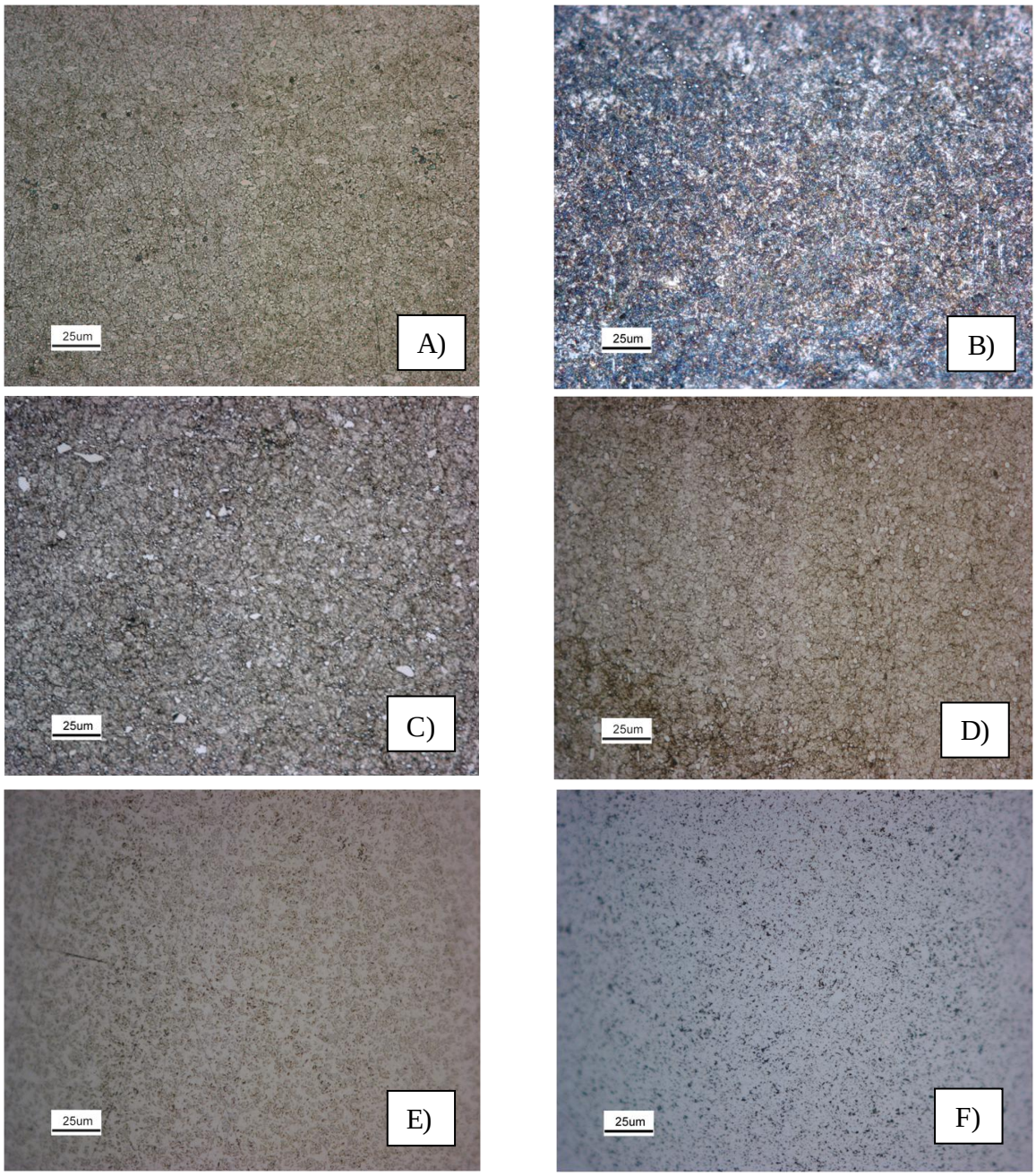


**Figure 3-3 Blade material microstructure: A) Baseline blade B) FPC blade C) Thick blade D) Chisel Blade E) Stainless steel thin blade F) Tungsten carbide blade**

## 3.5 Linear Cutter

### 3.5.1 Reason for Developing

In order to accurately observe and quantify the effects of changing various parameters of the chopping device, a means of acquiring force vs. displacement curves for the action of cutting a roving in a controlled manner was sought. As the industrial, rotary style cutter is difficult to instrument and acquire meaningful data clear of noise, a simplified version of the cutter was developed. The simplified version included a means of measuring the force of the blade on the fibers and backing material, the displacement of the blade with respect to the surface of the backing material, and a means of controlling the motion of the blade with respect to the backing. A linear motion was chosen to simplify displacement and load measurement as well as simplify the motion control. The intent was that the instrumented linear chopper would be able to characterize subtle differences between different chopper parameter set-ups.

### 3.5.2 Design Considerations

The linear instrumented chopper was designed with the following features in mind:

- Ability to mount blades of various geometry including variations in length, and thickness;
- Ability to test backing materials of varying dimensions including width, length and height;
- Ability to test backing materials of varying Durometer, or hardness;
- Ability to plunge the knife into the backing at different rates;

### 3.5.3 Functions

The basic functions of the linear chopper components are to interface with the tool holder of a CNC machine, and to couple a load cell, LVDT, and knife blade holder. The LVDT holder is adjustable in that it can clamp the LVDT housing at any height. This adjustability allows for blades of varying height to be used as well as backings, or backing fixtures, of varying height to be used. As can be seen in Figure 3-4, the LVDT holder is positioned below the load cell, which was chosen such that the displacement captured by the LVDT did not include the deflection of the load cell.

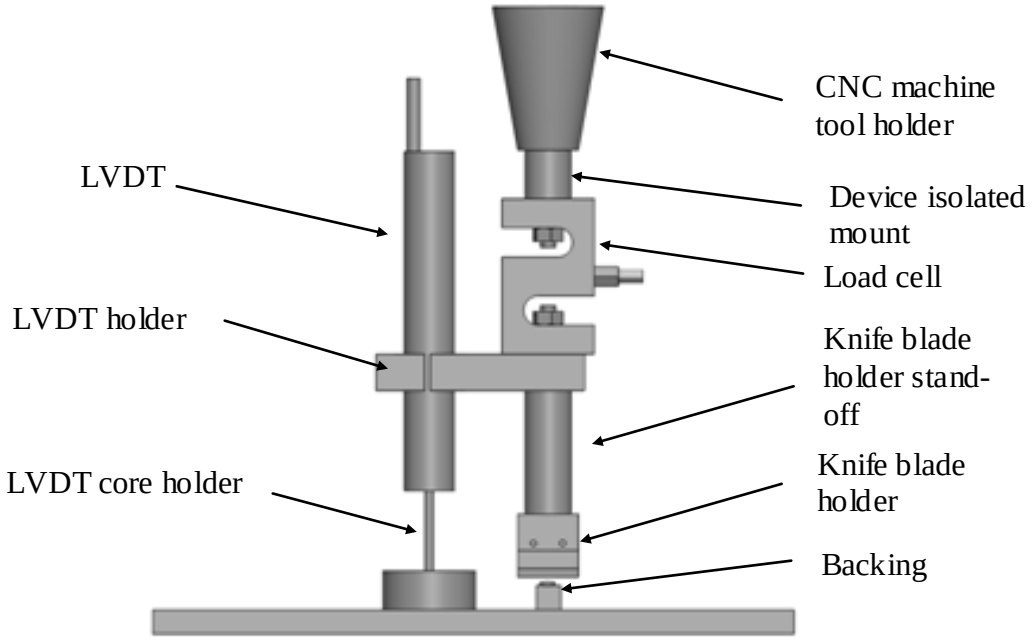


**Figure 3-4 Linear chopping device**

### 3.5.4 Details of Components

Device isolated mount: The device isolated mount is an acrylic coupler between the CNC machine tool holder and the load cell. It has been machined from acrylic in order to

separate the grounding of the CNC machine and the linear chopper. A metallic version of the mount had been implemented, but was replaced with the non conducting material after noise was found in the load cell signal while the CNC mill was in motion. A series of tests were performed to isolate the cause of the noise, and it was found that the electrical continuity of the linear chopper and the CNC machine tool holder was the source. After the holder was swapped to the acrylic version, the noise observed with the CNC machine motion was no longer observed.

Load cell: The load cell is an Omega LC101-25 strain gauge based load cell. This load cell has a linearity of +- 0.03 %, a repeatability of 0.01 % and hysteresis of +- 0.02 % as indicated from the specifications document. A calibration was performed on the load cell with a precision digital scale.

LVDT: The LVDT used in the linear chopper is the Measurement Specialties HR500. This sensor has a +- 12.7 mm displacement range with a linearity of 0.25 %. An annealed nickel alloy core is supported by a brass rod, which is supported on by a steel base. The LVDT was calibrated using precision ground plates.

LVDT holder: The LVDT holder is a component that couples the LVDT to the load cell and knife holder components. It has been fabricated from aluminum such that it is lightweight and therefore will have a low effect on the apparatus' natural frequency of vibration.

Knife blade holder: The knife blade holder is attached to the load cell through a stand-off. The holder fixtures the knife blades via 2 set screws. The blade holding groove is 1.6 mm wide and 4 mm deep, while the set screws are placed 12 mm apart. The blade holder can accommodate any blade that is taller than 4 mm, although extra depth is

preferred such that the tip of the blade protrudes typically 4-5 mm from the bottom of the blade holder, any blade with a thickness less than 1.6 mm, and any blade that is wider than 14 mm such that the set screws are able to bear down on to the blade surface.

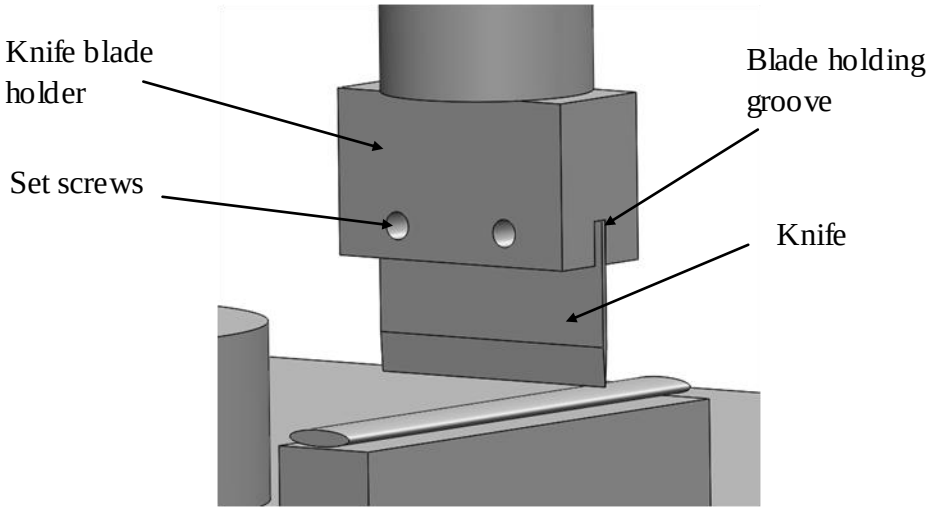


**Figure 3-5 Knife blade holder**

LVDT signal conditioner: A signal conditioner is required for a data acquisition card to be able to acquire a signal from an LVDT. The model chosen was the Penny and Giles UCM.

Data acquisition card: A data acquisition card was required to simultaneously collect data of the LVDT and load cell such that synchronized load vs. displacement curves could be easily generated. A card with high resolution and fast data transfer rates was desired. The NI USB-6210 card was recommended by a supplier. This card features 16 bit data acquisition at up to 25k samples/s.

Power supply: A BK Precision 1670A was recommended by the university electronics shop as an adequately stable, regulated and adjustable DC power supply. As the sensors

require power to operate, a consistent and noise free supply voltage contributes to a noise free signal from the sensors.

A personal computer with LabView 12 controlled the data acquisition card, and stored the data streams which were sampled at 15 kHz which was chosen to adequately acquire enough data as to not attenuate features and to minimize storage requirements. A LabView VI was developed to efficiently record and organize data.

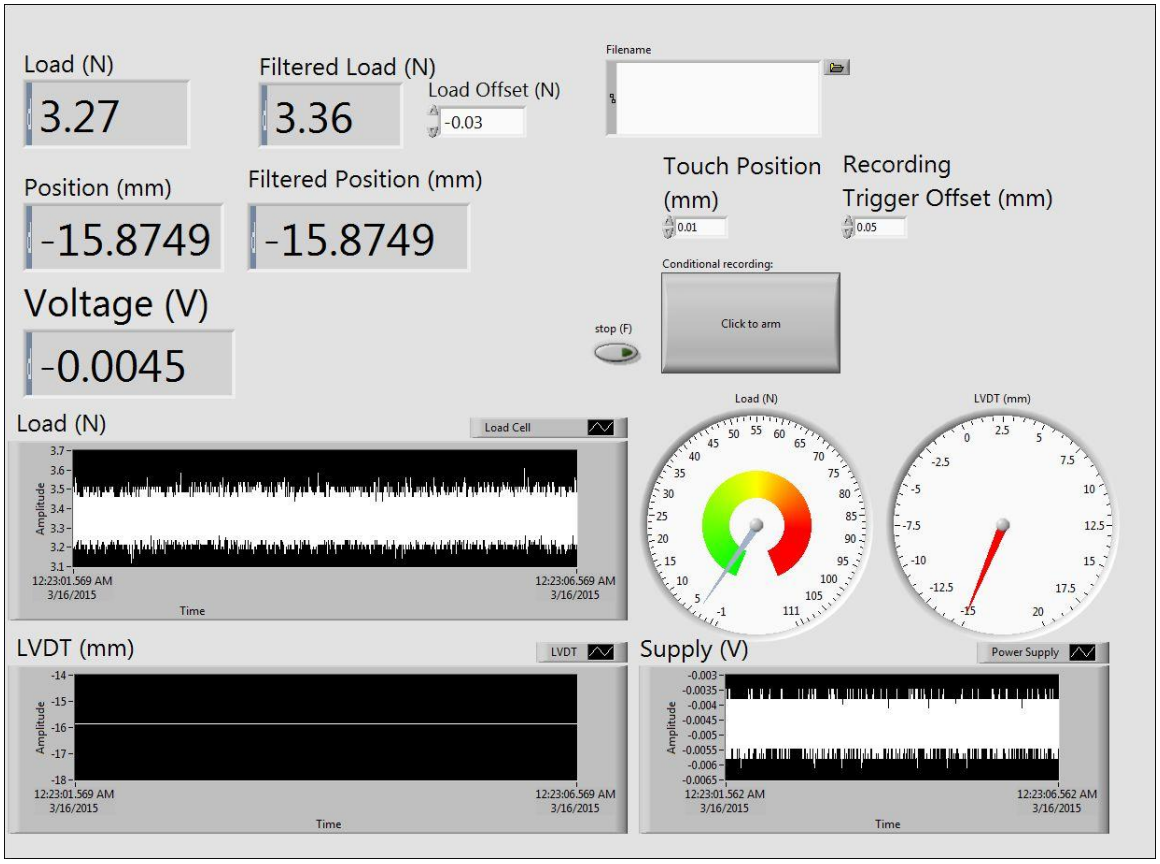


**Figure 3-6 LabView dashboard for linear chopper**

Figure 3-6 shows the LabView dashboard that was developed for use with the linear chopper and the block diagram is shown in Figure 3-7. Information, such as load and position data streams, is shown in real time which enabled rapid quality checking of experiments without the need to post process the data. If data showed that the plunge

depth of the experiment was not adequate, then the depth of plunge was updated and the test repeated. The supply voltage was continuously monitored unfiltered to ensure that the sensors were receiving a consistent 10 V supply.

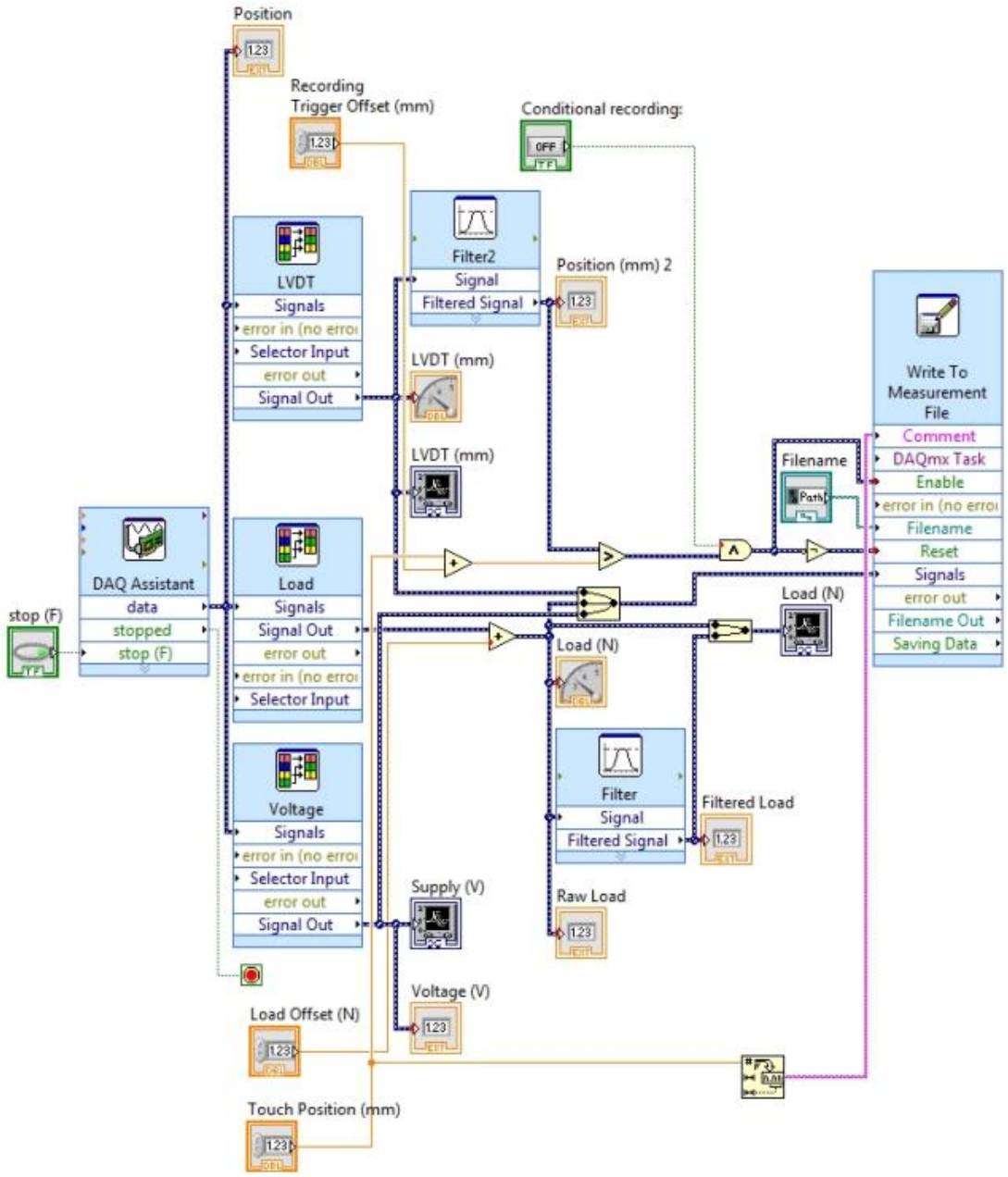


**Figure 3-7 LabView block diagram for linear chopper**

The load and position data streams were also monitored unfiltered which proved useful in detecting noisy signals that arose due to wiring issues. A load offset input box is present to tare the load cell when a new knife blade is mounted, and to account for any other variation. The touch position of the blade to the backing is inputted to allow for the post processor to be able to set the position datum for the test. A recording trigger offset was included, which controlled when the program automatically began recording data. The sequence of testing would be to set the CNC machine in motion from its control panel, and as the machine travelled in the z direction, the LVDT signal would be read by the LabView VI, when it reach the dictated offset from the indicated blade-to-backing touch position, recording would start. As the test came to completion and the CNC machine retracted past the offset position, the VI would halt recording of data and write it to a file indicated in the filename box. A "click to arm" button was required to be activated in order for the automatic data acquisition to function. This enabled manual set up of the test by positioning the CNC machine without triggering the data recorder.

### 3.5.5 Signal Processing

A signal processing program was developed in MatLab to perform the functions of trimming data at the beginning and ending of each test, filtering the data, plotting, and extracting key metrics that were identified. A multiple pass moving average filter that approximated a Gaussian filter with a cutoff frequency of 70 Hz was chosen because it adequately removed noise from the signals while capturing key features of the data. It was observed through excitation of the apparatus that the natural frequency of the apparatus was approximately 207 Hz using a fast Fourier transform on the recorded data as shown in Figure 3-8. The data shown was acquired while the apparatus was fixtured in

the CNC machining center, but showed similar natural frequency while removed from the machining center.

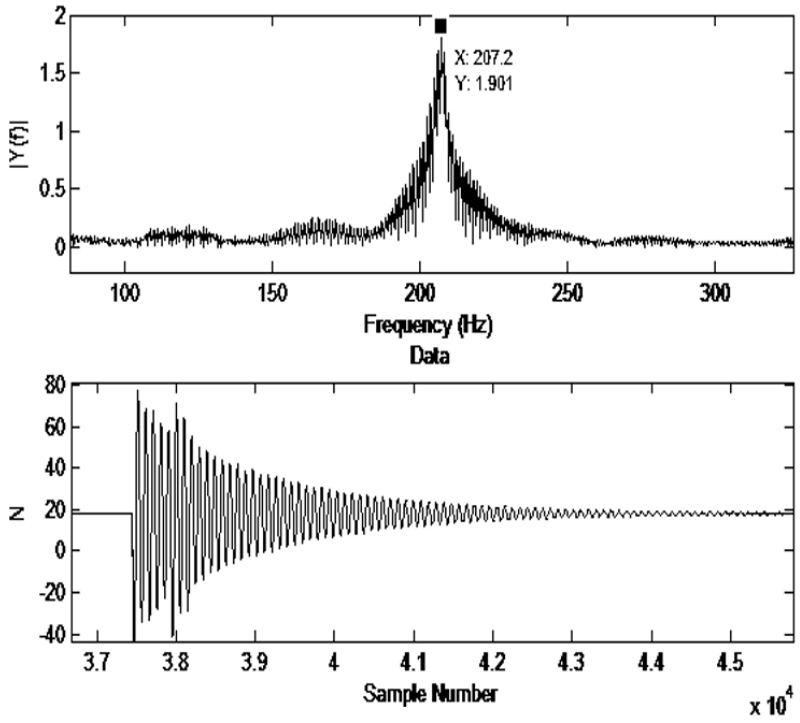


**Figure 3-8 Frequency of vibration of linear chopper.**

The apparatus is excited after a roving is cut with the testing apparatus, as the vibrations in the load signal are clearly visible in the data. Figure 3-9 shows the vibration picked up in the load signal post cutting of a roving against a soft backing. The blue curve is the filtered data curve. As the load rapidly drops as the fibers spontaneously sever and energy that has been built up in the load cell and apparatus is released, the apparatus vibrates at its natural frequency while being damped by the viscoelastic backing. Peak and minimum load finding is then carried out by the program to extract information about the test. Three points are of interest being the peak force during the cutting operation, the

local minimum force immediately after cutting, and the peak displacement of the test.

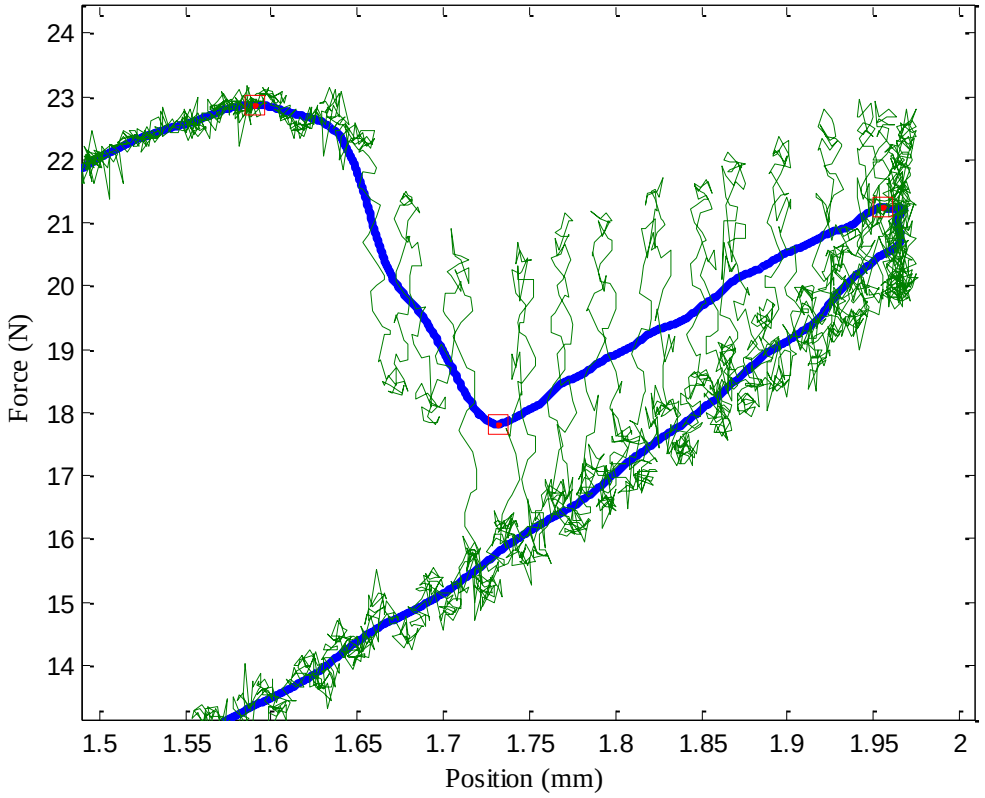


**Figure 3-9 Post cut excitation of apparatus**

These points are indicated in Figure 3-9 by red open squares. Finding these points of interest is accomplished in the program by finding data points that remain maximums or minimums in a window of data that is swept from the beginning to the end of the data set for the duration of time the point is within the window. Position data is shifted such that zero displacement corresponds to the position of the blade coming into contact with the backing with no fibers present.

### 3.5.6 Experimental Setup

Before each experiment, a setup procedure is followed to ensure that the range of motion of the blade is appropriate, that the data collected is in a consistent form and that

all important variables are recorded. For each combination of blade and backing material, the setup procedure consists of setting a position datum, determining the maximum plunge depth and collecting a baseline force vs. displacement curve without fibers being cut. The common position datum allows direct graphical comparison between experiments regardless of fiber tow size, or backing height. The datum also allows the depth to cut the fibers to be calculated. The maximum plunge depth is determined via manual positioning of the knife blade with fibers present to ensure that the automated experiment successfully cuts the fibers without plunging too deeply into the backing material. Finally, the collection of the baseline force-displacement curve permits calculation of the work to cut fibers without additional work required to compress the backing.

The datum height of a backing is measured by slowly bringing the knife into contact with the backing while observing the load signal for an increase in load. The displacement of the blade is taken as the datum when an increase in load due to displacement of the knife is observed.

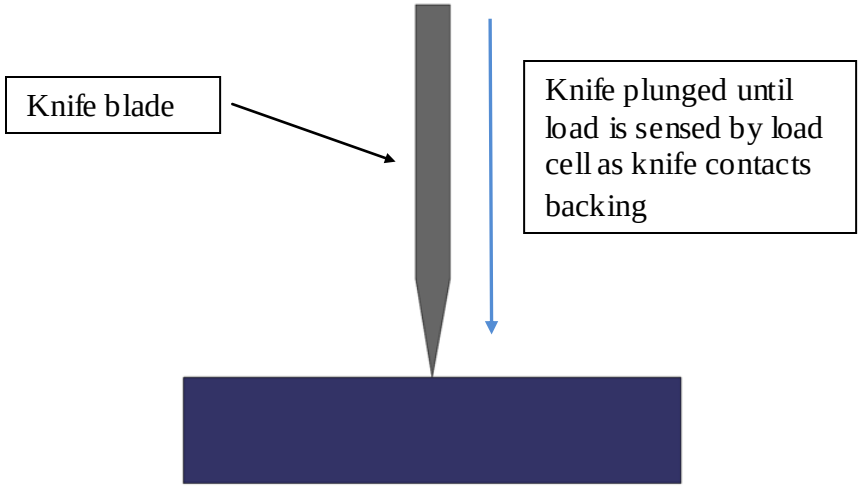


**Figure 3-10 Height datum procedure**

This observed load is typically in the order of 0.1 N and the maximum positional error associated with the datuming technique is +- 0.03 mm. This error in datum position has an effect on values obtained through data processing such as the height of the fiber tow, the depth of knife plunge to cut the fibers and the total depth of the knife plunge, but does not affect work or force measurements. After datuming the backing surface, the depth that the knife plunges into the backing during automated experiments is determined by performing a manual plunge with a roving under the knife to observe the displacement at which the roving is fully cut. This displacement corresponds to a sharp drop in the load signal. Once the displacement is recorded, the knife is manually positioned to the appropriate height above the backing such that the CNC program will stop plunging at the desired plunge depth which is typically 0.25 mm below the depth required to manually cut the roving. The CNC machine is programmed to plunge to the maximum depth at a desired rate, while the data acquisition hardware and software records position and force to acquire the baseline curve.

### 3.5.7 Characteristic Curve

Experiments run with both glass and carbon fibers have been observed to contain similar and repeatable characteristics. Figure 3-11 shows the characteristic curve with labeled points of interest. Upon close inspection, it can be observed that the initial force the curve begins with is slightly above zero. This is because the data trimming in the signal processing program is set to remove data that corresponds to load being below 0.35 N. This is performed in order to reliably trim the beginning and end of the experiment which corresponds to the blade not being in contact with the fibers nor backing. The beginning of the curve starts off in a slightly non-linear fashion until a linear region is reached. The

non-linear region could be due to the compaction and settling of the roving as the knife bears down upon it. Load and displacement continue to rise until the load drops off suddenly.

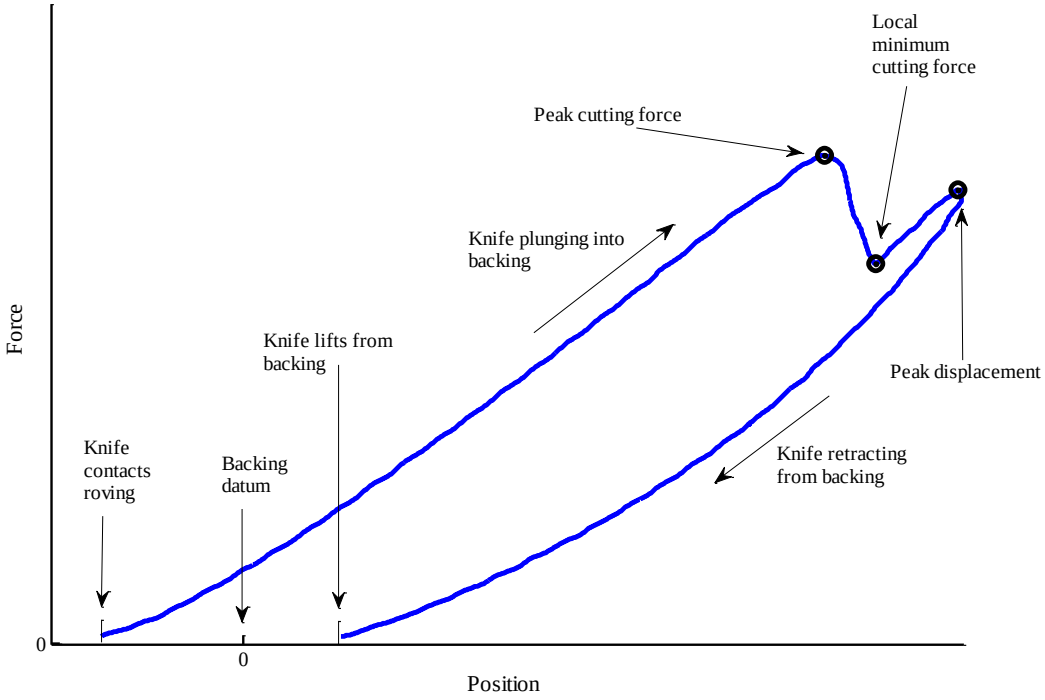


**Figure 3-11 Characteristic force vs. position curve of a roving being chopped.**

This drop off corresponds to the roving being cut. The load then reaches a local minimum and continues to rise until the CNC machine reverses its motion. The unloading curve is noticeably non-linear and the end of the curve does not correspond with the backing datum. These two observances can be explained by the viscoelastic nature of the backing material.

### 3.5.8 Extracted Data

After collection of the data, information of interest is then gathered using information from the peak finding algorithm. Below is a list of information that is catalogued with each experiment:

Roving height: The roving height is calculated by taking the position of the start of the force vs. displacement curve.

Work to cut fibers: The work to cut the fibers is taken as the area underneath the force vs. displacement curve up to the local minimum cutting force. This is depicted in Figure 3-12.

Total work: Total work corresponds to the area inside of the force vs. position curve as depicted in Figure 3-13.

Peak cut force: The peak cut force is the force value that the peak finding algorithm detects from the first peak.

Depth required to cut fibers: The depth required to cut is extracted from the local minimum value that has been found by the data combing algorithm.

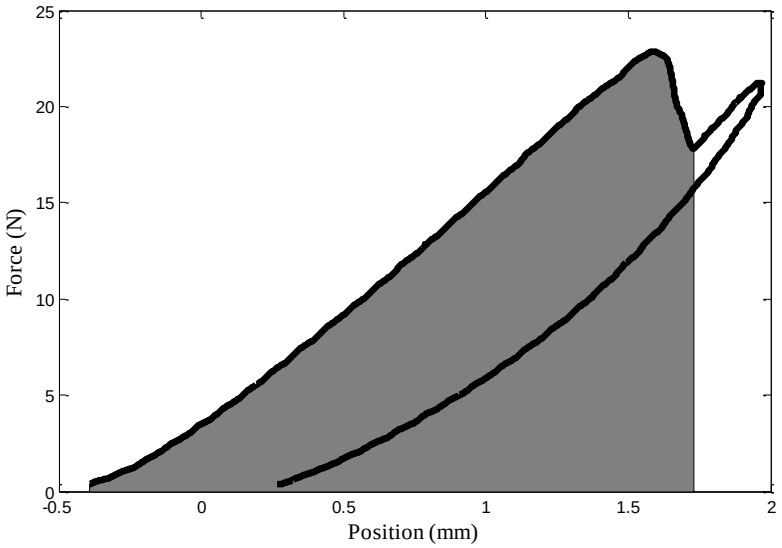


**Figure 3-12 Depiction of work to cut fibers.**

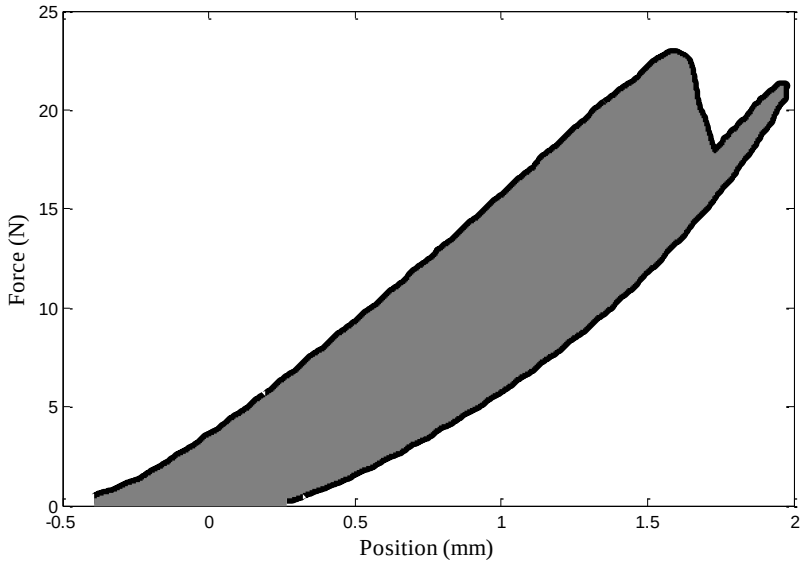


**Figure 3-13 Depiction of total work.**

## 3.6 Rotary Cutter

### 3.6.1 Motivation

As the means for characterizing the differences in process parameters with respect to force and displacement was accomplished with the linear chopper, a means of inducing the effects of continuous use on the chopping blades and backing in an apparatus that was close to the industrial chopper was sought after, such that different blades and backing materials could be compared. The used blades and backing from the rotary cutter could then be tested in the linear chopper to quantitatively measure the effects of usage. The rotary cutter was also developed to observe the effects of continuous use and to aid in determining the cause of fiber cutting failures. Specific emphasis was placed on observing if blade wear progressed such that the radius of curvature of the blade tip exceeded the critical radius of the fiber.

### 3.6.2 Design Considerations

The rotary chopper shared many design considerations with the linear chopper in that a versatile platform where many combinations of blades and backings could be tested. Blades of varying thicknesses and heights were accommodated with a variation of the blade holding mechanism of the linear chopper. The knife holding roll also allows a range in the knife protrusion height which is important if backings of different Durometer are to be tested as the depth of plunge has been found to change with backing Durometer during initial testing. A stiffer backing requires less knife plunge and hence less knife protrusion than a softer backing. To increase the amount of chops per blade per linear unit of roving, the amount of blades was kept to a minimum while still being able to mount 2 samples of the different blades being examined. Not counting a baseline wear test involving the chosen baseline blade, this brought the number of blades simultaneously mounted to 10. The chopper was designed to cut rovings in increments of close to 25 mm, the same increment as the industrial chopper at the FPC. With 10 blades and roughly 25 mm spacing between each blade, the diameter of the knife roll was set to 76.2 mm or 3” to match the diameter of commercially available backing material of 3” diameter. The spacing between each knife blade at the surface of the knife roll was then

set to 23.9 mm as measured as an arc.

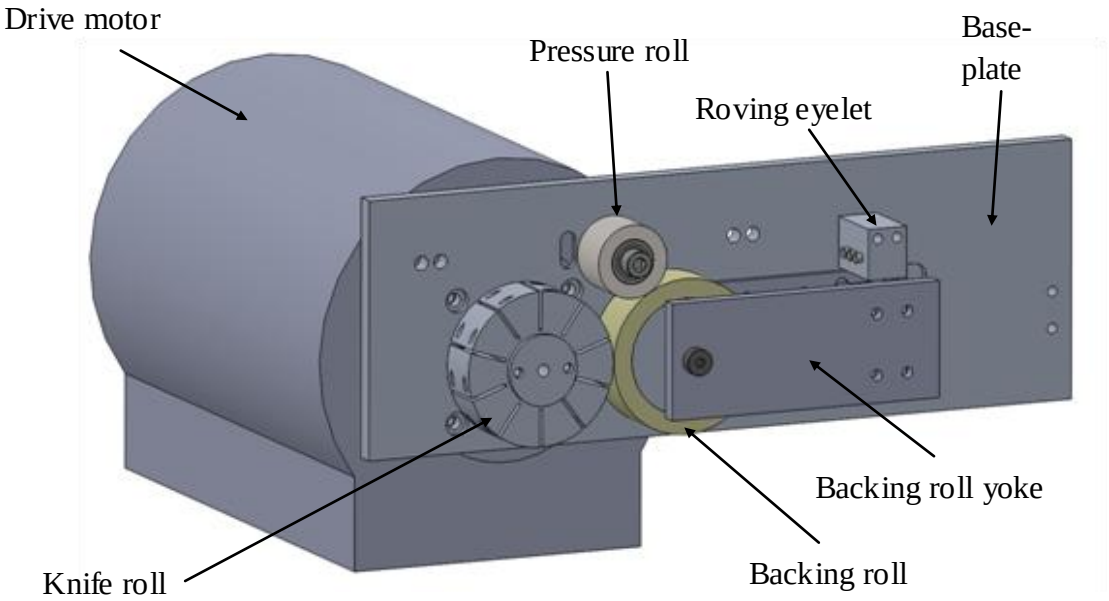


**Figure 3-14 Rotary chopper.**

The feed rate of the rotary was required to be controllable such that the surface cutting speed of the industrial chopper could be matched. This ensured that the cutting action was as close as possible to the industrial chopper. Differences between the rotary chopper testing device and the industrial chopper are that the roll diameter, and number of blades present on the knife roll are smaller on the testing unit. The industrial unit holds 24 blades, whereas the testing unit holds 10. The effect that the difference in roll diameter has on the cutting action is that the testing unit's knives will sweep through a greater angular range during contact with either fiber or backing given a constant knife protrusion as compared to the industrial chopper. Figure 3-15 shows that with a change in roll diameter while knife protrusion is kept constant, the angle that the knife contacts the backing roll changes such that with a smaller roll a larger contact angle is present.

The rolls in Figure 3-15 A) are equal diameter, as are the rolls in Figure 3-15 B). The effect that the contact angle has on the mechanics of the rotary chopper is that a small degree of translation of the knife tip will occur with respect to the backing surface if the angular velocity of the rolls remains equal to each other as in the case of being meshed via gearing or another mechanism. Alternatively, no translation may occur between the knife blade tip and the backing roll only if the angular velocities of the two rolls are allowed to change with respect of each other.

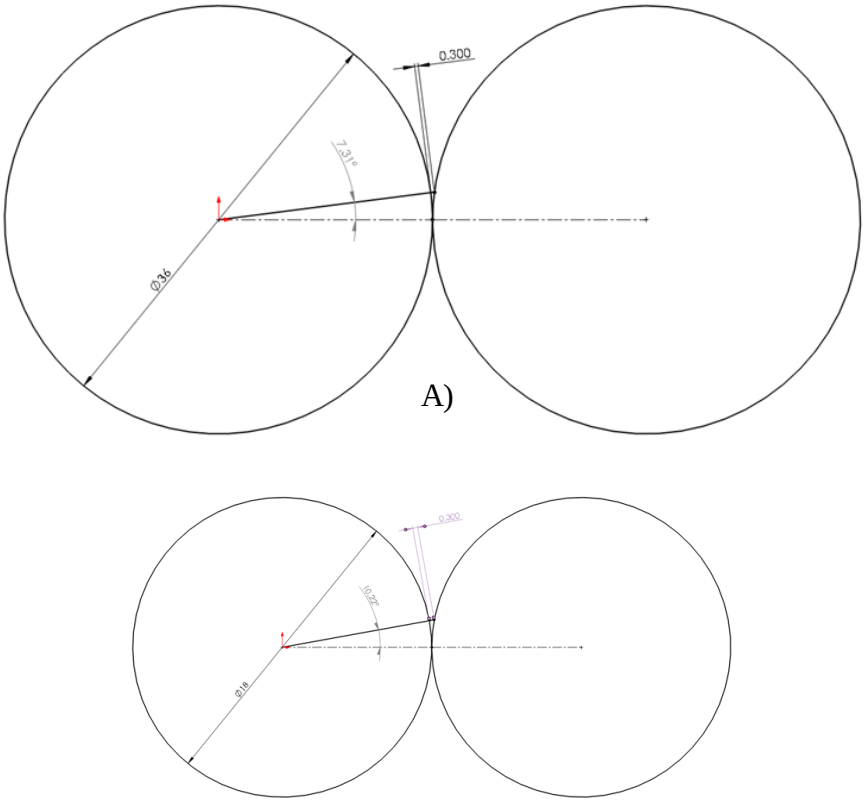


**Figure 3-15 Contact angle of knife to backing roll for different diameter rolls: A) Large B) Small**

In the case of the industrial chopper, the knife roll carries the blades in helical grooves in order to reduce vibration as only a small portion of a blade will initiate contact with the backing roll as opposed to the full length of the blade initiating contact in a straight blade holding groove scenario. As such, it is likely that the angular speeds of the rolls in the industrial chopper are forced to be equal to each other due to the contact with many blades simultaneously. For the industrial chopper, it would then be reasonable to assume that a small amount of translation of the blade tip with respect to the fiber roving and backing surface occur during chopping. The effect of blade translation during chopping is not clearly known, although it is suspected that it increases the wear rate of the blades and backing.

The rotary chopper testing unit as shown in Figure 3-14 is configured with the knife roll coupled to the drive motor. This arrangement has been chosen to mimic the industrial chopper's arrangement of the knife blade being driven. All testing conducted within the scope of this thesis has had this particular arrangement. For research purposes, the backing roll may be coupled to the motor instead of the knife roll.

As the diameters for the backing roll vary, the backing roll fixturing was required to be adjustable. The adjustment for the positioning of the backing roll with respect to the knife roll also allowed for adjustment of force between the backing roll and the knife roll.

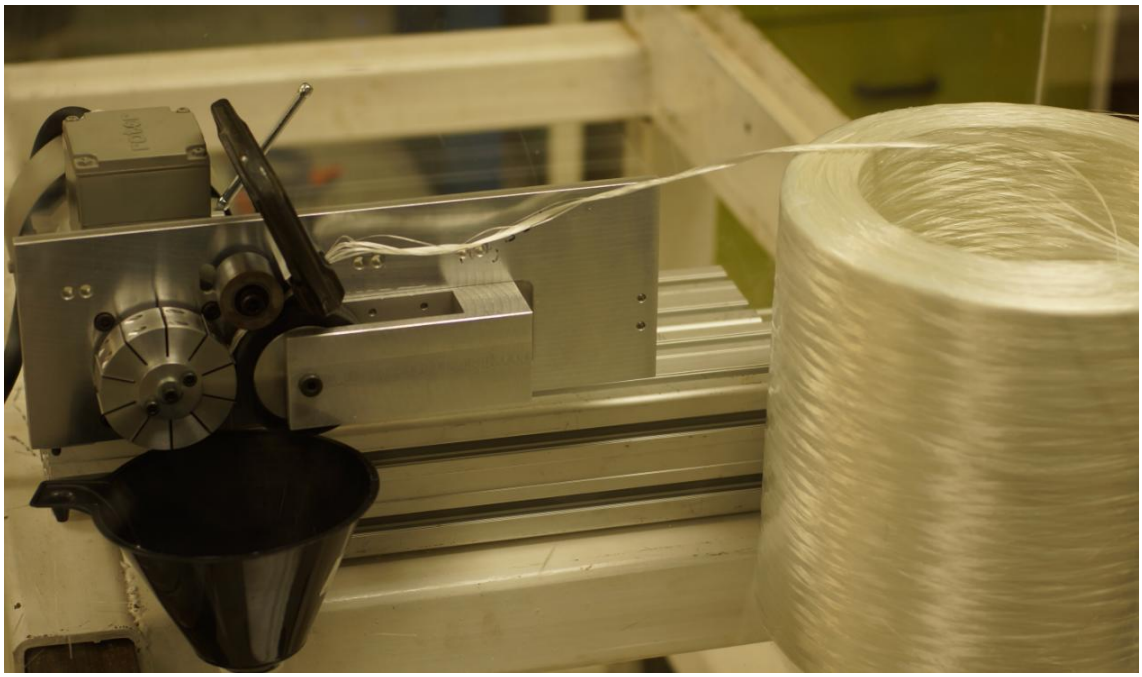

**Figure 3-16 Rotary chopper tester.**

### 3.6.3 Function

The functions of the various components have been summarized below:

Motor: Provides power to the device for all the moving components

Knife roll: Fixtures the knifes at the correct depth of cut and transmits power from the motor to the backing roll through contact friction

Backing roll: Provides a compliant surface such that the knifes may bend the fibers to failure

Pressure roll: Also described as the pinch roll, the pressure roll presses the roving against the backing roll to grip the roving and draw it into the contact region between the knife and backing roll. This roll is mounted on a slot in the backing plate, and its pressure against the backing roll is adjustable.

Roving eyelet: The roving eyelet acts as a guide for the roving such that the roving does not wander off the backing roll as it is being fed.

Backing roll yoke: The backing roll yoke rigidly supports the backing roll

As the motor is the sole power unit for the device, a means of drawing the fiber from the spool into the cutting region using the power from the motor is required. This is accomplished by maintaining contact between the knife roll (driving roll coupled to the motor shaft) and backing roll, and between the backing roll and the pressure roll. Other variations on this style of chopper have the knife roll only in contact with the backing roll through the knives. The necessary driving of the backing roll and pressure is accomplished via gearing between the knife roll and backing roll.

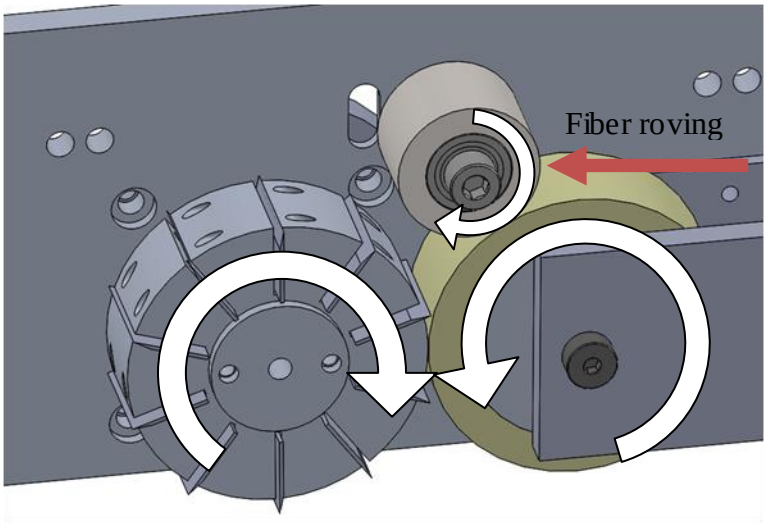


**Figure 3-17 Power transmission of the rotary chopper.**

### 3.6.4 Blade Positioning

A method of consistently positioning the blades in the blade holder's grooves was necessary to ensure that plunge depth from blade to blade was consistent and minimized as blades that plunge deeper into the backing could generate accelerated wear. Ensuring that the blade edge was aligned parallel to the axis of rotation was also considered important as deviation from this arrangement would result in an uneven pressure

distribution along the blade edge, uneven blade and backing wear. In order to accomplish these goals, custom blade positioning tools were machined from acrylic blocks that had a slot with a depth of the target blade protrusion. The knife roll was placed on a table top and a blade installed, lightly held by the set screws, protruding beyond the desired position. The blade was manually pushed downward into the table and the blade positioning tool was used to press the blade into the knife roll until it made contact with the knife roll. The set screws were then carefully tightened alternating from one to the other. Figure 3-18 shows the blade insertion procedure.

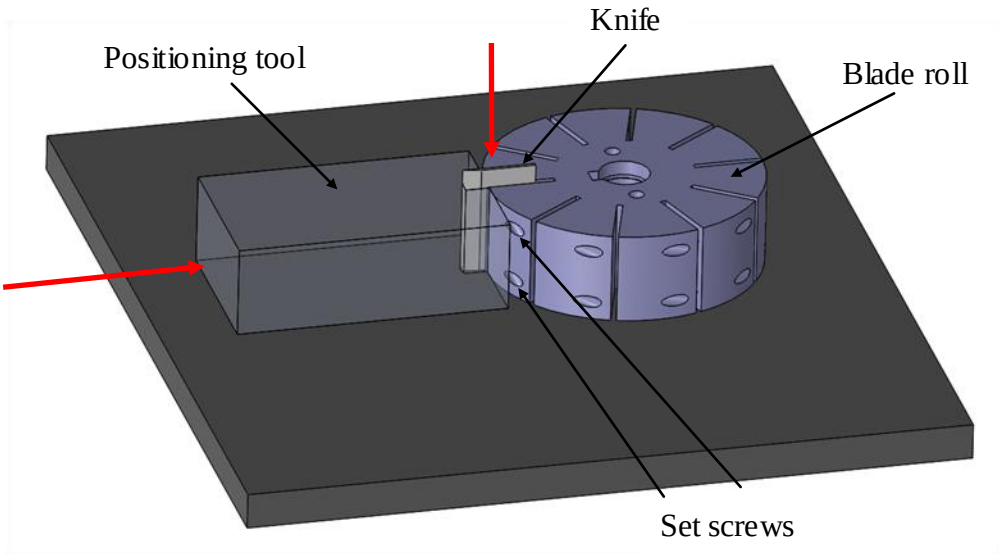


**Figure 3-18 Rotary chopper blade insertion procedure; red arrows indicate force application vectors.**

### 3.6.5 Backing Material Source

The backing material was sourced from McMaster-Carr.com, which conveniently carried a range of wear resistant polyurethane tubes at 3” outer diameter, with 3/8” wall thickness, which was similar to the 10 mm thickness of the backing installed at the FPC. These dimensions suited the design of the chopper well, and custom material was not

needed. The backing material was chosen to have similar properties as the material that the industry partner has on the D-SMC fiber chopper. Therefore, a Durometer of 60 shore A was chosen. The tensile strength rating for the material claimed by the supplier was 27.6 MPa. After receiving the material it was tested for hardness with a shore A Durometer and was found to be 64 A.

## 3.7 Wear Testing Design of Experiments

A testing scheme was developed to observe how each blade reacted to continuous chopping in the rotary chopping device while quantifying the effects of use at pre-determined intervals using the linear chopper. Two rounds of testing were performed, an extended wear test with baseline blades, and a multiple blade test with the remainder of the blades.

### 3.7.1 Baseline Extended Wear Testing Description

The extended wear test was performed to observe the effect of prolonged usage on cutting blades in the rotary chopper. During pre-determined intervals, blades were removed from the blade roll and replaced with new blades such that at the end of testing the blades would have a progression of wear from an unused state to the most used state. The chosen stages of wear for the baseline wear test in terms of thousands of chops that each knife performed were: 2.5, 5, 10, 20, 30, 40, 50, 60, 80, 100, 120, 140, 150, 160, 170, 180, 190, 195, 197.5. 200 thousand chops per blade represents 40 kg of carbon fiber chopped in the rotary chopper for all the blades. If scaled to the production unit, which featured 2.4 x the number of blades, 24 x the number of rovings, and approximately ¼ the effective wear on the blades as the industrial chopper translates the rovings along the

cutting edge surface in an alternating fashion such that a roving is only in one location on the blade ¼ of the time, and the rest of the time, the knife does not cut, then this would represent 9,216 kg of carbon fiber. Assuming a 30% fiber volume fraction, which is typical for SMC and a matrix density of 1600 kg /m3, the equivalent total mass of composite material produced from the equivalent number of chops with the same roving weight in the industrial unit is 28,300 kg. At full production speed this represents 66 hours of operation or approximately 8.25, 8 hour shifts.

At each increment, the testing machine was stopped and the blade and backing were removed and placed within the linear chopper. Force vs. displacement curves were obtained as outlined in Section 3.5.

The intention with this test would be to simulate continuous usage comparable to an acceptable life cycle time of the blades in the industrial unit. This would afford the ability to observe if the chopping mechanism ceased to function as well as to quantify the effects of wear on the blades as usage continued.

### 3.7.2 Blade Geometry and Material Testing Description

A similar testing routine was performed with the remainder of the blade types. This test differed in that the 5 remaining blade types were placed on the knife roll simultaneously with 2 blades of each type being mounted. For this test the increments were determined to be 10, 30, and 50 thousand chops as there was a limited supply of carbon fiber available for testing. The intent with this test was that the blades would be compared against each other with moderate amounts of wear.

## 3.8 Blade Wear Measurements

### 3.8.1 Motivation

Quantifying the effects of blade wear was identified as an important means of assessing the performance of the blades. A means of tracking the change in the plunge depth of the blade into the backing as blade wear progressed was sought after because the plunge depth of the blade has been isolated as a critical factor in the ability for a blade to cut a roving of carbon fibers. Even if a blade is sufficiently sharp, it will not be able to cut a roving unless a critical plunge depth is reached. One of the sources of change in depth of plunge is that as more and more chops are performed by a blade, the blade edge is eroded away from its initial position. This distance change will translate to a loss in plunge depth of the blade into the backing and, if sufficient erosion has occurred, will reduce the plunge depth below the critical value necessary to sever all of the filaments in the roving. If the tip erosion depth can be tracked for different blades, the blades can be ranked accordingly, and characteristics of the blades can be isolated that are responsible for the difference in performance.

As bending the fibers to the critical radius has been identified as a means to cut the fibers, measurement of the blade tip curvature is of interest. If a blade has been worn down and the tip radius of curvature exceeds the critical radius of the fiber, the cutting mechanism could not be solely a bending mechanism. Conversely, if the blade tip radius of curvature on a worn blade that does not have the ability to cut is below that of the critical radius of the fiber, another explanation for its failure to cut must be generated as the fiber should be able to reach the critical radius if conformed to the blade tip. Comparing the data obtained from the linear chopping testing apparatus from worn blades with the blade tip

radius of curvature measurements gives insight on the effect of the tip radius of curvature vs. other forms of wear.

### 3.8.2 Techniques

Various techniques were developed in order to measure the effects of blade usage.

#### 3.8.2.1 Front View Datum Edge Comparison

Front view datum edge comparison involves taking a blade and placing its face on the microscope stage. Another blade of similar thickness is placed such that its bottom, non cutting, edge is placed in contact with the cutting edge of the blade that is being measured. The blades are viewed under the microscope at 50x magnification in order to increase the depth of field of the image. The depth of field is an important factor for the measurement as the datum edge is resting in a different focal plane than the cutting edge of the blade. This separation of focal planes has been minimized but cannot be practically eliminated as positioning the cutting edge of the blade against the datum edge would be increasingly difficult. The likelihood of the cutting edge resting on top of the datum edge instead of against it increases as the planes approach each other. In order for a high contrast between the datum and cutting edge vs. the background to occur, a white background was used. The field of view was restored until the region with the largest visual gap between the blade and datum were found. A schematic of the procedure is shown in Figure 3-19. An image was captured at this position and then imported to SolidWorks CAD software in order to measure. The method of importing the image was to sketch on a plane and use the ‘sketch picture’ function to import the picture. Each image from the optical microscope has a scale bar present in the bottom left hand corner of the image. Within the sketch containing the picture a line was drawn at the length of

the scale bar. To begin and terminate the line, the viewport was zoomed in as far as practical in order to reduce the error between the sketch line length and the scale bar length. After the line was drawn, its length and position were fixed and a dimension was used to show the line length in the Solidworks sketch scale.

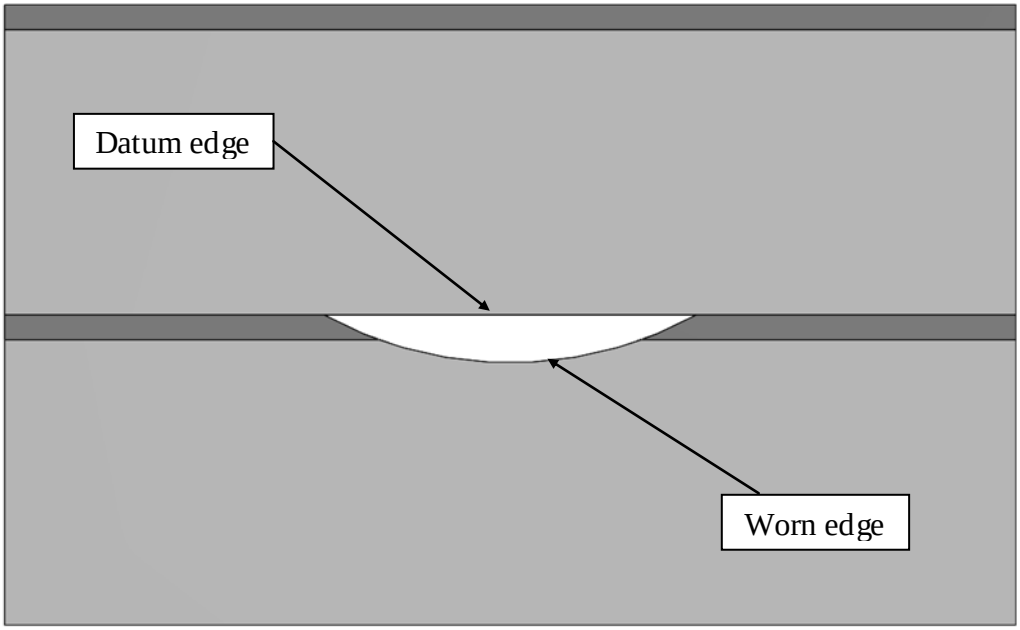


**Figure 3-19 Schematic of front view datum edge comparison.**

A line was then drawn that spanned the largest gap in between the blade cutting edge and the datum edge. The length and position of this line was fixed and a dimension was applied to it. The values of the lines were then entered into a spreadsheet. Sources of error for this type of measurement include the fact that the sides of the blade that contacted the straight edge datum were not measured for wear. Therefore, if wear were present on either side, it would reduce the measured wear. If the blade edge quality was such that it was not perfectly straight, which must be assumed, the wear measurement would be skewed. If the straight edge datum that was used was significantly curved, the

wear measurement would have error associated with it in much the same way as if the blade edge were not straight. As the optical microscope was used to generate the measurements any error associated with the scale bar present on the captured image would result in error in the measurement. Any irregularities in the optics of the microscope would result in measurement error. The fact that the datum edge and the blade edge were in different focal planes would also generate error in the measurements. Error could be generated if the blade edge extremities were not in proper contact with the datum edge. This type of error could either increase or decrease the measurement through the following scenarios:

If one of the blade edges were overlapping the datum edge, then the measurement would be lower than the true value.

If one or both of the blade edges were separated from the datum edge the measurement would be greater than the true value.

A technique was used to decrease the error associated with these two scenarios. This technique involved carefully positioning the blade edge in contact with the datum edge while using oil based modeling clay to reduce the amount of movement the blades experience as the operator's fingers are removed from contact with the blades and the base. The oil based modeling clay was chosen as a fixturing material as it is highly plastic, which ensured little spring back or blade movement after placement. It was also convenient to store and use, as opposed to water based clay because it is non-drying and residue is easily cleaned from the blades and microscope base. It also has the advantages that little shrinkage occurs after placement, and it does not dry and/or crack which would

increase the amount of error in the measurements. After the blades were positioned a visual inspection was performed to warrant further investigation under the microscope. If the positioning failed visual inspection, the procedure was repeated until no visual gap at the blade edge extremities or any blade edge overlapping occurred. The extremities were then inspected under the microscope to verify that contact was made between the blade edge and datum and that no overlapping was present. Images were captured at each extremity to ensure this procedure had been performed and for traceability purposes such as if a measurement did not follow a trend, the positioning could be evaluated and inspected closer to ensure proper placement. As can be seen from the image below, there is error associated with the position of the red mark to the position of greatest wear.

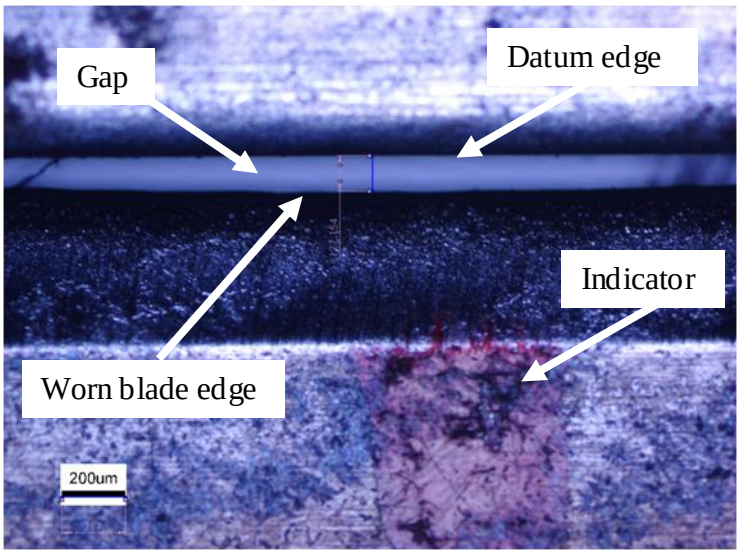


**Figure 3-20 Sample image of front view datum edge comparison.**

Figure 3-20 shows the worn blade edge at bottom with scale bar visible in the bottom left hand corner. The Solidworks lines for the scaling bar and gap are visible with their dimensions. Also visible in this image is the red mark that roughly indicates the region

where the roving was most likely to be cut in the rotary chopping device. This red mark was used to align the rovings to be cut in the linear chopping testing apparatus.

### 3.8.2.2 SEM Imaging

**SEM imaging was completed on all the blades under investigation at each increment of wear to give insight on the progression of wear from both a subjective and objective point of view. SEM was chosen to image the blades as it is a non destructive means of viewing the blades at high magnification while maintaining a very large depth of field as compared to an optical microscope. The top of the blade cutting edge has been imaged and measurements taken of the shaded region at the blade edge which corresponds to the worn region. This measurement gives the effective width of wear on the blade edge, and does not give direct insight on the depth of wear from the initial tip position or the radius of curvature of the tip of the blade. The SEM images are able to show in great detail the morphology and microstructure of the blades as they have progressively more and more wear. The width measurements taken from the SEM images can be compared with other wear measurements to observe correlations. As can be seen in**

Figure 3-21, multiple measurements were made per blade, and the measurements were capturing the width of the worn region as denoted by shading and striations.

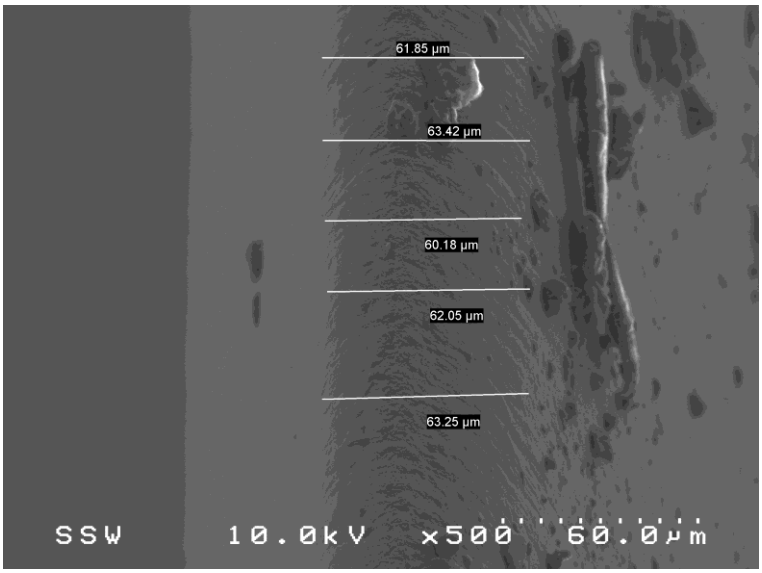


**Figure 3-21 Sample SEM image of worn blade tip with measurements.**

#### 3.8.2.3 Cross Section Tip Curvature

After all testing had been completed on the blades, as well as front view depth measurements, the blades were mounted in Bakelite, ground and polished to be viewed under an optical metallographic microscope. As the likelihood of a roving being chopped on a particular region of the blade edge changes along the length of the blade edge, it was particularly important to capture the cross section at the region of highest wear. This region was determined by using information from the front view datum edge comparison, markings that were present on the knife carrier roll that indicate a high likelihood of a roving being cut, as well as the fact that the blades had a common datum as installed on the rotary chopper knife roll. A mark with a red, fine tipped marker was placed on each blade at the peak of this marking, and the distance from the datum edge of the knife roll to the peak of this marking was taken. During the front view datum edge comparison measurement technique, the region of most wear could be compared to the placement of the red marking to ensure that the region of highest wear was accurately targeted. The region of highest wear could be assumed to be the same distance from the blade datum edge for all the blades, as the installation of the knife roll on the rotary chopper consistently positioned the knife roll with respect to the backing roll and the roving eyelet. The blades were then positioned in the vice of a diamond wafering saw perpendicular to the length axis of the blades using a square block such that the knife blades were cut off leaving the region of highest wear adjacent to the wafering blade edge.

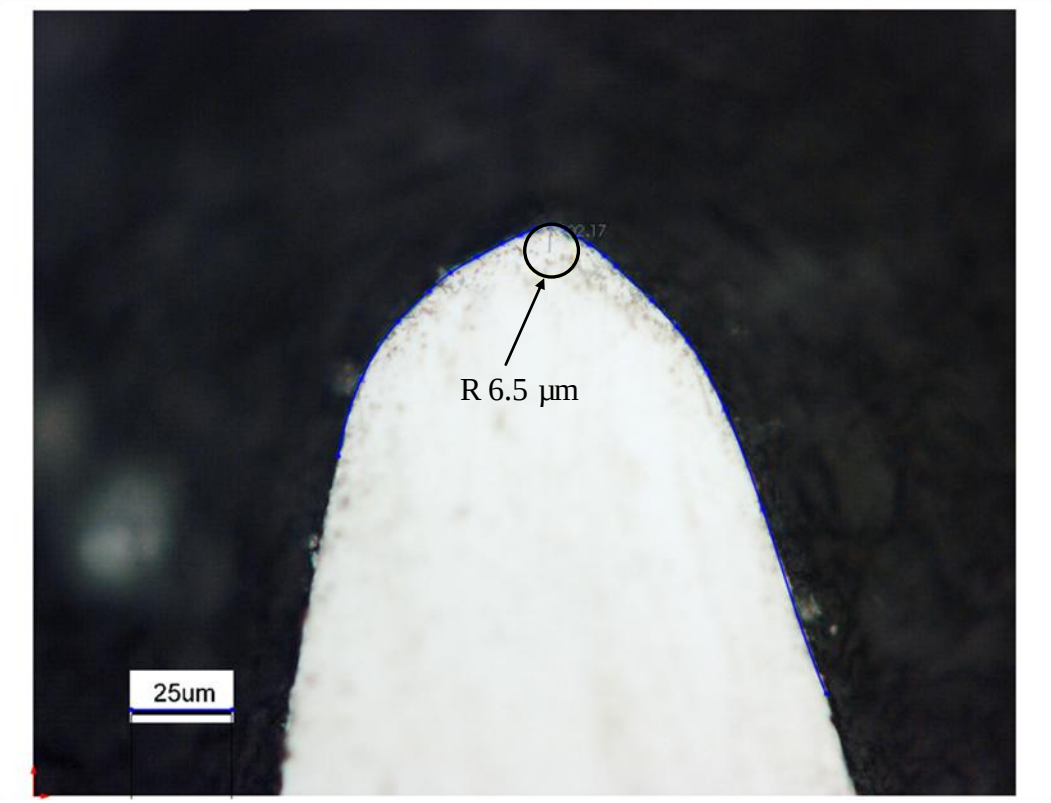


**Figure 3-22 Measurement of tip radius of curvature**

The blades were then carefully de-burred and positioned in the Bakelite mold with spring clips ensuring that all the blade sections were in contact with the mold bottom. After mounting, the samples were progressively finished using 300-2000 grid grinding paper followed by polishing with 0.5 micron alumina. The samples were then imaged at 500x magnification in an optical metallographic microscope. The images were then imported to a CAD software program and the outline of the tip of the blade was manually traced with a spline. A feature was used to show the minimum radius of curvature of the spline as shown in Figure 3-22. The value for each blade's radius of curvature was then recorded in a spreadsheet with a scaling factor applied to account for the difference between the CAD dimension and the scale bar dimension present on the image.

#### 3.8.2.4 Cross Section Edge Projection Depth Measurement

Measurement of the depth of wear from the initial blade tip to the worn blade tip was accomplished with analysis of the images taken of the knife cross sections as mounted in Bakelite. In order to generate a depth of wear measurement, a datum must be generated for each image as there is no feature present on the image indicating the position of the original tip of the knife blade. This datum was generated via the largely unaffected grind flanks present in the image. An unused blade was mounted in Bakelite and lines were drawn along the ground edges and were projected to an intersection of the two lines. Lines were also drawn along the honed edges and were projected to an intersection. The distance from the visible tip of the blade to the intersection point of the honed edge lines was recorded as well as the distance from the intersection of the ground edge lines to the visible tip of the new blade. An estimate of the distance that the tip of the blade has progressed from the new condition to the worn condition could then be made by measuring the distance from the ground edge intersection to the visible tip of the worn blade and subtracting the distance from the ground edge intersection to the visible tip measured with the new blade specimen. Figure 3-23 shows that with a heavily used blade, the wear progresses such that the hone region is no longer discernible from the tip region and therefore the honed edges cannot be used to measure depth. Thus the grind edges must be used as the datum for wear measurements as they are clearly visible on the

worn blade.

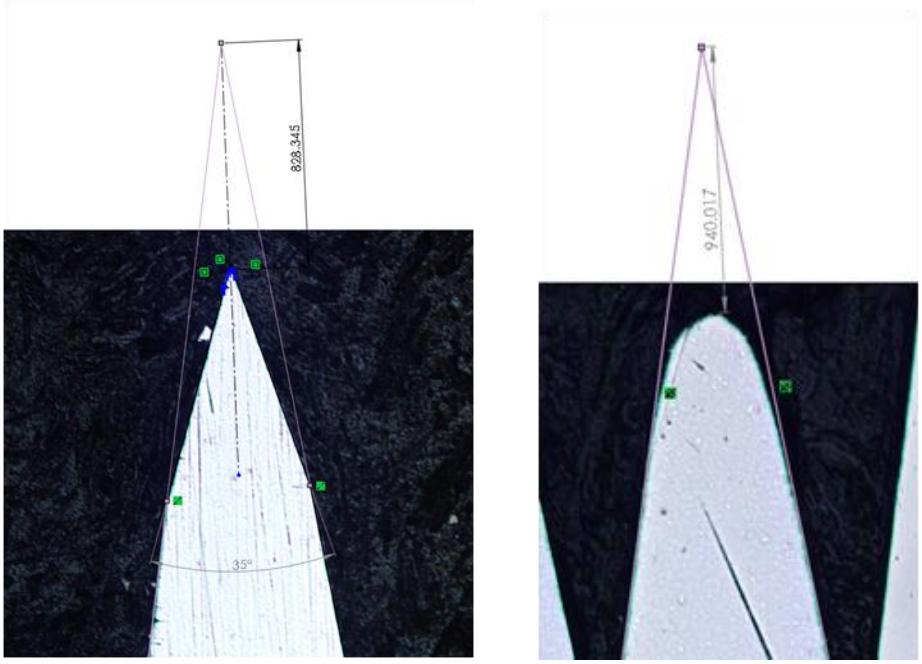


A) B)

**Figure 3-23 Measurement of depth of blade wear: A) New blade B) Used blade**

A study was performed on a number of minimally worn blades to establish confidence in using the ground edges of the blades as a datum for wear depth measurement. The study involved projecting both the honed edges and the ground edges to a point and measuring the distance between the two points. The values are presented in Table 3-3. The standard deviation of the values is then taken as the error associated with this portion of the measurement technique. The fact that the blades could not be cut, mounted, ground and polished to match up with the region of most wear that was observed with the front view datum edge measurement technique also introduces error into the measurement.

**Table 3-3 Study on ground edge consistency.**

| # of chops performed on blade | Distance between grind intersection and hone intersection-µm | grind angle | hone angle |
|---|---|---|---|
| 0 | 147.00 | 18.65 | 30.53 |
| 2500 | 142.90 | 19.35 | 30.82 |
| 5000 | 143.85 | 19.31 | 31.16 |
| 10000 | 144.79 | 19.75 | 30.52 |
| 20000 | 154.26 | 19.79 | 31.26 |
| Average | 146.56 | 19.37 | 30.86 |
| Standard deviation | 4.08 | 0.41 | 0.31 |

The estimated deviation from the plane of greatest wear is 0.75 mm. From analyzing the front view datum edge technique images, the error associated with the cross section being in the range of 0.75 mm is -4 % of the depth of the measurement.

# Chapter 4

# 4 Results and Discussion

In this chapter the results and observations of the experiments that have been outlined in chapter 3 are discussed.

## 4.1 Various Cutting Methods Test

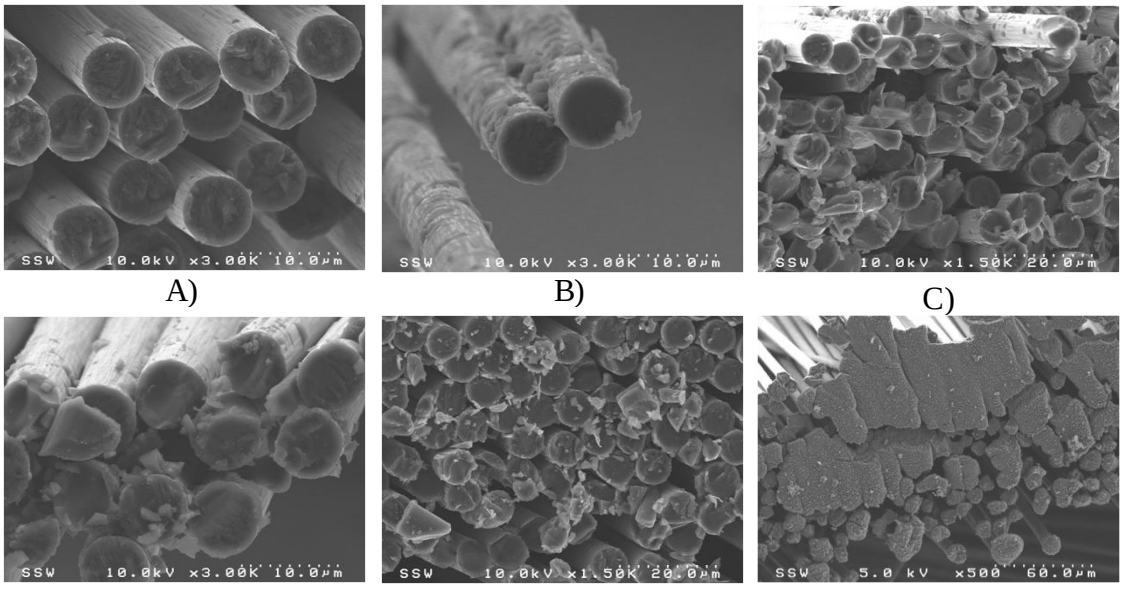


**Figure 4-1 SEM images of fiber ends through various cutting methods A) Bend failure B) Tensile failure C) Scissor cut D) Slice cut E) Crush cut F) Laser cut**

Figure 4-1 shows images obtained of the fiber ends through various cutting methods. As can be seen in the images, a varying amount of dust particles can be observed. Methods of severing the fibers that did not have high shear loading components appear to produce the least amount of dust such as bend failure, tensile failure and laser cutting. In fibers severed via bend failure, regions of tensile and compressive stresses may be discerned as also observed by Naito et al and DaSilva et al[39, 40]. In tensile failed fibers, the end

condition of the fiber is most homogenous although a failure initiation zone can be identified (as was also observed by Naito et al[41]). In the tensile failed fibers, a change in morphology to the surface of the fiber can be observed as flaking is present in Figure 4-1 B). Comparing the surface of the tensile failed fibers to the bend failed fibers, there appears to be a higher degree of fiber surface degradation. Naito et al observed the opposite effect in that the tensile failed fibers had a smoother surface while the bend failed fibers had the flaked[41]. The cause of the surface morphology change is unknown but may be caused by handling prior or post severing, or a rapid, energy release event.

## 4.2 Fiber Loop Testing

Results of fiber loop tests performed on T700 carbon fibers and JM272 E glass fibers are outlined in Table 4-1.

**Table 4-1 Critical radius measurement**

| Critical Radii | | | | |
|---|---|---|---|---|
| Sample | Radius (μm) | | Sample | Radius (μm) |
| Carbon 1 | 66.5 | | Glass 1 | 160.6 |
| Carbon 2 | 60.7 | | Glass 2 | 198.1 |
| Carbon 3 | 56.6 | | Glass 3 | 124.3 |
| mean | 61.3 | | mean | 161.0 |
| std. dev. | 5.0 | | std. dev. | 36.9 |

The carbon fibers consistently showed a smaller critical radius by a mean factor of 2.6. The relatively large difference in critical radius may explain difficulty in transitioning from glass to carbon fibers if blade edges do not have an edge that can produce the critical radius that the carbon fibers demand. The drastic difference in critical radius between the carbon and glass fibers may be explained partially by the difference in

diameter of the carbon fibers and glass fibers. Table 4-2 summarizes filament diameter measurements from optical microscope images.

**Table 4-2 Fiber diameter measurements**

| Fiber Diameters | | | | |
|---|---|---|---|---|
| Sample | Diameter (µm) | | Sample | Diameter (µm) |
| Carbon 1 | 7.3 | | Glass 1 | 13.6 |
| Carbon 2 | 7.9 | | Glass 2 | 13.7 |
| Carbon 3 | 7.0 | | Glass 3 | 13.8 |
| Carbon 4 | 6.4 | | Glass 4 | 13.5 |
| Carbon 5 | 7.0 | | Glass 5 | 13.8 |
| Carbon 6 | 7.1 | | mean | 13.7 |
| Carbon 7 | 7.0 | | std. dev. | 0.1 |
| mean | 7.1 | | | |
| std. dev. | 0.4 | | | |

If the properties from Table 2-1(assuming a tensile strength of 3445 MPa and a modulus of 80 GPa for E-glass) were used along with Equation 2.1 to predict the critical radius of the fibers the results would be that the E-glass would have a critical radius of 160 µm and the T700S carbon would have a critical radius of 165 µm. Comparing the experimental results to the theoretical results shows that the average value for the glass fibers is close to that of the predicted value (101%), but for the carbon fibers the experimental value is 37% of the predicted value. This could be explained by the anisotropy of the carbon fiber as compared to glass' isotropic structure[9].

## 4.3 Wear testing

### 4.3.1 Blade Wear Measurements

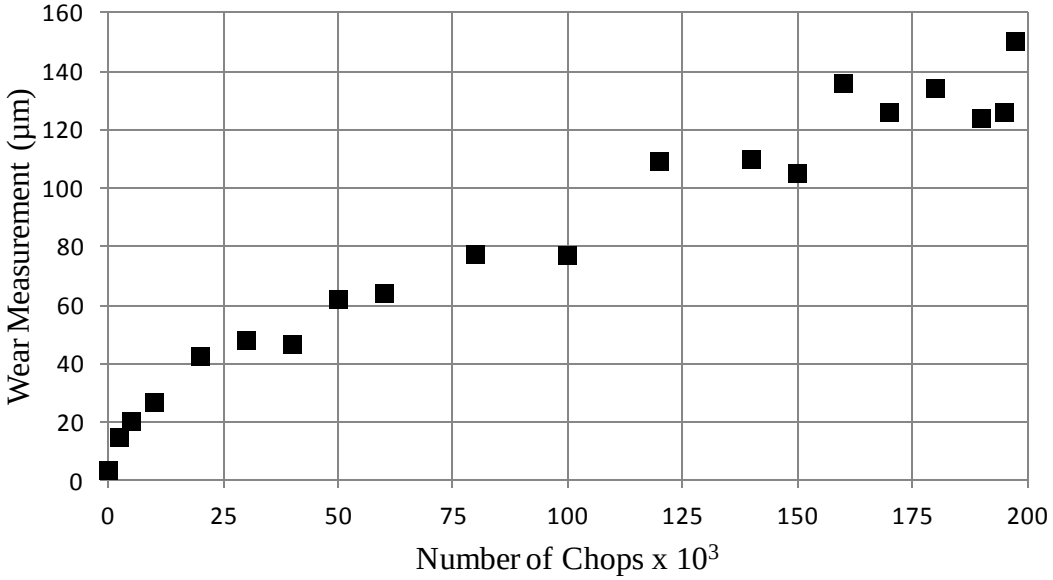


**Figure 4-2 Cross section depth of wear measurements for baseline blades.**

As can be seen in Figure 4-2, the depth of wear for the baseline blades throughout the extended wear test follows a linear relationship. At the early stages of wear, however, the depth of wear increases in a more rapid fashion as compared to the later stages (25,000 chops – 200,000 chops). This is consistent with observations by Lau et al.[35]. As wear progresses the effective depth that the blade engages into the backing material is diminished and as such the plunge depth may decrease to the point where the roving may not completely cut. The observed wear depth does not continuously rise from this measurement technique and may be due to a number of factors including variations in hardness of each blade sample, variation in set up in the rotary chopping device,

deviation of the viewing plane of the cross section from the region of greatest wear in the blade and eccentricity of the backing roll and blade roll.

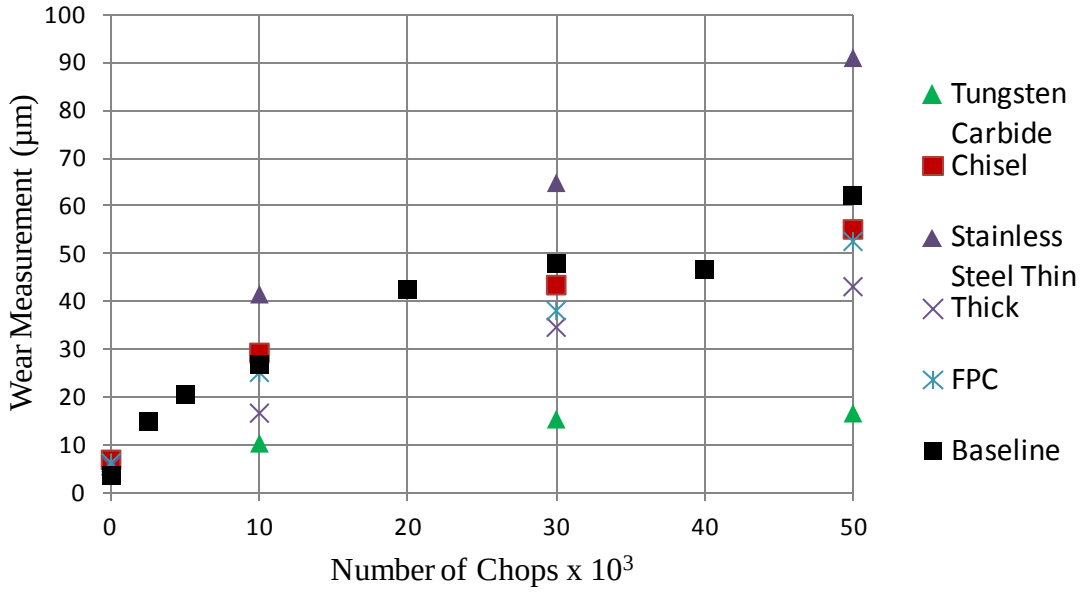


**Figure 4-3 Cross section depth of wear measurements.**

Figure 4-3 shows the progression of blade height loss over number of chops for various blades. This graph allows comparison between the various blades, but over a smaller duration than with the baseline extended wear test. The blade that showed the least amount of wear according to this metric was the tungsten carbide blade. The stainless steel thin blade showed significantly more wear than the other blades, while the FPC, thick, and chisel blade were grouped closer together between the tungsten carbide blade and the stainless steel thin blade. Figure 4-3 also shows the initial region of wear for the baseline blade extended wear test, with a break in region of increased wear rate, followed by a region that was more linear from 20000 chops onward.

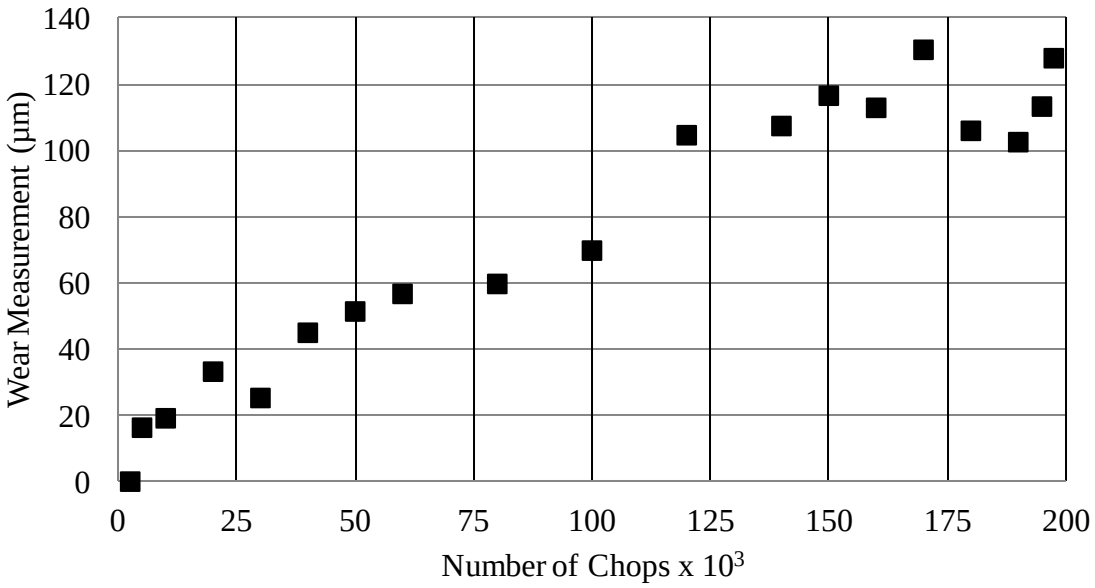


**Figure 4-4 Front view depth of wear measurement for baseline blades.**

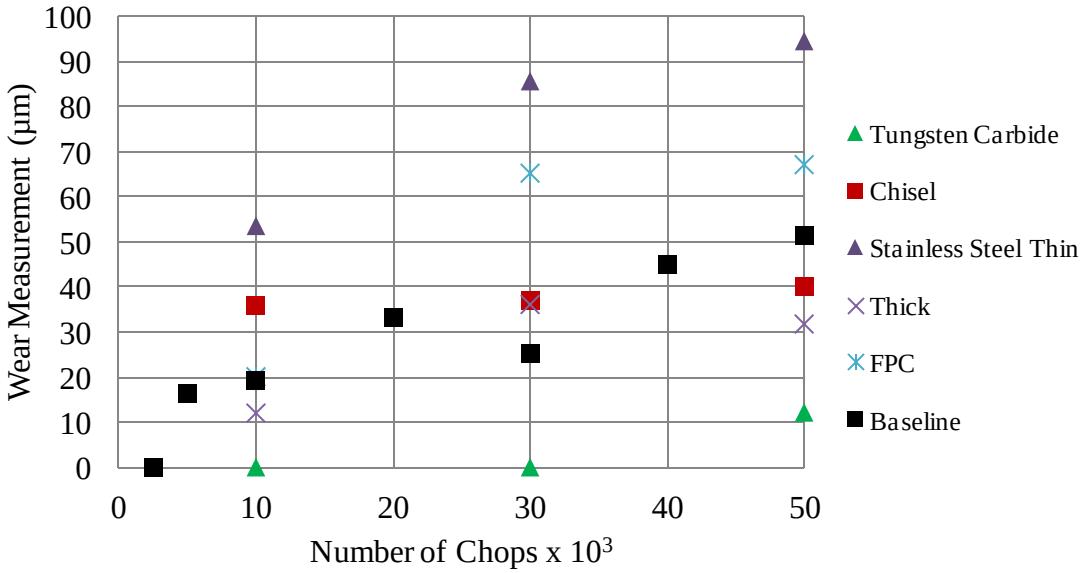


**Figure 4-5 Front view depth of wear measurements.**

Figure 4-4 and Figure 4-5 show consistent results with respect to general trends as compared with Figure 4-2 and Figure 4-3. The absolute value of depth of wear between

cross section and front view measurements differ slightly with the front view measurements being roughly 10% lower than the cross section measurements. This discrepancy can be explained with the errors described in the experimental procedures section. It is interesting to note that the tungsten carbide blade showed approximately the same wear at 50,000 chops than the baseline blade showed at 2,500 chops in both measurement techniques.

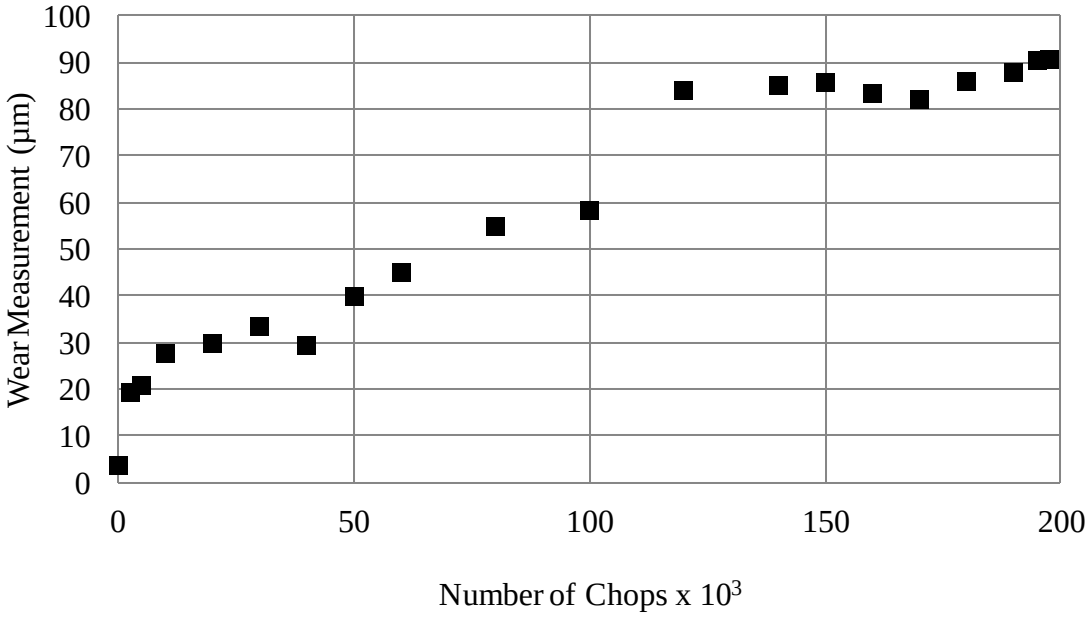


**Figure 4-6 SEM width of wear measurements for baseline blades.**

Width of wear region measurements as taken from SEM images of the blade tip shows an increasing width with usage. A marked jump however can be seen after 100000 chops on the baseline blade in Figure 4-6. The trend of increasing wear is less linear than cross section depth of wear measurements, but shows a similar high wear rate at the beginning of the wear testing (from 0 to 2,500 chops). After this initial break in, the width of wear continues linearly until 100,000 chops. It was observed that shortly after 100,000 chops a

set of grooves was worn into the backing roll and that the knife blades were consistently meshing with the grooves.

**Figure 4-7 Worn backing with grooves generated.**

A)

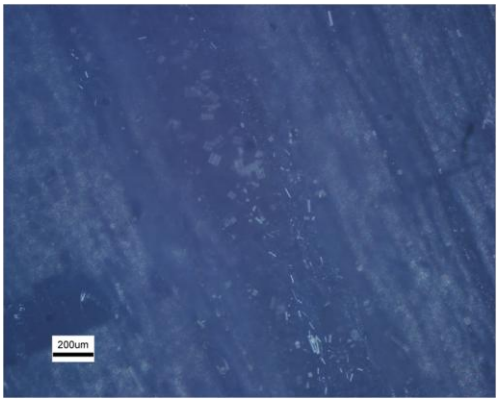


B)

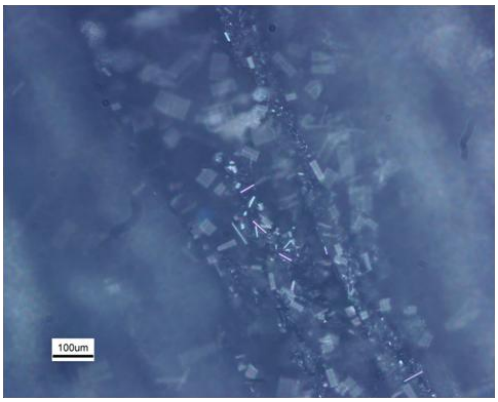


C)

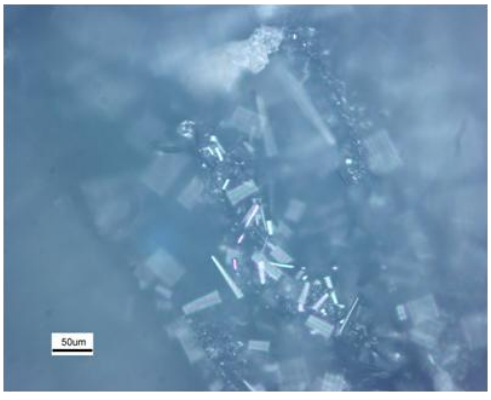


D)

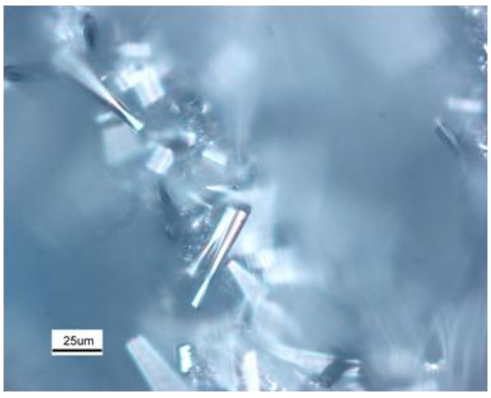


**Figure 4-8 Optical microscope images of carbon fiber particles embedded in backing groove: A) 50x B) 100x C) 200x D) 500x**

The backing was observed under an optical microscope and it was found that an accumulation of carbon fiber particles existed in the grooves which may have been a factor in the marked increase in wear rate just after 100,000 chops as reported in Figure 4-4 and Figure 4-6.

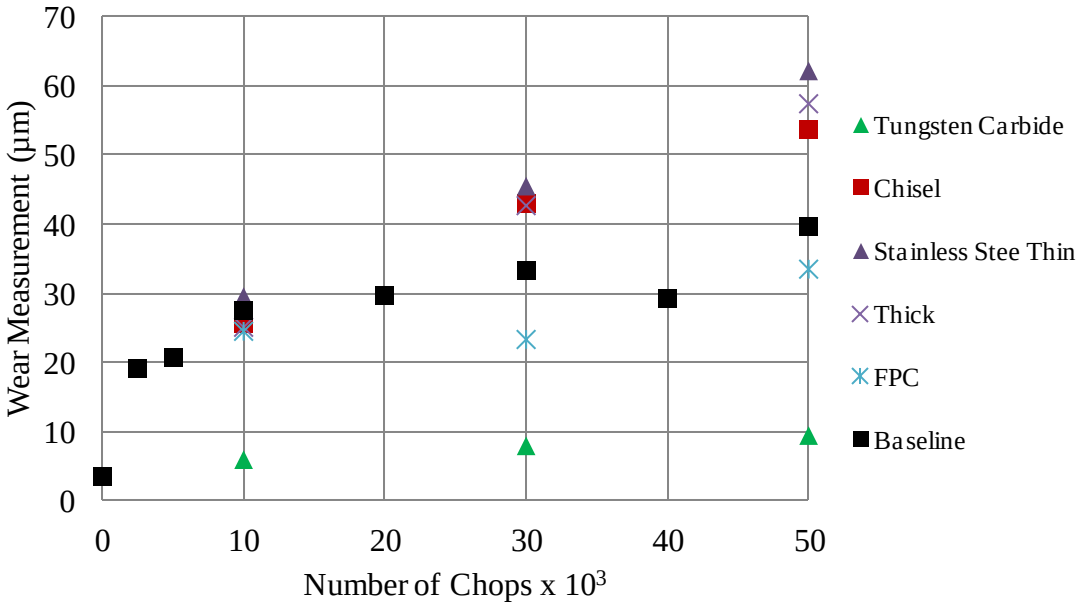


**Figure 4-9 SEM width of wear measurements.**

Comparing the wear width measurements of the different blade models, the trends appear similar to the depth measurements, where the tungsten carbide blades showed the least wear, and the stainless steel thin blades showed the most wear. The order of the blades in between the stainless steel thin blade and the tungsten carbide blades is not consistent between the various methods of quantifying wear. SEM images of each blade type through increasing stages of wear are show in Figure 4-10 through Figure 4-15.

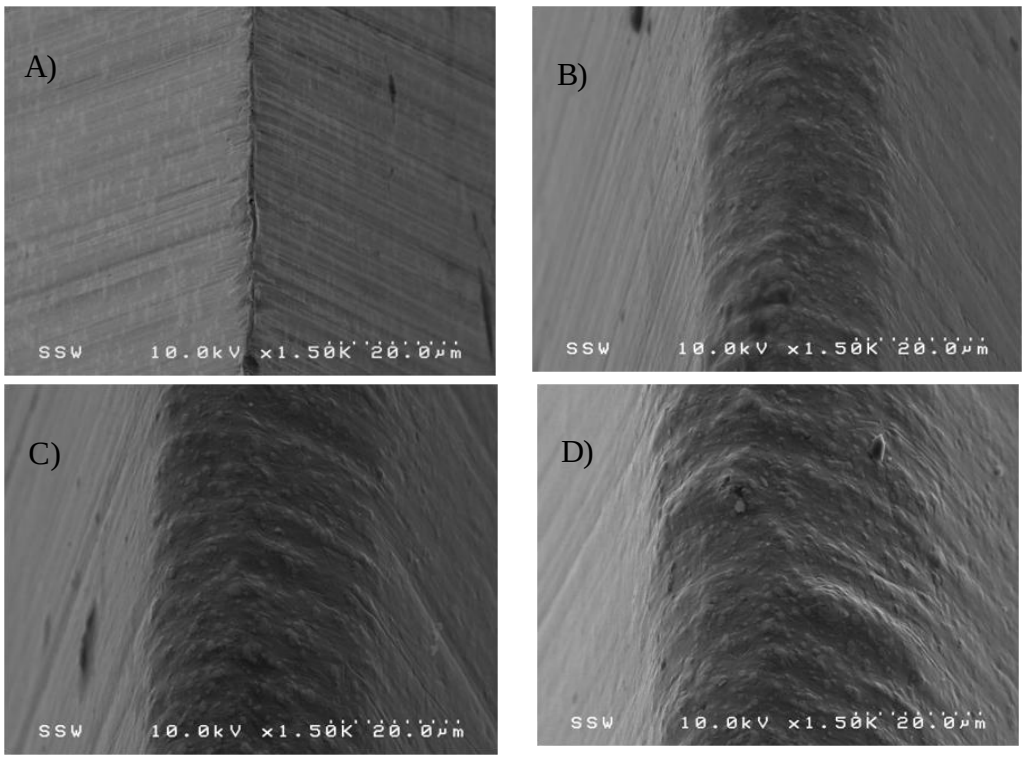


**Figure 4-10 SEM images of baseline blades through increasing stages of wear: A) Unused B) 10000 chops C) 30000 chops D) 50000 chops**

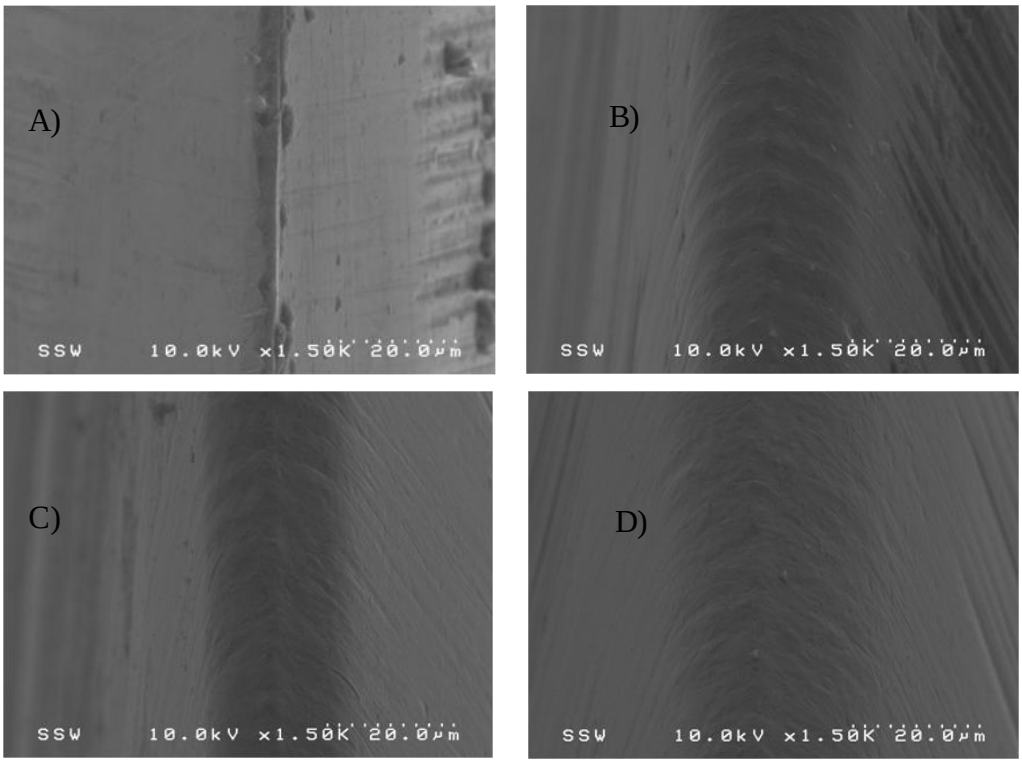


**Figure 4-11 SEM images of FPC blades through increasing stages of wear: A) Unused B) 10000 C) 30000 D) 50000**

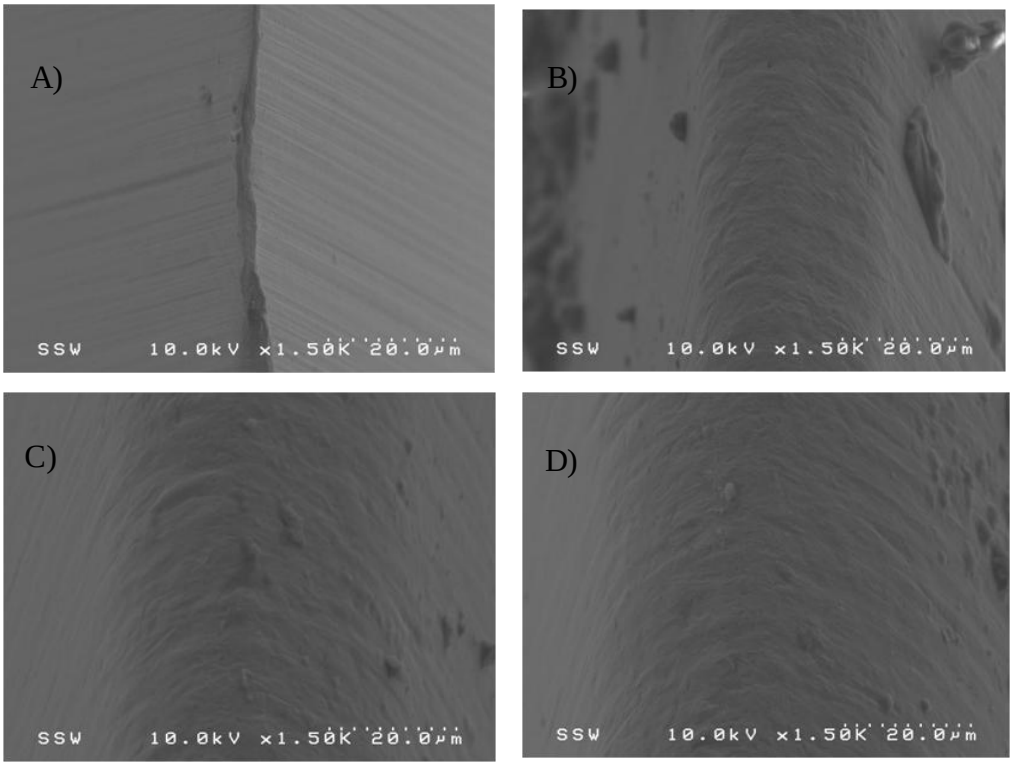


**Figure 4-12 SEM images of stainless steel thin blades through increasing stages of wear: A) Unused B) 10000 C) 30000 D) 50000**

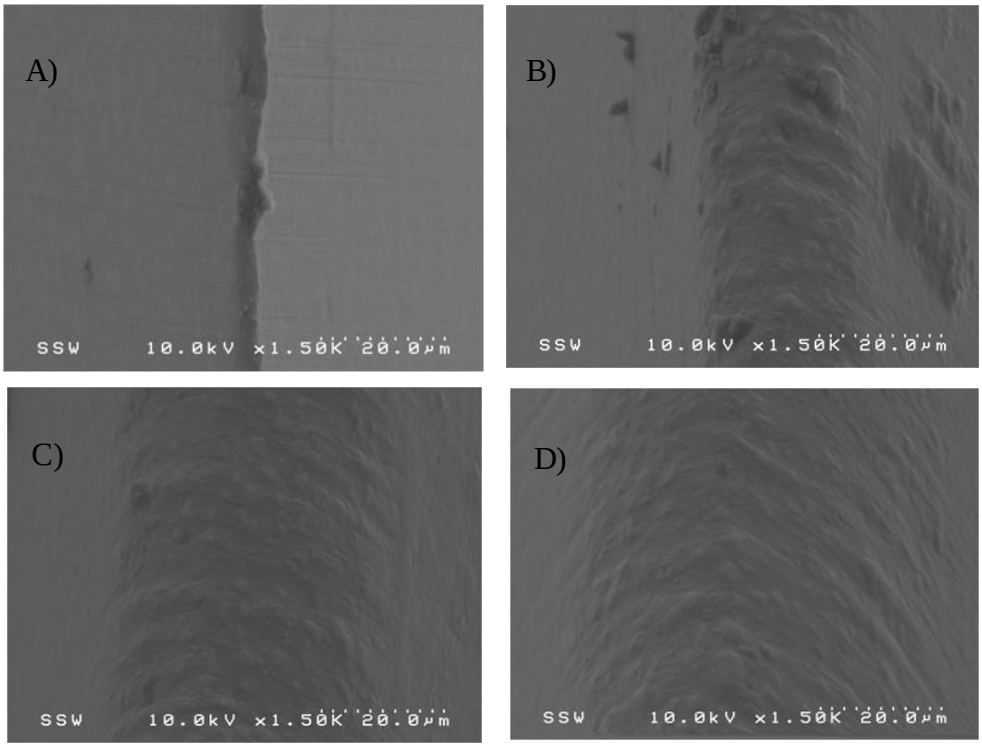


**Figure 4-13 SEM images of thick blades through increasing stages of wear: A) Unused B) 10000 C) 30000 D) 50000**

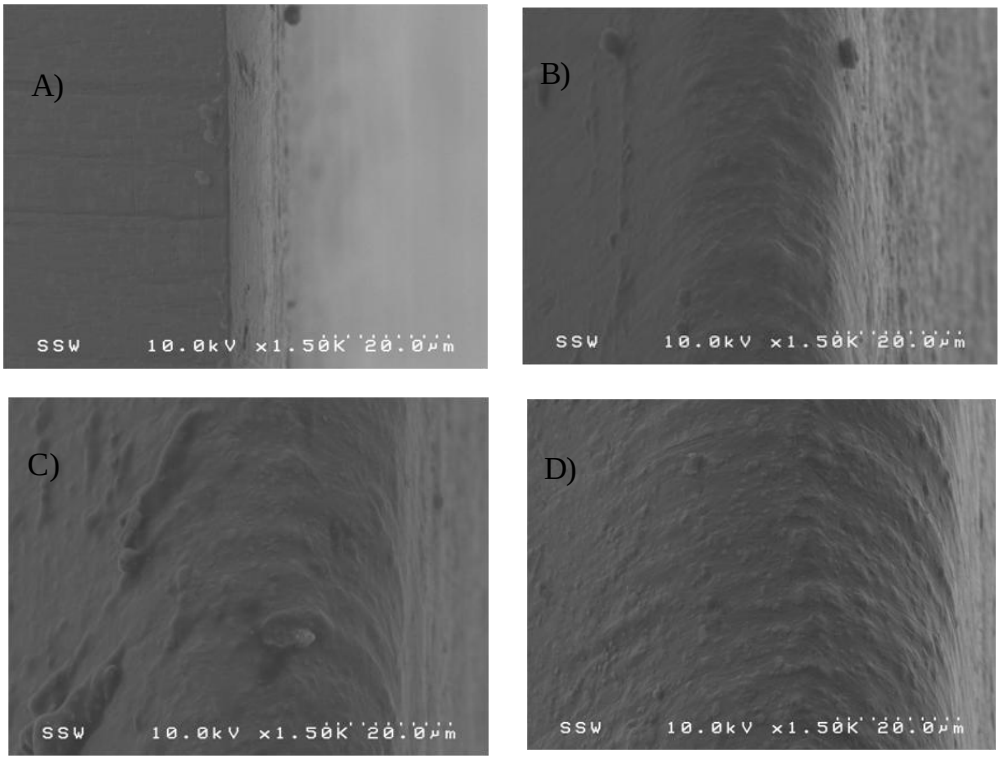


**Figure 4-14 SEM images of chisel blades through increasing stages of wear: A) Unused B) 10000 chops C) 30000 chops D) 50000 chops**

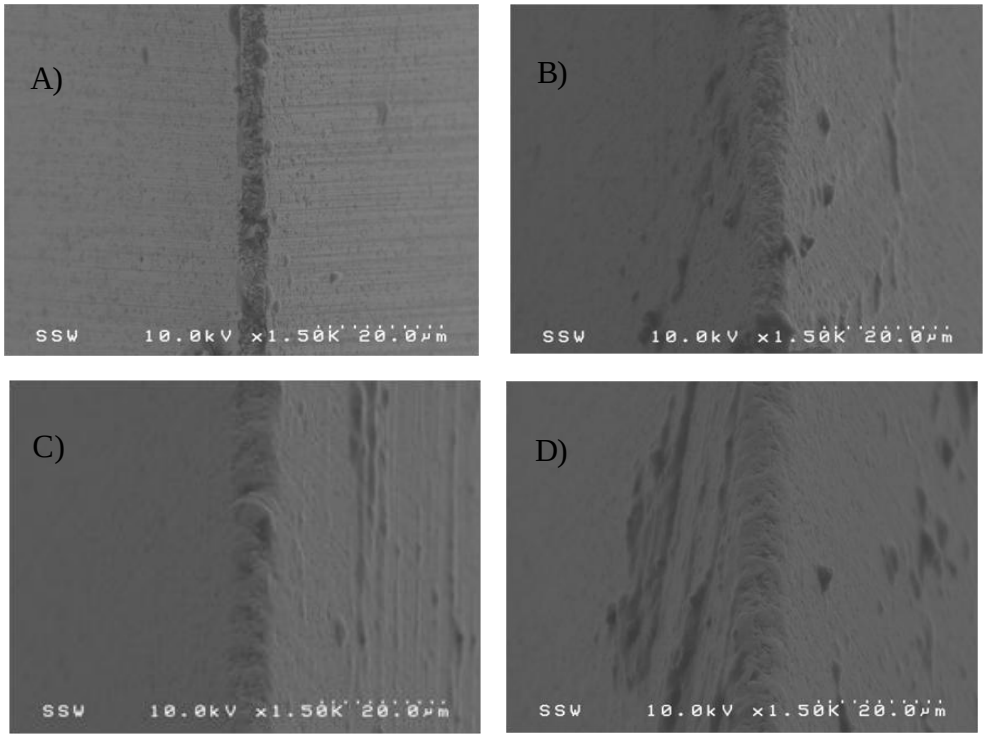


**Figure 4-15 SEM images of tungsten carbide blades through increasing stages of wear: A) Unused B) 10000 chops C) 30000 chops D) 50000 chops**

The most notable differences between the blade types and wear are that the tungsten carbide blade clearly shows less wear through 50,000 chops and that the microstructures of the blades differ. It appears that the tungsten carbide blade has worn less through 50,000 chops than the other blades have through 10,000 chops. Close inspection of the SEM images shows that different phases may be seen on the M2 steel blades, a granular structure can be observed in the tungsten carbide blades, and the microstructure of the FPC blades and the stainless steel thin blades appear homogenous and smooth. Ridges are noticed that run perpendicular to the axis of the blades in the majority of the blades with the exception of the tungsten carbide blade.

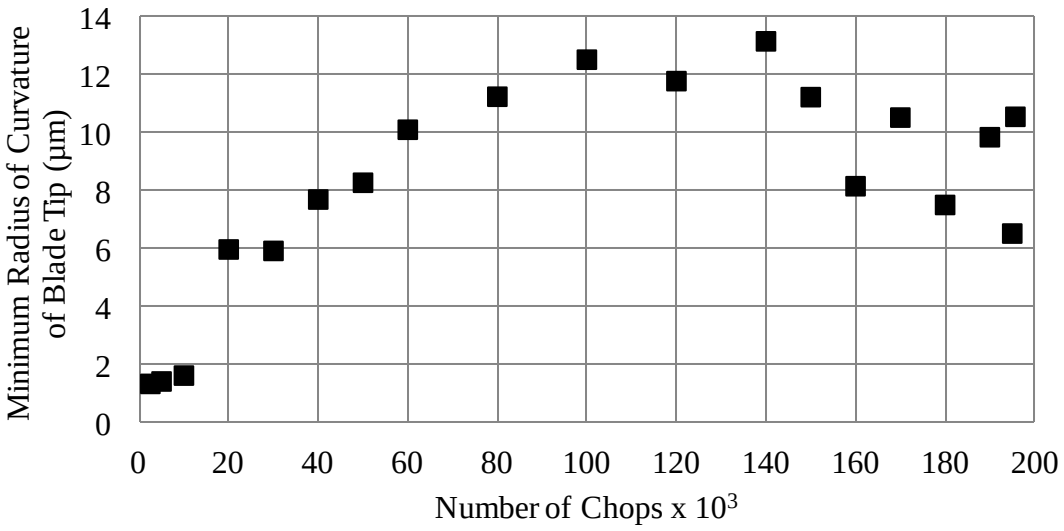


**Figure 4-16 Baseline blade tip radius of curvature measurements.**

Interestingly, the blade tip radius of curvature did not follow the same trend as depth, and width of wear. It can be observed that after 100,000 chops that the tip radius of curvature levels off and even begins to fall after 150,000 chops. This observation may be due to

the presence of the backing grooves that were significant in size and meshed with the knives after 100,000 chops.

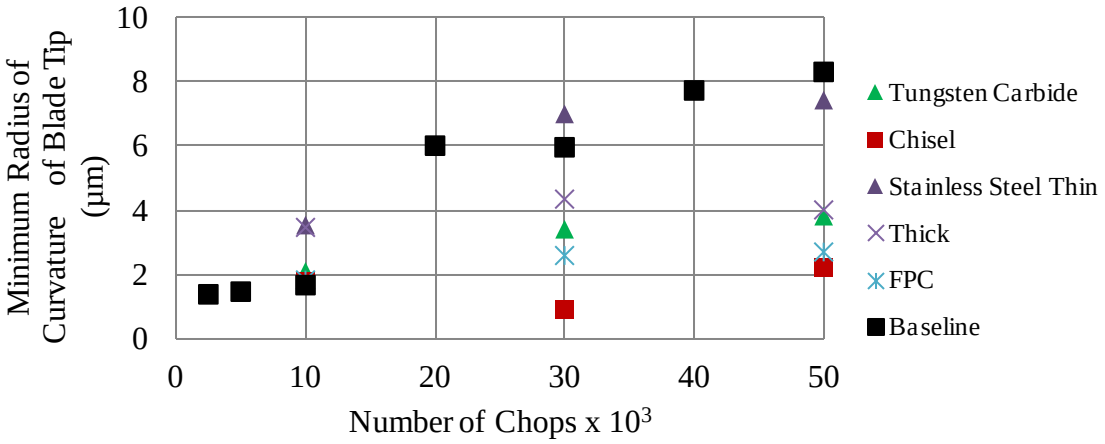


**Figure 4-17 Blade tip radius of curvature measurements.**

Figure 4-15 shows the blade tip radius of curvature measurements of the different blades. The data from this graph is somewhat scattered and consistent trends are difficult to ascertain. The stainless steel thin blades and the baseline blades appear to exhibit the largest tip radius of curvature with the other blades scattered somewhat lower than these two. The tip radius of curvature of all of the blades up to 50,000 chops and the baseline blades up to 197,500 chops do not appear to be closing in on the critical radius of the carbon fibers as observed to be roughly 60 µm.

### 4.3.2 Force vs. Position Graphs and Extracted Data

Figure 4-18 through Figure 4-28 show force vs. position graphs of different combinations of curves. Due to the large number of experiments, the data can be compared in many different ways. The presentation begins with comparing all the different blades at a given stage of wear on one graph and then transitions to comparing a particular blade at different stages of wear on one graph. This is intended to show the differences between

blades and the differences due to usage independent from one another. In the unused condition the curves are relatively close to each other as compared to the 50,000 chops condition. In the unused condition the blades with a more acute tip angle showed slightly lower force to cut the fibers, and required slightly less plunge to cut the fibers. By 50,000 chops, a significant amount of wear had been developed, enough to alter the shapes of the graphs such that the chisel blade and the baseline blade showed increased depth and force required to cut the fibers. The chisel blade surprisingly required a larger increase in force to cut the fibers than most of the other blades, which did not correspond with the measurements of wear. This could be due to the orientation of the chisel blade in the blade holder of the linear chopper as the wedge angle of the blade is asymmetric about the axis of travel as compared to the other blades in which the wedge is symmetric. From inspection of the graphs of a particular blade's curves through increasing amounts of wear, Figure 4-22 through Figure 4-27, it can be seen that there is a marked jump from the unused condition to the condition from 10,000 chops onward except for the tungsten carbide blade which remained most constant. Figure 4-28 shows sample force vs. displacement curves from the baseline blade extended wear study up to 197,500 chops. After 100,000 chops the force and displacement required to chop the fibers jumps drastically. A 10 mm wide backing was required for testing these blades as the force required to chop on a 25 mm backing for the blades beyond 100,000 chops exceeded the load cell rating. This trend is surprisingly not echoed by the radius of curvature measurements as depicted in Figure 4-16. The width of wear measurements from Figure 4-6 show a closer correlation, but do not correlate with the increased force to cut at the 197,500 chop interval.

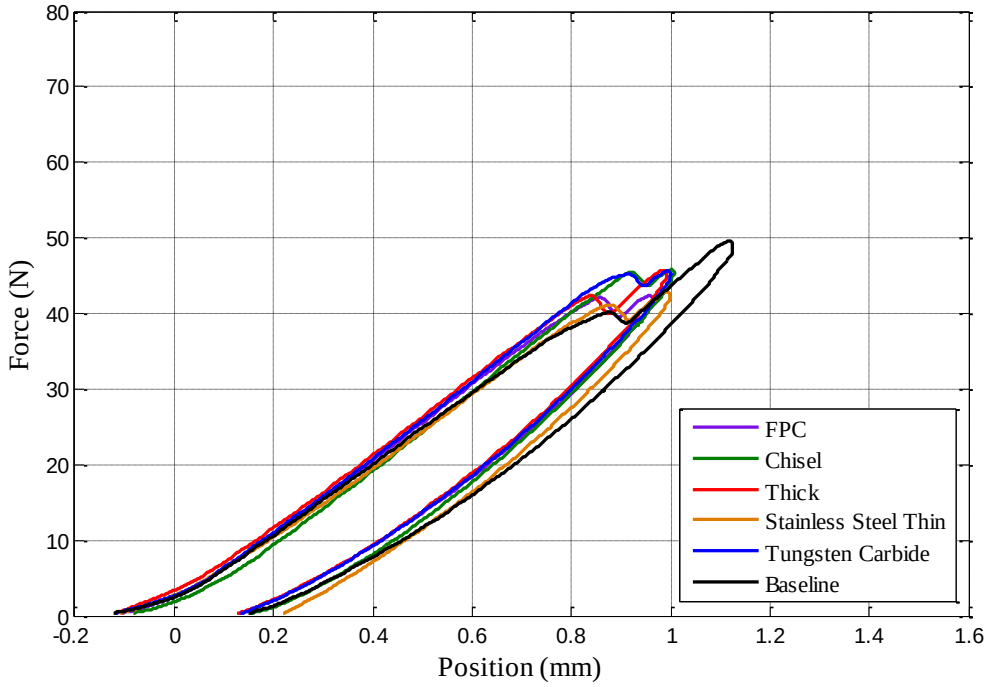


**Figure 4-18 New blades cutting on new backing.**

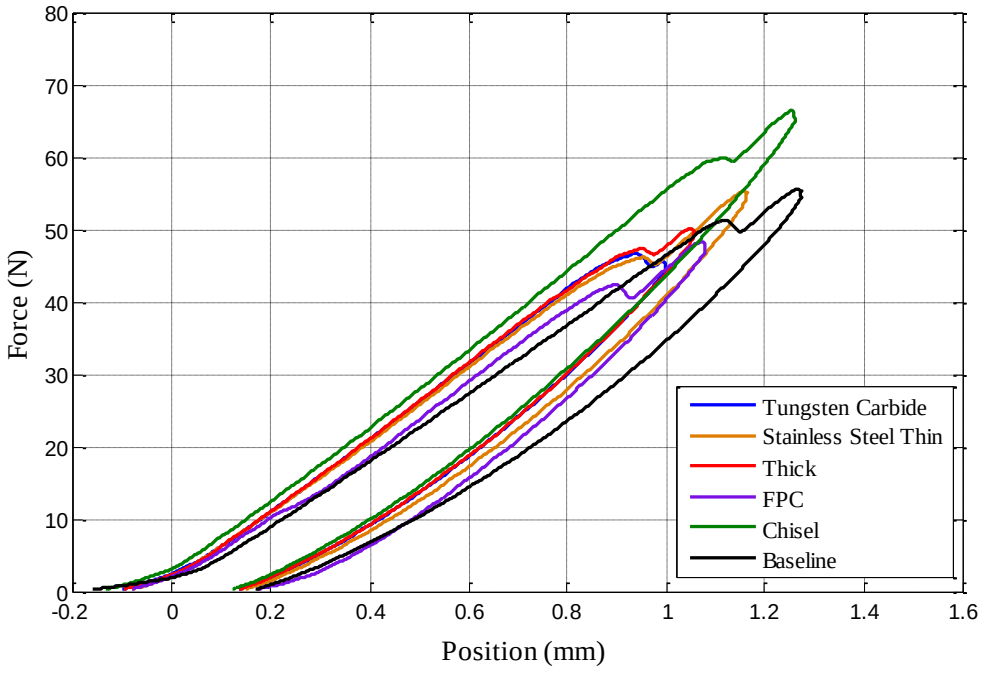


**Figure 4-19 Blades with 10,000 chops cutting on new backing.**

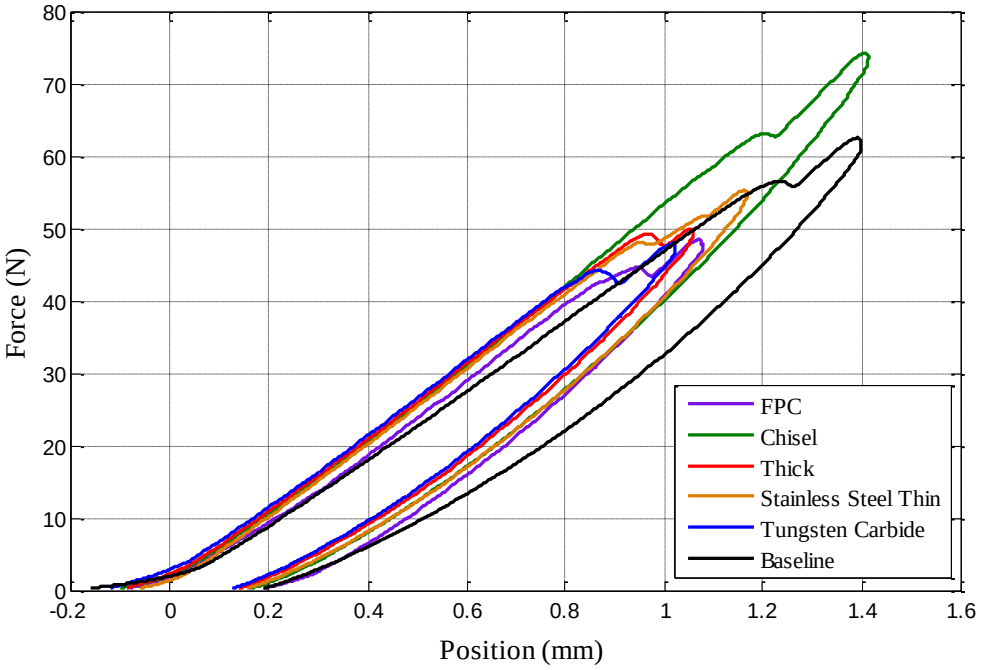


**Figure 4-20 Blades with 30,000 chops cutting on new backing.**

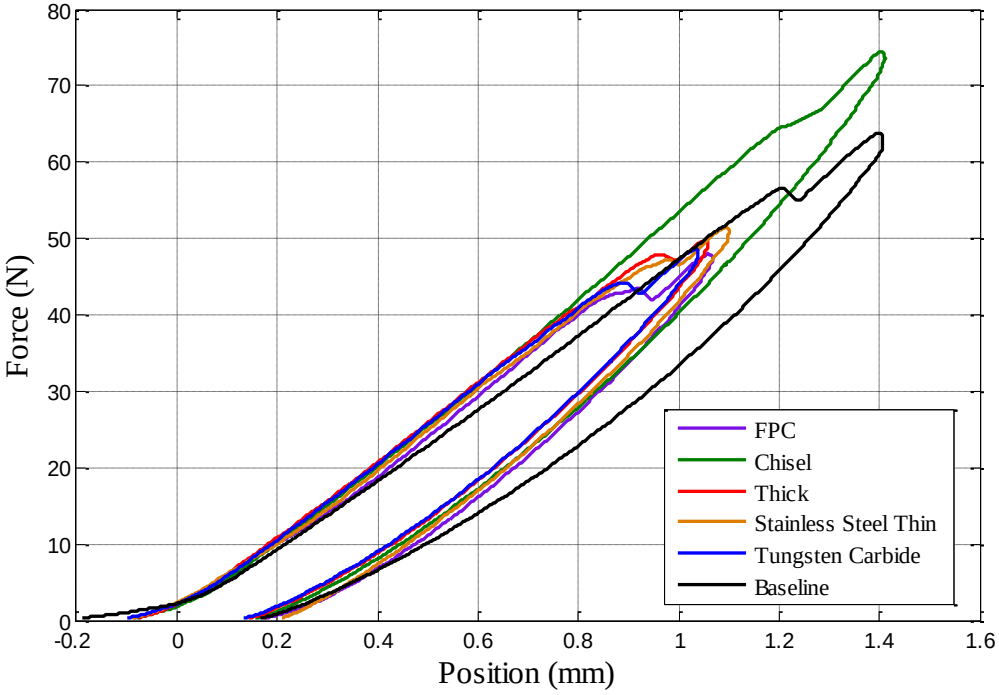


**Figure 4-21 Blades with 50,000 chops cutting on new backing.**

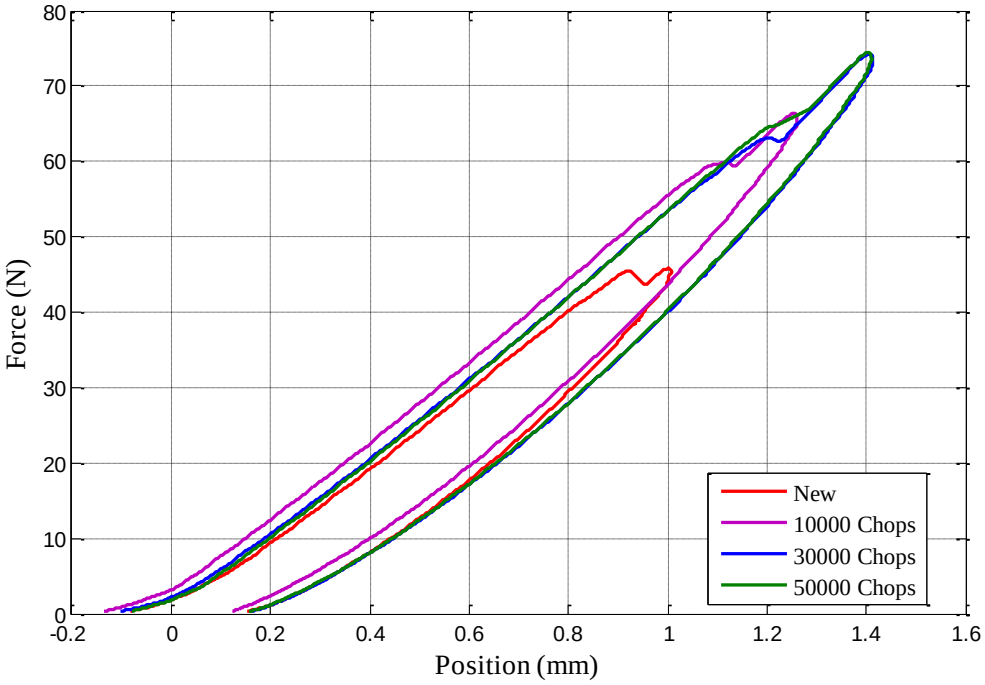


**Figure 4-22 Chisel blades with increasing usage cutting on a new backing.**

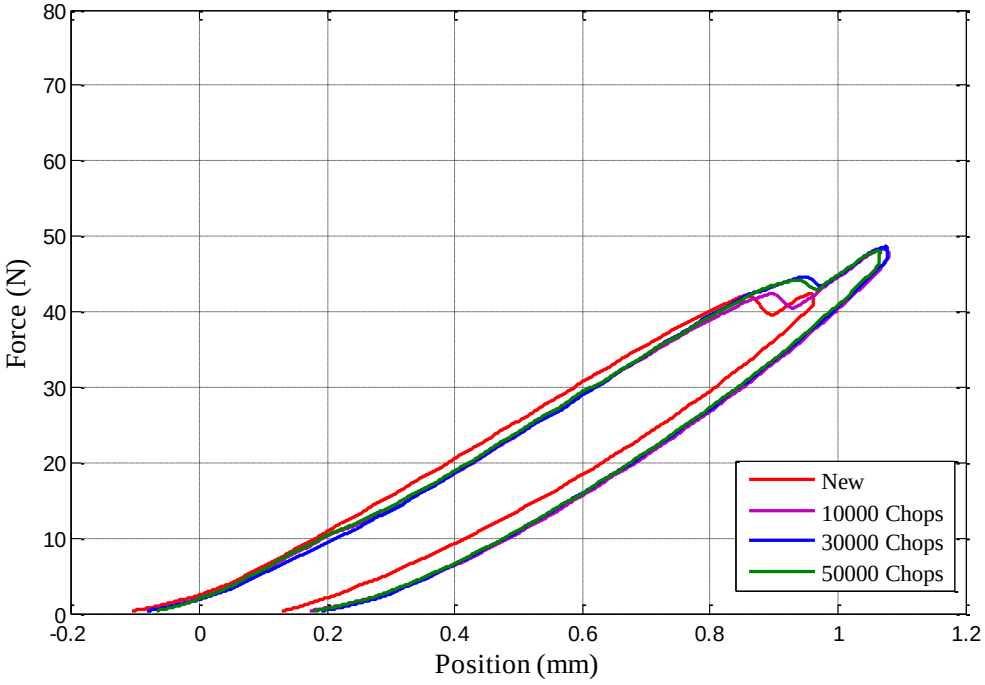


**Figure 4-23 FPC blades with increasing usage cutting on new backing.**

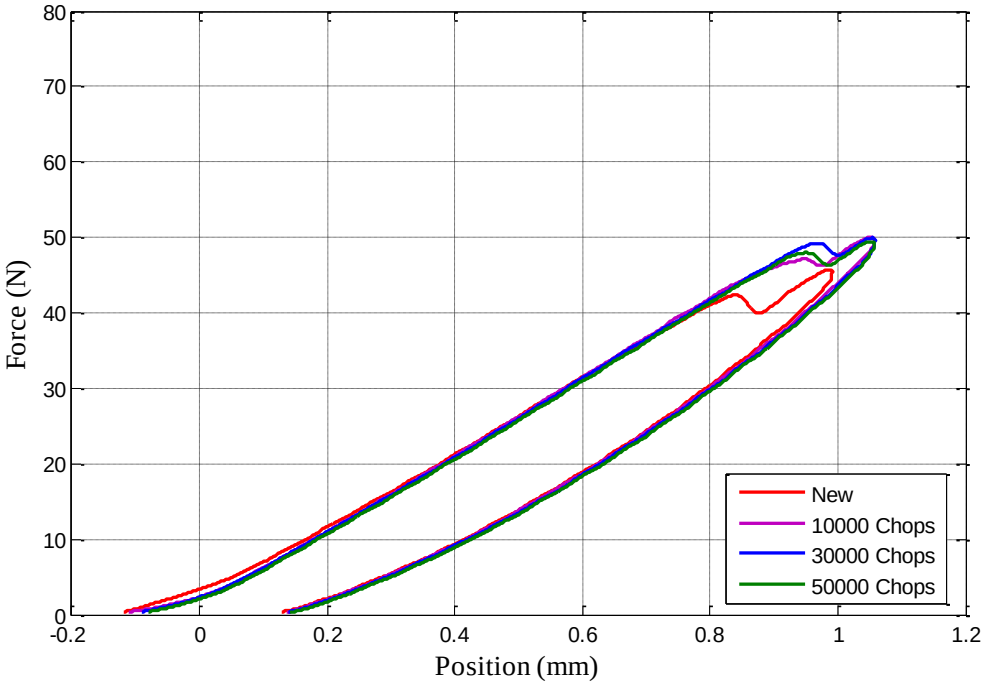


**Figure 4-24 Thick blades with increasing usage cutting on new backing.**

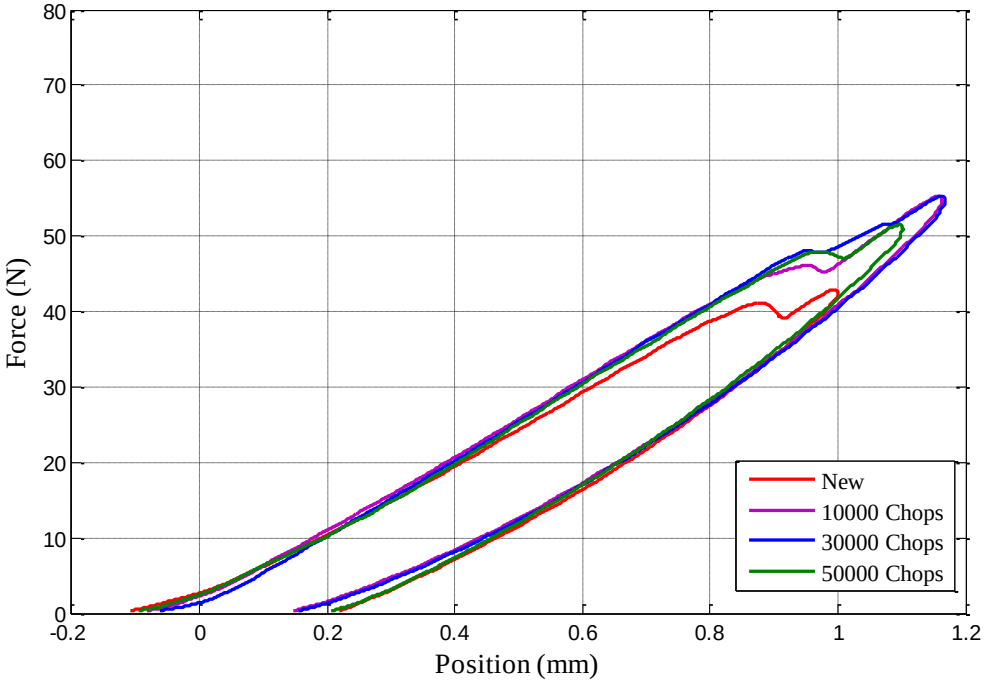


**Figure 4-25 Stainless steel thin blades with increasing usage cutting on new backing.**

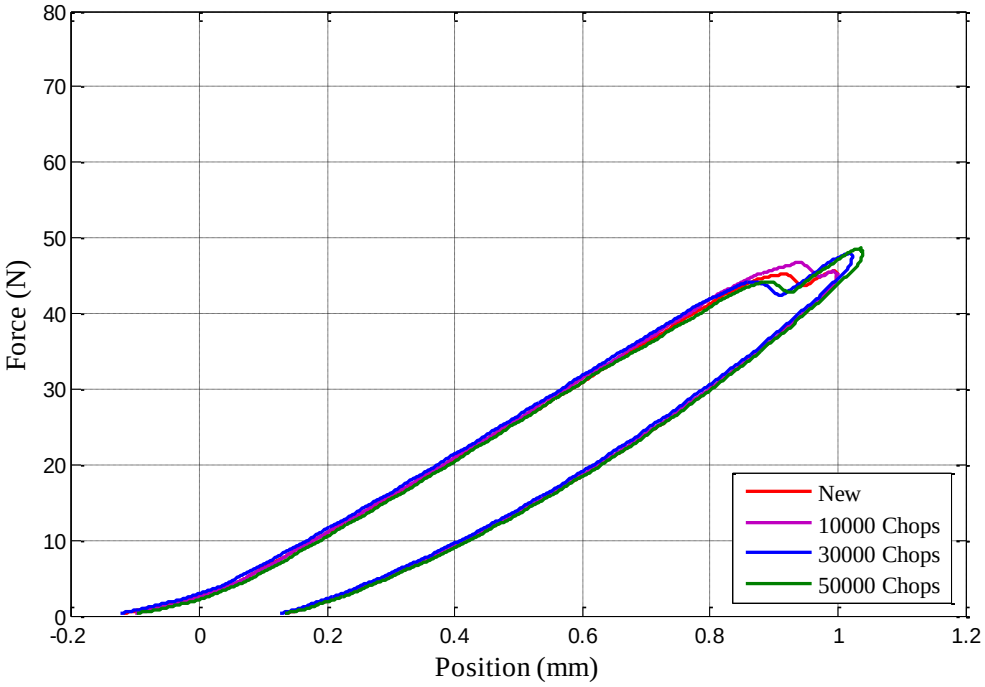


**Figure 4-26 Tungsten carbide blade with increasing usage cutting on new backing.**

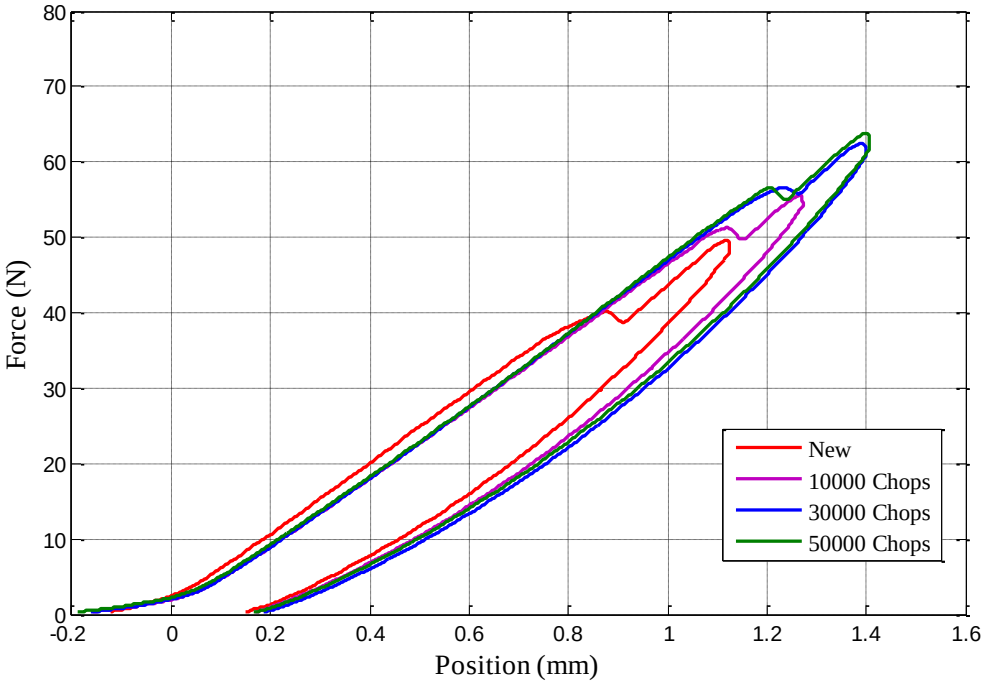


**Figure 4-27 Baseline blades with increasing usage cutting on new backing.**

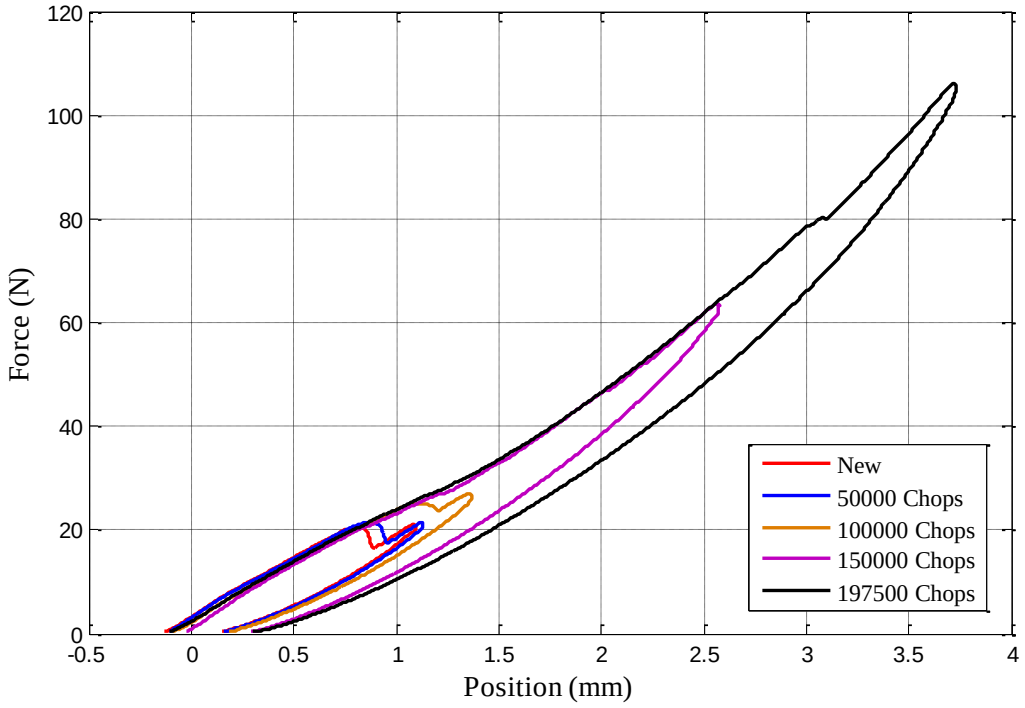


**Figure 4-28 Baseline blades from extended wear study cutting on 10 mm wide new backing.**

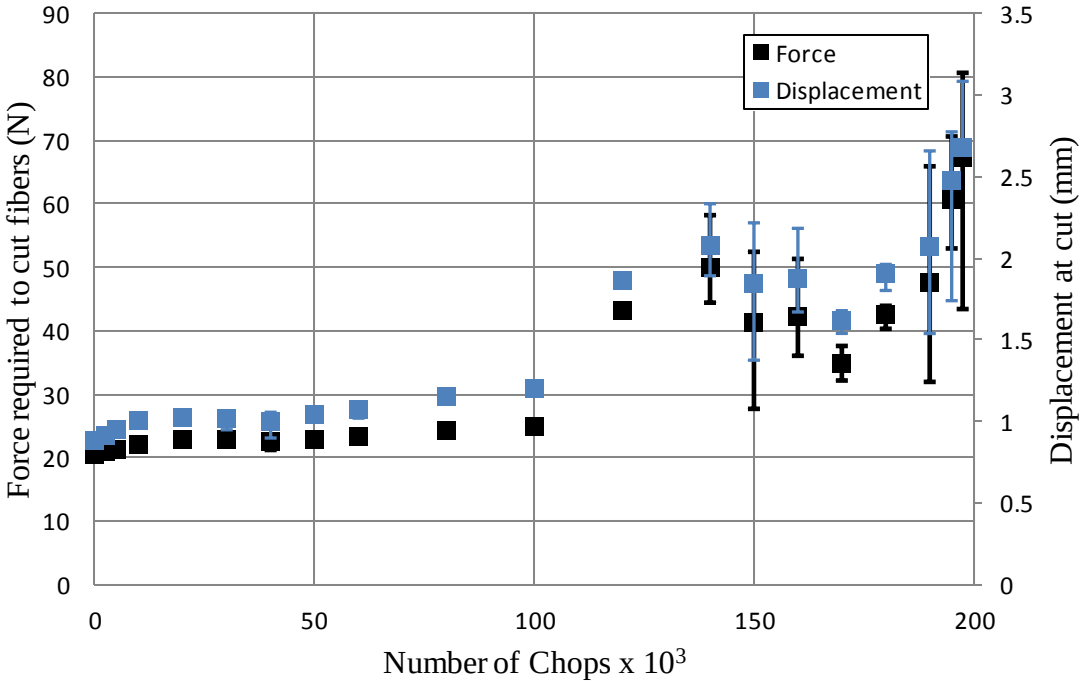


**Figure 4-29 Force and displacement required to cut roving for baseline blades with increasing usage on a new 10mm wide backing-Error bars indicate max and min values.**

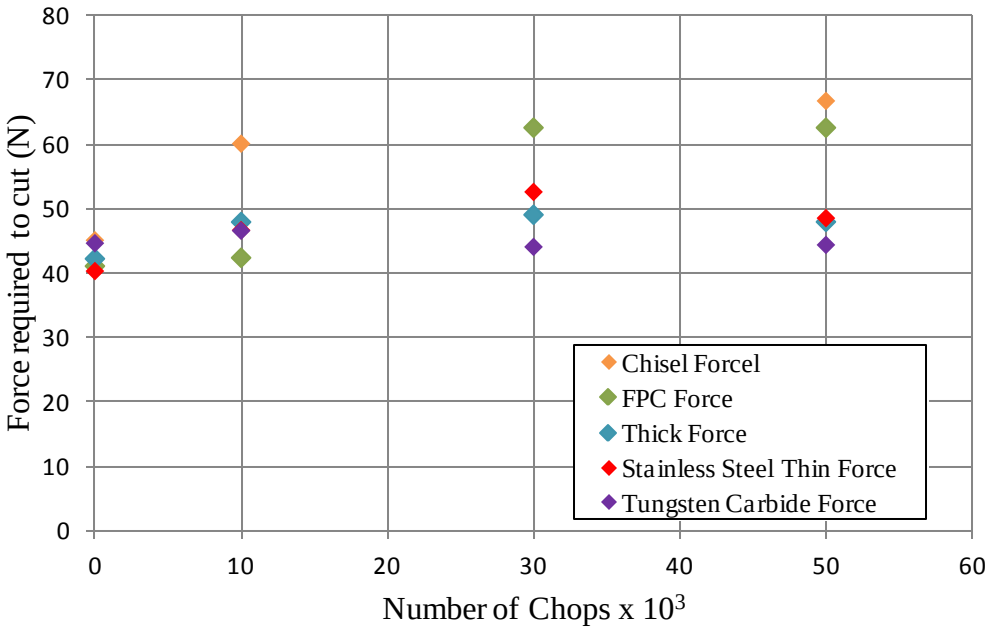


**Figure 4-30 Force required to cut roving for blades with increasing usage.**

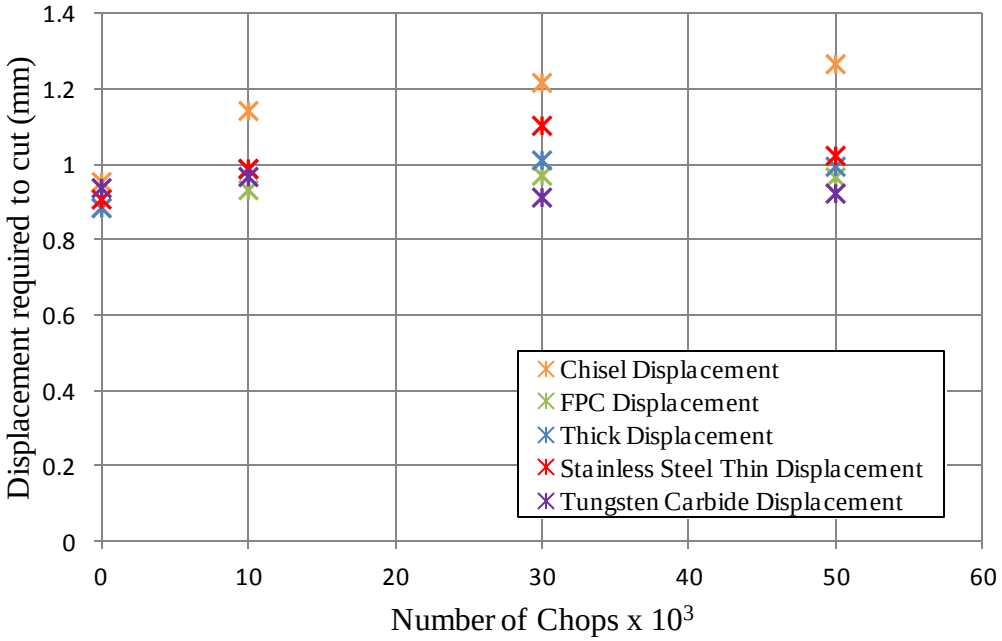


**Figure 4-31 Displacement required to cut roving for blades with increasing usage.**

The extracted data of the force required to cut the fibers and the displacement required to cut the fibers for the extended baseline wear study and the multiple blade wear study are

shown in Figure 4-29 and Figure 4-30. A strong correlation between force required to cut, and depth required to cut can be observed. This may be explained by the fairly linear increase in load vs. increase in plunge depth of the knife which is observed in the force vs. displacement curves. For the linear chop tests shown in Figure 4-28, the backing was required to be reduced to 10mm wide in order to be able to chop rovings with the higher wear blades. Figure 4-30 shows that initially the tungsten carbide blade had the highest force to cut and by 50,000 chops it required the least force and displacement to cut. It may be said that initially the blade geometry dictates the force and displacement to cut but with worn blades the amount of wear present on the blades is a more dominant factor. A factor that may be contributing to the increased amount of force required to cut at greater amounts of wear is the fact that the blades had not worn out evenly along their cutting edge. This uneven wear means that the outer edges of the blade would plunge into more backing material than they normally would have given the same amount of plunge into the backing directly underneath the roving and region of high wear of the blade. Figure 4-32 shows the distribution of wear on a highly worn baseline blade that has been run though the rotary chopper. A line is present spanning from edge to edge of the blade acting as a reference line and an estimation of the initial position of the blade cutting edge. It can be seen that the blade has worn closest to the center, and it should be noted that there was an overhang of the blade with respect to the backing at the left hand

side of the image.

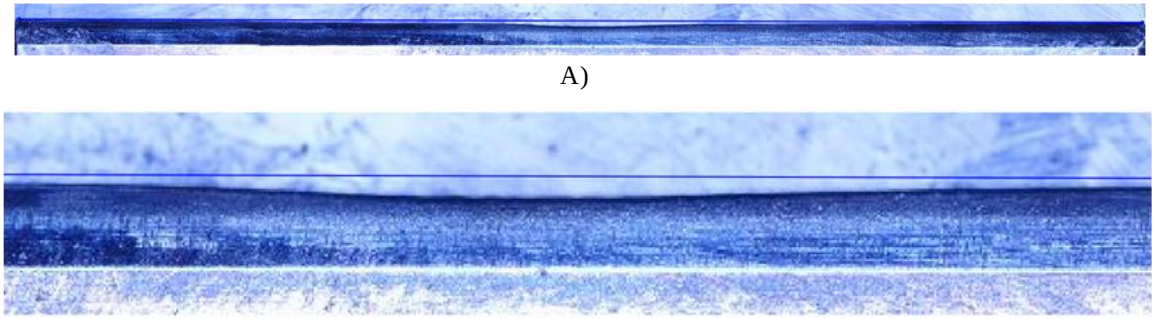

A)

B)

**Figure 4-32 Optical microscope assembled image of blade with 197,500 chops: A) Full blade B) Region of high wear**

To test with the absence of uneven wear on the effect of blade sharpness, the wire EDM formed blades were tested in the linear chopper. The wire EDM formed blades have a consistent edge, and would not have the same effect of uneven wear as described above and shown in Figure 4-32. Figure 4-33 shows that the EDM blades that had a target radius of curvature of 60 and 80 µm required greater force to cut a roving than the sharper 20 µm and 40µm target blades. One should also note that the 80 µm blade failed to cut all the filaments in the chop test. As the higher wear blades in the baseline extended wear test required a significant amount more depth to cut as compared to the blades with less wear, a reason of why the blades continued to cut in the rotary chopper was needed as the plunge depth of the blades was not set deep enough to accomplish the cut. One explanation could be that as the rotary chopper operated at a higher speed than the linear chopper, the viscoelastic properties of the backing material would effectively stiffen the backing and as a result may increase the force the backing exerts on the knife at a given depth. Another explanation could be that since the backing roll is pressed and deformed against the blade roll in the set up of the rotary chopper, an additional depth of plunge of the knife into the backing is induced. During the operation of the chopper in

the region of 100,000 chops to 197,500 chops, the knives were observed to be consistently landing in grooves worn into the backing material. A series of experiments were performed to compare force vs. displacement curves of cutting within the groove and cutting outside of the groove on the backing surface. The result was that cutting within the groove had a significant effect on the force required to cut the roving. The effect of the groove was so significant that the force required to cut the roving with the highly worn blade was less than a new blade required on a new backing. The effect on the depth to cut the fibers is also significant and may explain how the rotary chopper continued to operate with highly worn blades. Figure 4-34 displays the in groove and out of groove curves.

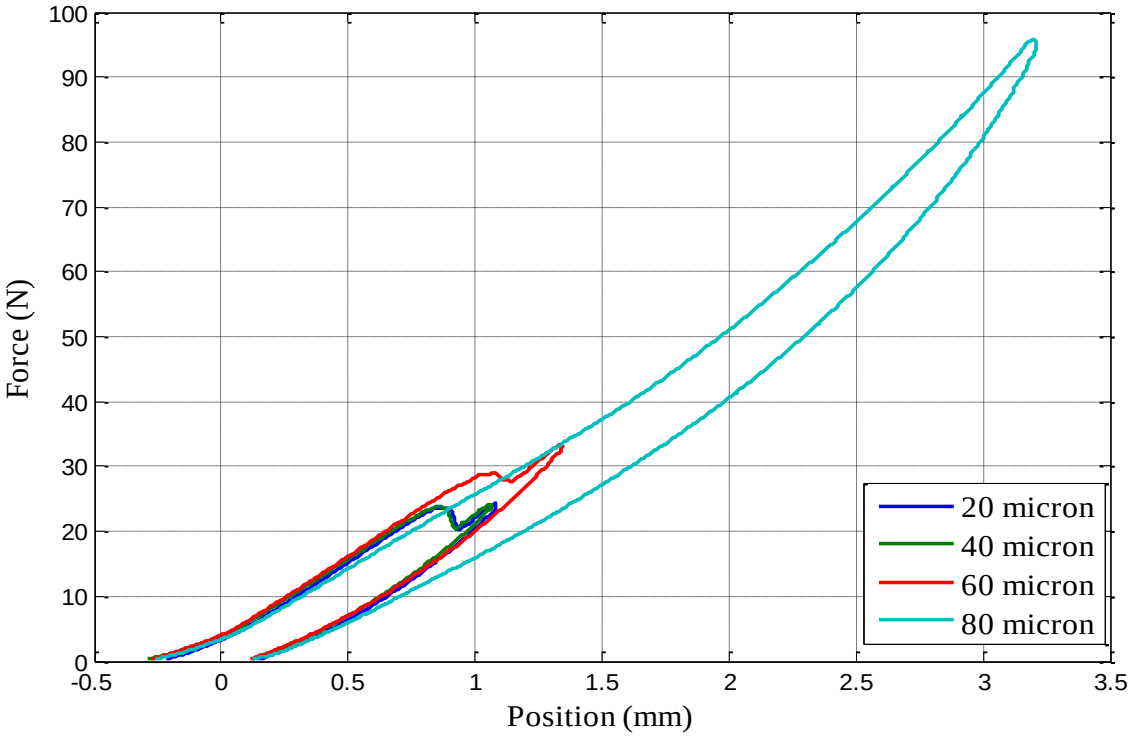


**Figure 4-33 Force vs. position curves for EDM blades of various sharpness.**

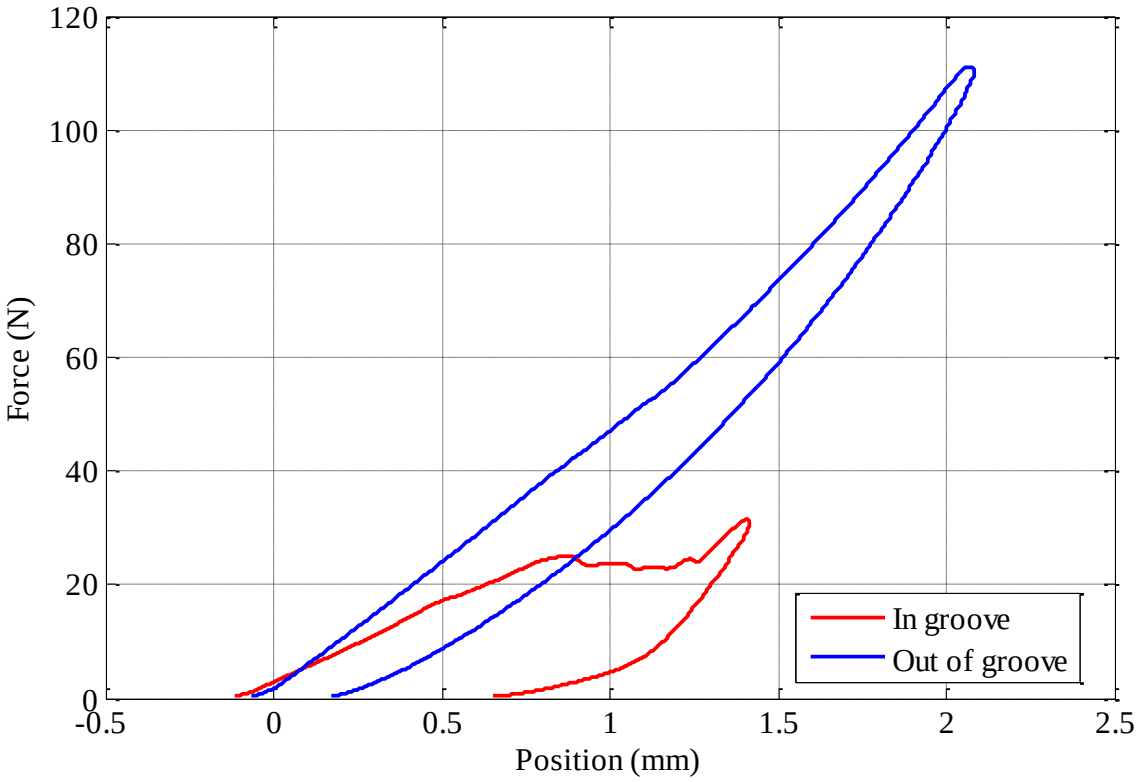


**Figure 4-34 Force vs. position curves of baseline blade with 197,500 chops in groove and out of groove.**

### 4.3.3 Blade Cross Sections

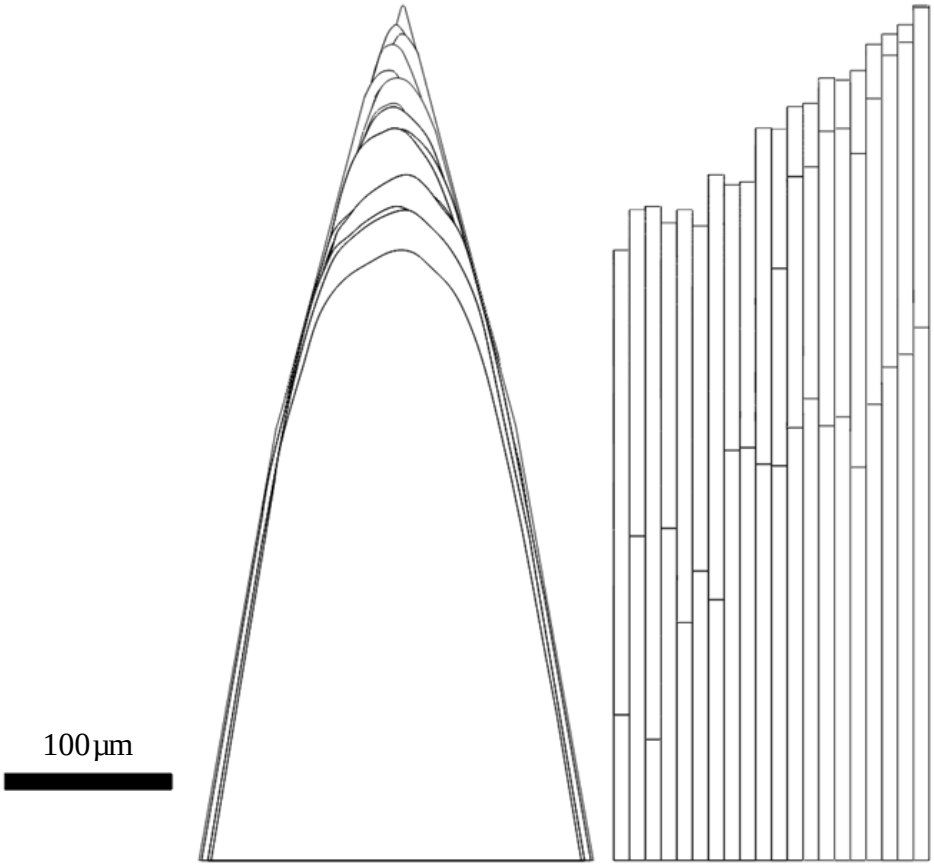


**Figure 4-35 Cross section of baseline blades from new condition to 197,500 chops.**

Figure 4-35 and Figure 4-36 are overlays of blades with increasing amounts of wear for qualitative comparison. For the baseline extended wear study blade stack up shown in Figure 4-35, a trend of increasing wear depth is not observed, although for the other blade types there exists a trend of increasing wear depth. The shape of the worn tip of the blades in all of the examples do not follow a consistent curvature, as there is a trend that there are two sides with a gentle curve that meet to a region of higher curvature.

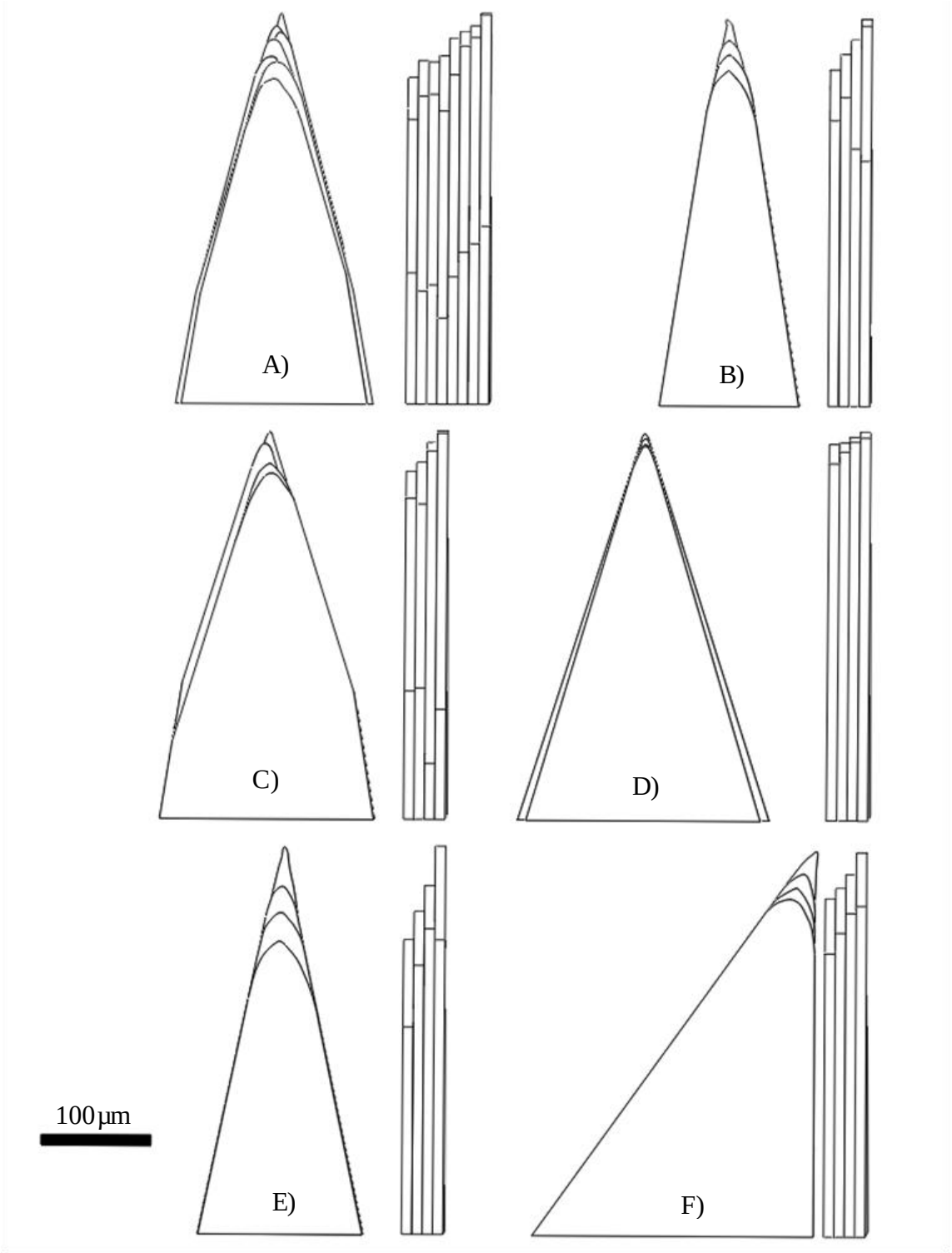


**Figure 4-36 Cross sections of blades from new condition to 50,000 chops: A) Baseline B) FPC C) Thick D) Tungsten carbide E) Stainless steel thin F) Chisel**

# Chapter 5

# 5 Conclusions and Future Work

## 5.1 Summary

Apparatus have been developed to quantify the effects of blade wear on the force and displacement requirement of a thin edge blade to cut brittle fibers against a soft backing and to simulate extended usage. Measurement techniques have been developed to quantify blade wear in terms of blade height loss and tip radius of curvature. Blades of varying hardness (material) and geometry have been compared against each other after being subjected to repeated use.

## 5.2 Conclusions

This study has shown the effects of varying the geometry and material of knife blades in the operation of chopping carbon fibers in an apparatus similar to the D-SMC fiber chopper installed at the FPC. The results may be applied to similar equipment and mechanisms that involve the cutting of carbon fiber or other brittle fibers.

Blade wear has been shown to affect the operation of cutting in two ways. The first being that the effective depth of plunge that a blade has into a backing may be significantly diminished with wear as the overall height of the blade is reduced. This effect of the wear is only significant if the knife blades are set to protrude a set distance from the knife holding roll and if the backing material bottoms out on the knife roll adjacent to the knives as they are on the chopping unit at the FPC. The amount of depth change may be easily tracked on an industrial chopping machine my measuring the protrusion height of the knife edges from the blade roll surface. If problems in chopping arise, the height that

the blades protrude from the surface of the roll may need to be increased or the knives replaced. The second being that as blades are used and worn, the tip geometry changes such that a greater application force and plunge into the backing is required to be able to chop the fibers. The tip geometry of the blades in a significantly dulled condition, in that the force required to cut fibers has doubled, has been shown to still maintain a minimum radius of curvature well below the critical radius of the fiber. The effect of increased required force and plunge depth is accompanied with the loss in plunge depth due to the decreasing protrusion height generated from the blade wear as described above. Blades in a dulled condition may still be able to cut fibers if grooves are present in the backing roll as the grooves have been shown to decrease the force and plunge depth required to cut fibers with worn blades. It is therefore recommended to change the cutting blades if a backing roll that has grooves in it is being replaced.

Blade hardness has been shown to have an effect on blade wear, and therefore the lifecycle of the blades. The hardest blade tested in this study, manufactured from tungsten carbide-cobalt cemented carbide, showed significantly less wear than all the other blades being tested. The tungsten carbide blade showed a wear rate roughly 1/5 to 1/3 of the current industrially implemented blade, depending on the wear measurement. The challenge with using such a material in an industrial unit is that blades of this material are currently unavailable in the length required. Multiple blades may need to be fixtured side by side in the chopping unit to be able to span the required width. If the blades were to be fixture as such, problems may arise in chopping due to small gaps between the blades. The cost of the tungsten carbide blades is greater than that of the steel blades, and transferring over to tungsten carbide blades may not reduce overall cost

of operation unless the life cycle increase compensates for the higher initial cost. The tungsten carbide blade may be of interest if the preventative maintenance interval of the steel blades interferes with operations to the point where it does not allow for an uninterrupted shift, or becomes cumbersome. Softer blades than the currently used FPC blade, such as the stainless steel thin blade, have shown to have slightly more wear under similar testing conditions than the other blades studied, but the difference in wear was not as drastic as the difference between the tungsten carbide blade and any of the steel blades.

The effect of blade geometry was difficult to make hard conclusions on based on the data presented. The initial effect (blades in new condition) was shown to be a slight increase in force required to cut fibers. In the worn condition, the effect of geometry was not consistent and depended on the method of wear measurement.

The overall significance of the study is that the blade material has the largest impact on wear rates and that a change to a harder material such as tungsten carbide-cobalt may be required to satisfy the demands of mass production. The study also found that the effect of grooves in the backing is beneficial in that it reduces the force and plunge depth required to cut fibers.

## 5.3 Future Work

Proposed future work would be to run experiments with glass fibers to compare the amount of wear with carbon fibers. As grooves in the backing developed and there is evidence that the blade wear characteristics were altered as a result, more testing should be done with an intentionally grooved backing to assess blade wear progression as compared to a backing without a groove. The phenomenon of the reduction in cutting

force and depth of plunge while cutting against a grooved backing is poorly understood and merits further research. Testing with blades that are installed side by side in the knife roll to observe the effects on chopping may provide insightful if the use of tungsten carbide blades is of interest in the industrial chopping machine. The effect that laser cutting has on carbon fibers is not well documented and the material that is formed on the surface of the laser cut carbon fibers such as in Figure 4-1 is unknown. The material may have interesting properties that may be useful in other applications or the process may act to enhance interfacial bond strength in a composite. As blades with hard surface coatings were not included in the scope of this project, but have been shown to increase the life of other cutting tools, studying the effect of hard coatings may show positive results.

# References


1. Stewart, R., *Lightweighting the automotive market*. Reinforced Plastics, 2009. **53**(2): p. 14-21.

2. Cheah, L.W., *Cars on a diet: the material and energy impacts of passenger vehicle weight reduction in the US*. 2010, Massachusetts Institute of Technology.

3. Swentek, I., *On the Interfacial Fracture Mechanics of Long-Fibre Reinforced Polymer Composites*. 2014, Universtiy of Western Ontario.

4. Schmidt, W., W. Puri, and H. Meerkamm, *Strategies and rules for lightweight design*. Design methods for performance and sustainability. Professional Engineering Publishing, London, 2001: p. 27-34.

5. Stewart, R., *Automotive composites offer lighter solutions.* Reinforced Plastics, 2010. **54**(2): p. 22-28.

6. Whelan, T. and J. Goff, *Sheet Molding Compound,* in *Molding of Thermosetting Plastics*. 1990, Springer. p. 75-85.

7. Bruderick, M., et al. *Applications of carbon/fiber SMC for the 2003 Dodge Viper*. in *Second SPE Automotive Composites Conference*. 2002.

8. Siwajek, M. *Light Weight Class 'A' SMC Body Panels-TCA Lite*. in *Society of Plastics Engineers Automotive Conference*. 2010.

9. Hull, D. and T. Clyne, *An introduction to composite materials*. 1996: Cambridge university press.

10. Chung, D., *Carbon fiber composites*. 2012: Butterworth-Heinemann.

11. Reynolds, W. and J. Sharp, *Crystal shear limit to carbon fibre strength.* Carbon, 1974. **12**(2): p. 103-110.

12. Kozey, V., et al., *Compressive behavior of materials: Part II. High performance fibers.* Journal of Materials Research, 1994. **10**(4): p. 1044-1061.

13. Kumar, S., D.P. Anderson, and A.S. Crasto, *Carbon fibre compressive strength and its dependence on structure and morphology.* Journal of Materials Science, 1993. **28**: p. 423-439.

14. Mallick, P.K., *Composites engineering handbook*. 1997: CRC Press.

15. Wallenberger, F.T., J.C. Watson, and H. Li, *Glass fibers.* Materials Park, OH: ASM International, 2001., 2001: p. 27-34.

16. Van Der Mast, W.F., *Method and device for cutting fibres*. 2002, WIPO 2002055770A1.

17. Van Der Mast, W.F., *Method and device for cutting fibres into pieces of a short length*. 2005, WIPO 2005087993A1.

18. John, M., *Stable fiber cutter*. 1967, US Patent 3353431.

19. Brussel, R., *Cutting device for shear-cutting of fibre strands*. 2013, US Patent 8438959.

20. Minifibers, I., *Method and apparatus for cutting continuous fibrous material*. 1986, European Patent Number 0026107B1.

21. Farmer, E. and G. Keith, *Apparatus for cutting tow into staple fiber*. 1973, US Patent Number 3768355.

22. Harris, L.D., *Method and apparatus for cutting fiber tow inside-out*. 2000, US Patent Number 6029552.

23. Keith, G.B., *Method and apparatus for cutting continuous fibrous material*. 1984, US Patent Number 4445408.

24. Farmer, T., C.R. Keith, and G.B. Keith, *Apparatus for cutting fibrous tow into staple*. 1976, US Patent Number 3978751.

25. Laird, W.F., D.I. Walsh, and G.E. Corneau, *Precision cutter*. 1975, US Patent Number 3861257.

26. Gay, B.A., *Continuous cutter for a glass fiber chopper*. 1983, US Patent Number 4373650.

27. Sinclair, D., *A bending method for measurement of the tensile strength and Young's modulus of glass fibers.* Journal of Applied Physics, 1950. **21**(5): p. 380-386.

28. Williams, W.S., D. Steffens, and R. Bacon, *Bending behavior and tensile strength of carbon fibers.* Journal of Applied Physics, 1970. **41**(12): p. 4893-4901.

29. Krucinska, I., *Evaluation of the intrinsic mechanical properties of carbon fibres.* Composites Science and Technology, 1991. **41**(3): p. 287-301.

30. Dobb, M., D. Johnson, and B. Saville, *Compressional behaviour of Kevlar fibres.* Polymer, 1981. **22**(7): p. 960-965.

31. Greenwood, J. and P. Rose, *Compressive behaviour of Kevlar 49 fibres and composites.* Journal of materials science, 1974. **9**(11): p. 1809-1814.

32. Hawthorne, H., *On non-Hookean behaviour of carbon fibres in bending.* Journal of materials science, 1993. **28**(9): p. 2531-2535.

33. Levien, R., *The elastica: a mathematical history.* Electrical Engineering and Computer Sciences University of California at Berkeley, 2008.

34. McCarthy, C.T., A.N. Annaidh, and M. Gilchrist, *On the sharpness of straight edge blades in cutting soft solids: Part II–Analysis of blade geometry.* Engineering Fracture Mechanics, 2010. **77**(3): p. 437-451.

35. Lau, K.H., et al., *Wear Characteristics and mechanisms of a thin edge cutting blade.* Journal of Materials Processing Technology, 2000. **102**: p. 203-207.

36. Le, D.H., *Wheatstone bridge-type transducers with reduced thermal shift*. 1987, US Patent Number 4658651.

37. Smith, S.W., *The scientist and engineer's guide to digital signal processing.* 1997.

38. *Vol. 9.* Metallography and Microstructures, ASM Handbook, 1985.

39. Naito, K., et al., *Flexural Properties of PAN-and Pitch-Based Carbon Fibers.* Journal of the American Ceramic Society, 2009. **92**(1): p. 186-192.

40. Da Silva, J. and D. Johnson, *Flexural studies of carbon fibres.* Journal of materials science, 1984. **19**(10): p. 3201-3210.

41. Naito, K., et al., *Tensile and Flexural Properties of Single Carbon Fibres*, in *International Committee on Composite Materials-17*. 2009.

# Appendix A: Component Drawings

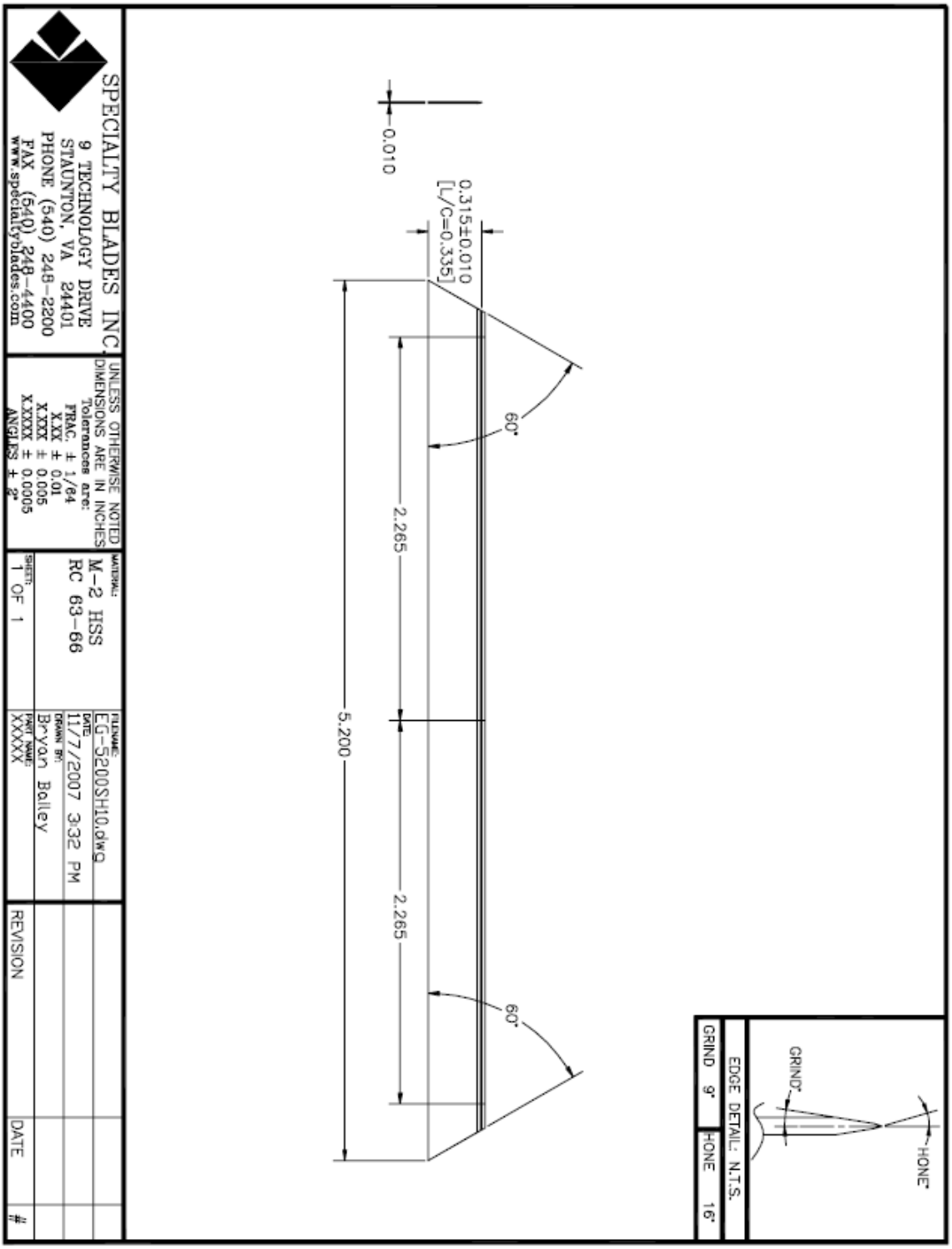


**Figure A. 1 Baseline blade drawing.**

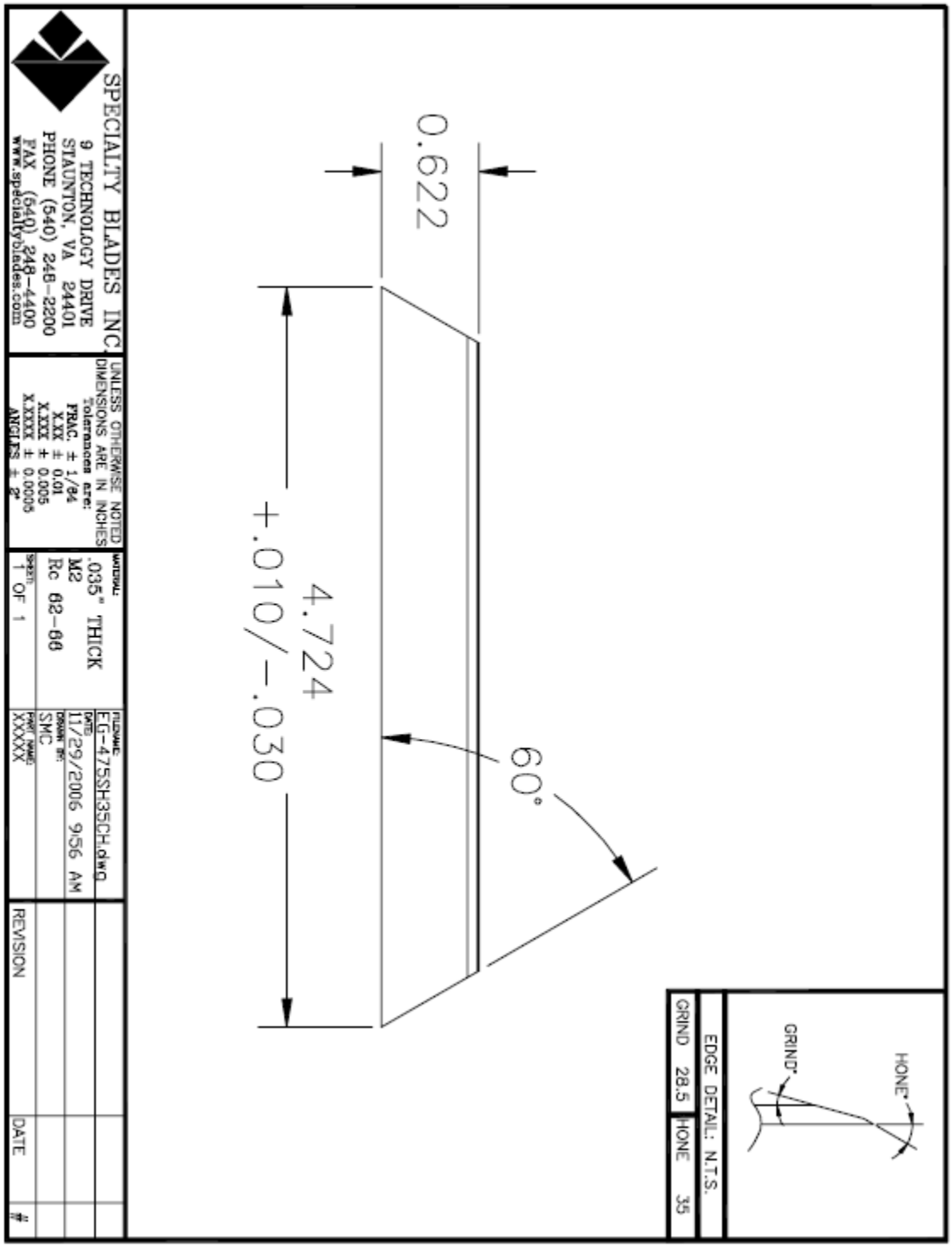


**Figure A. 2 Chisel blade drawing.**

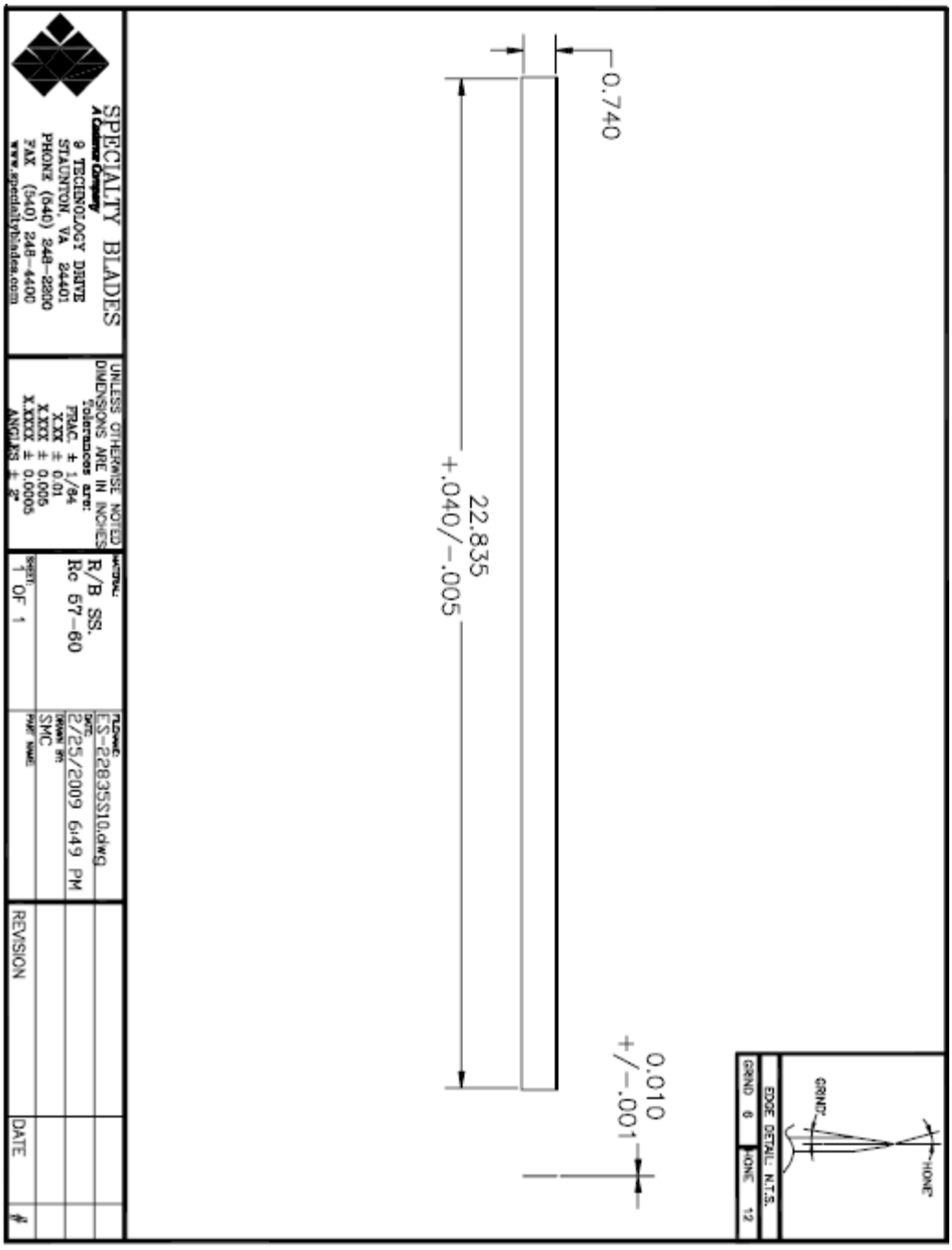


**Figure A. 3 Stainless steel thin drawing.**

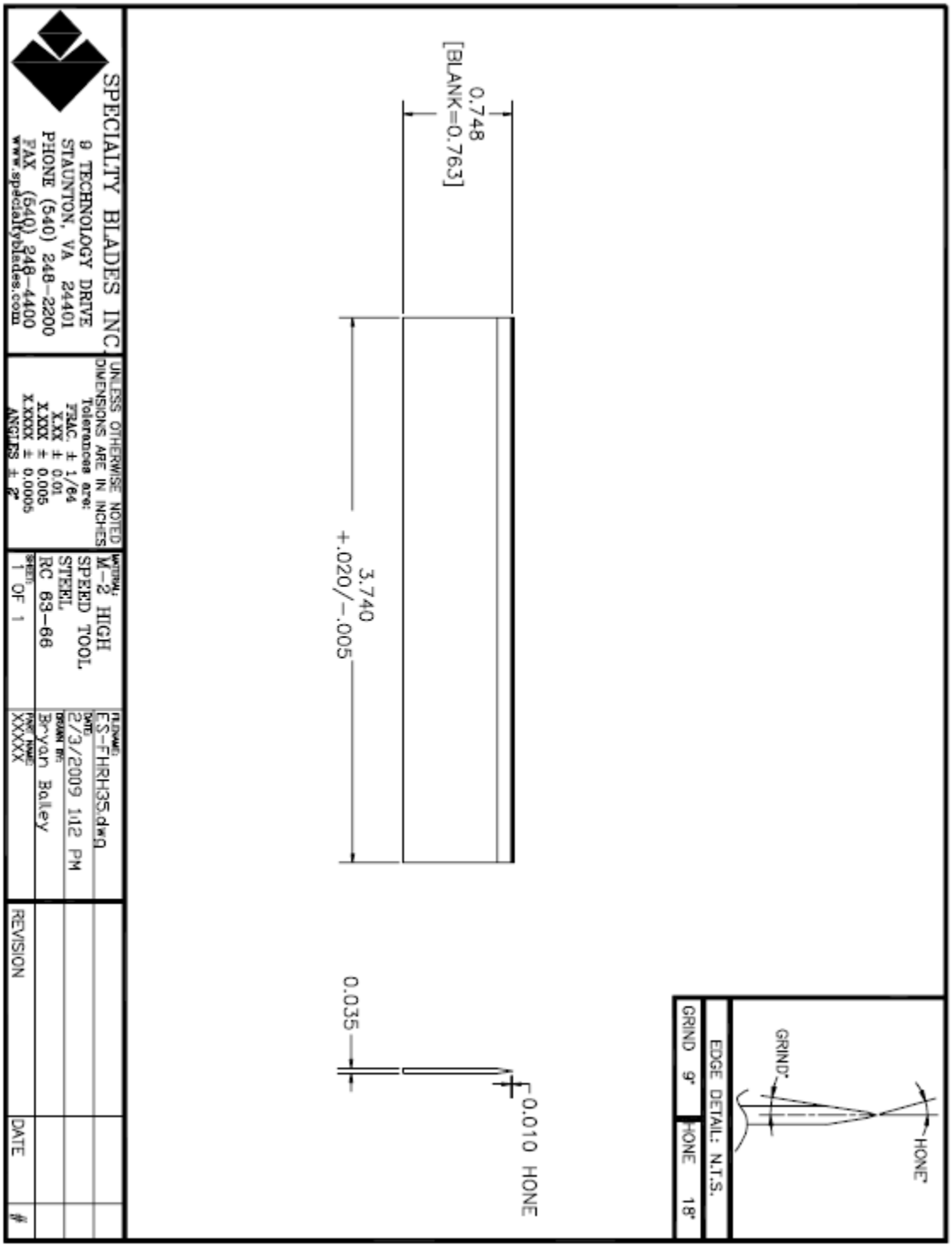


**Figure A. 4 Thick blade drawing.**

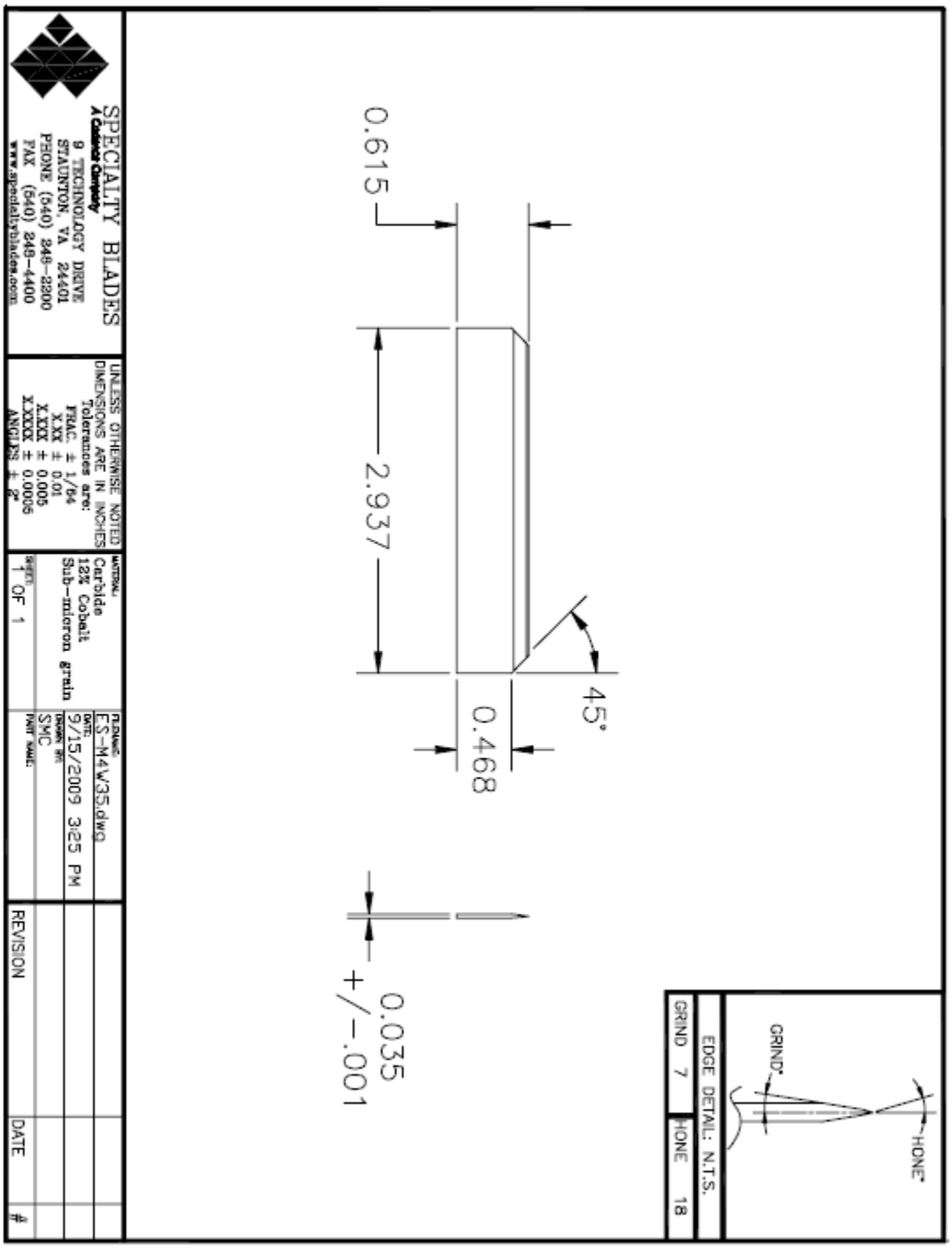


**Figure A. 5 Tungsten carbide blade drawing.**

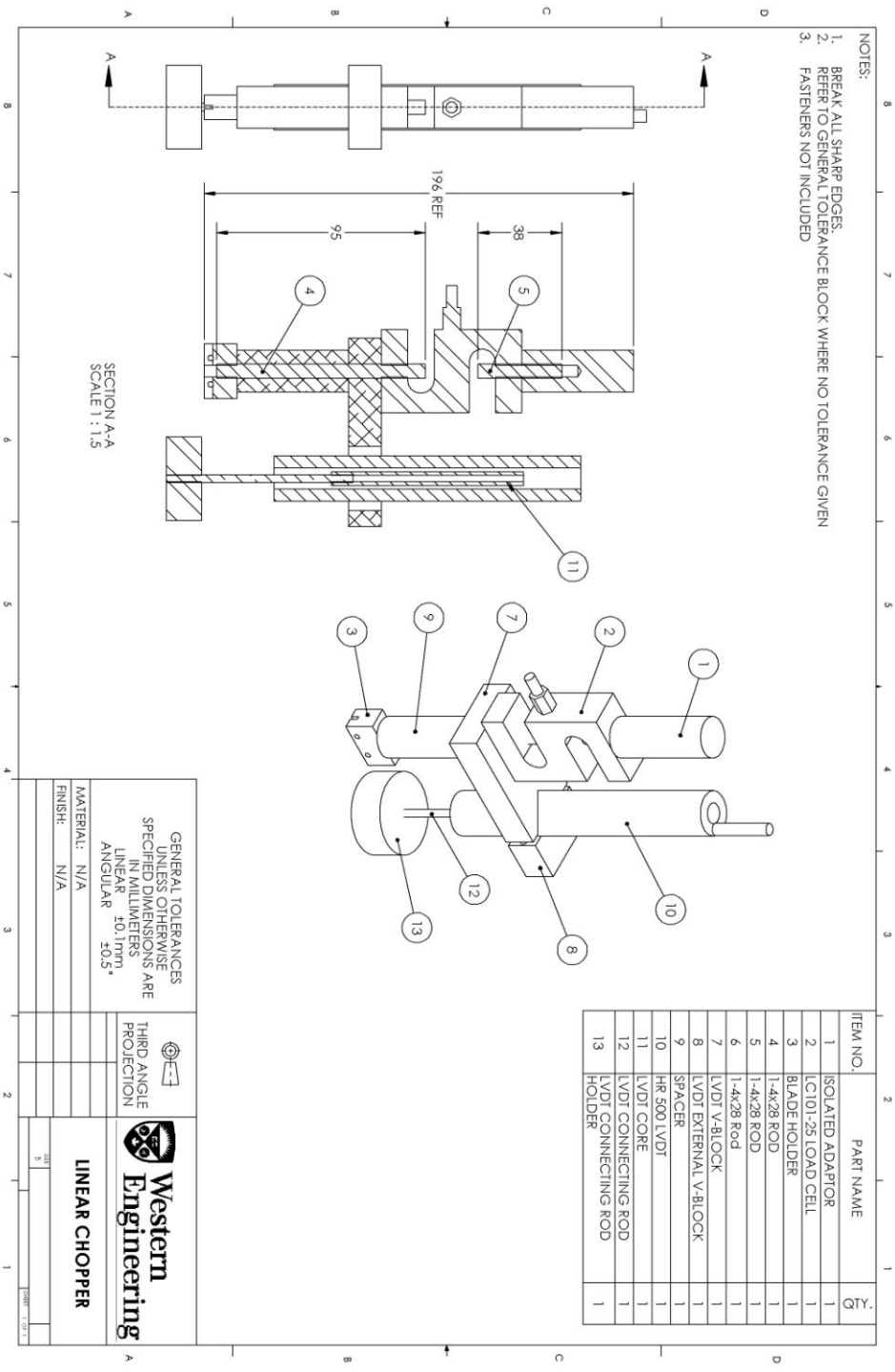


**Figure A. 6 Linear chopper drawing.**

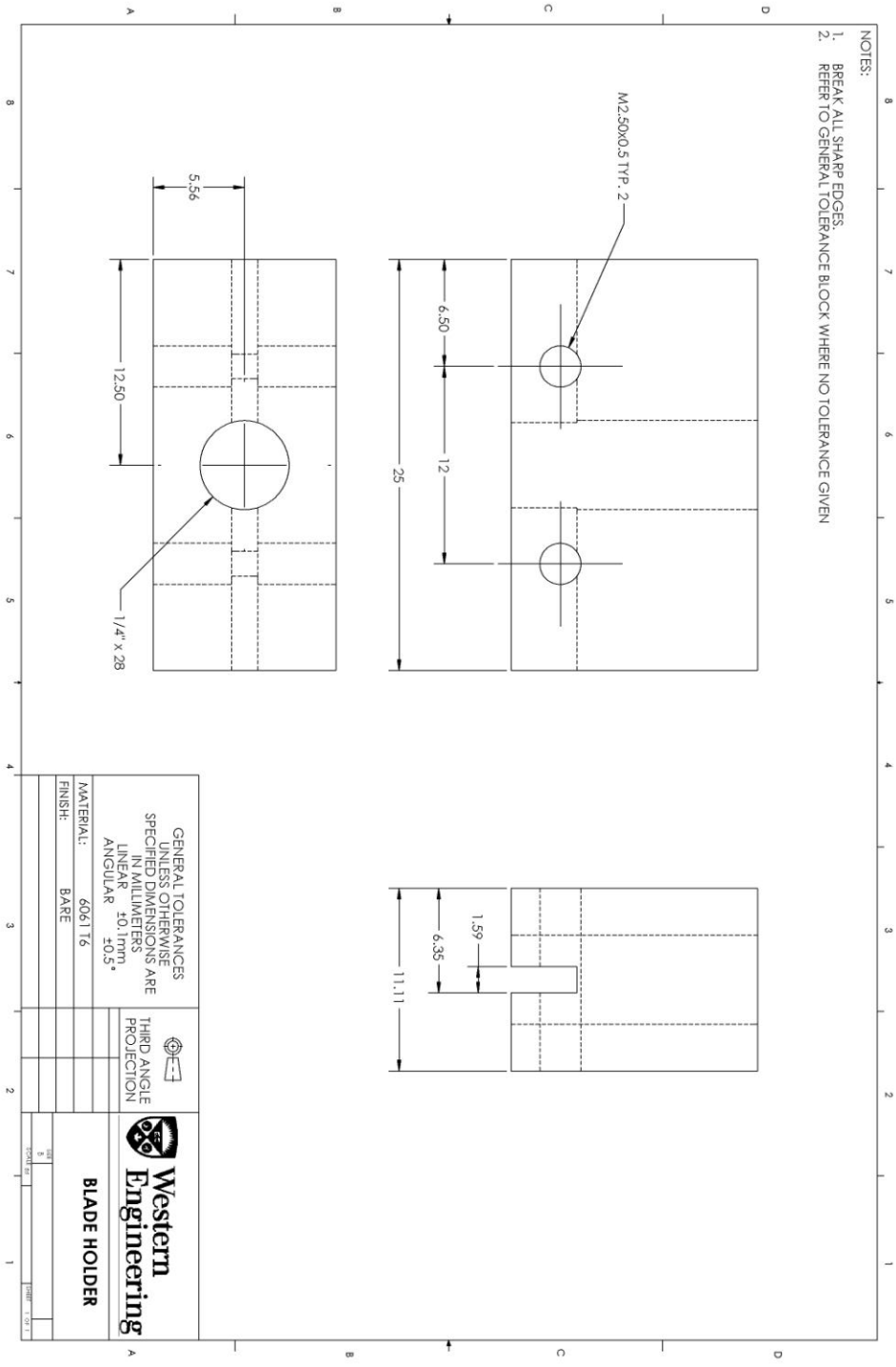


**Figure A. 7 Blade holder drawing.**

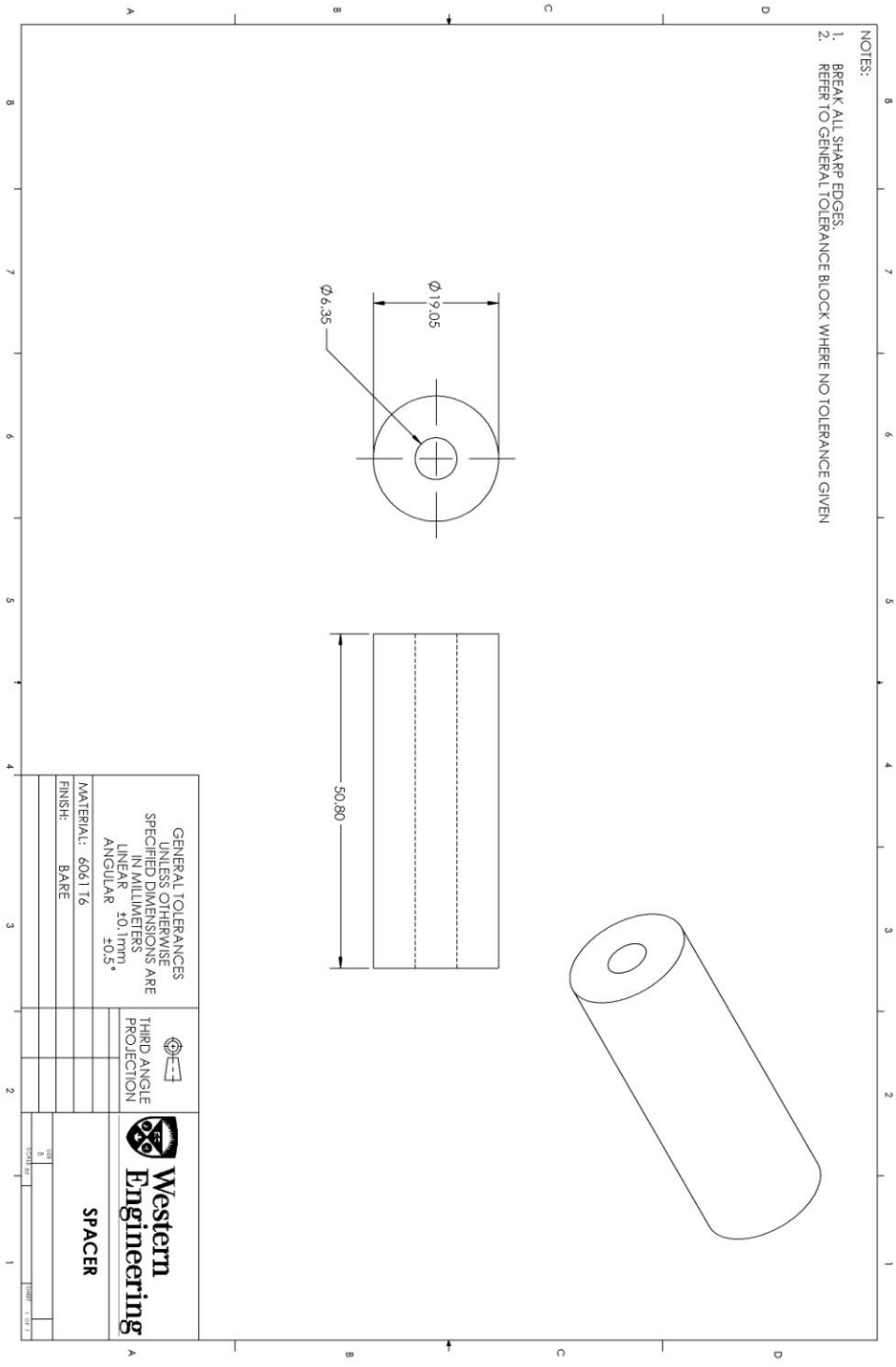


**Figure A. 8 Spacer drawing.**

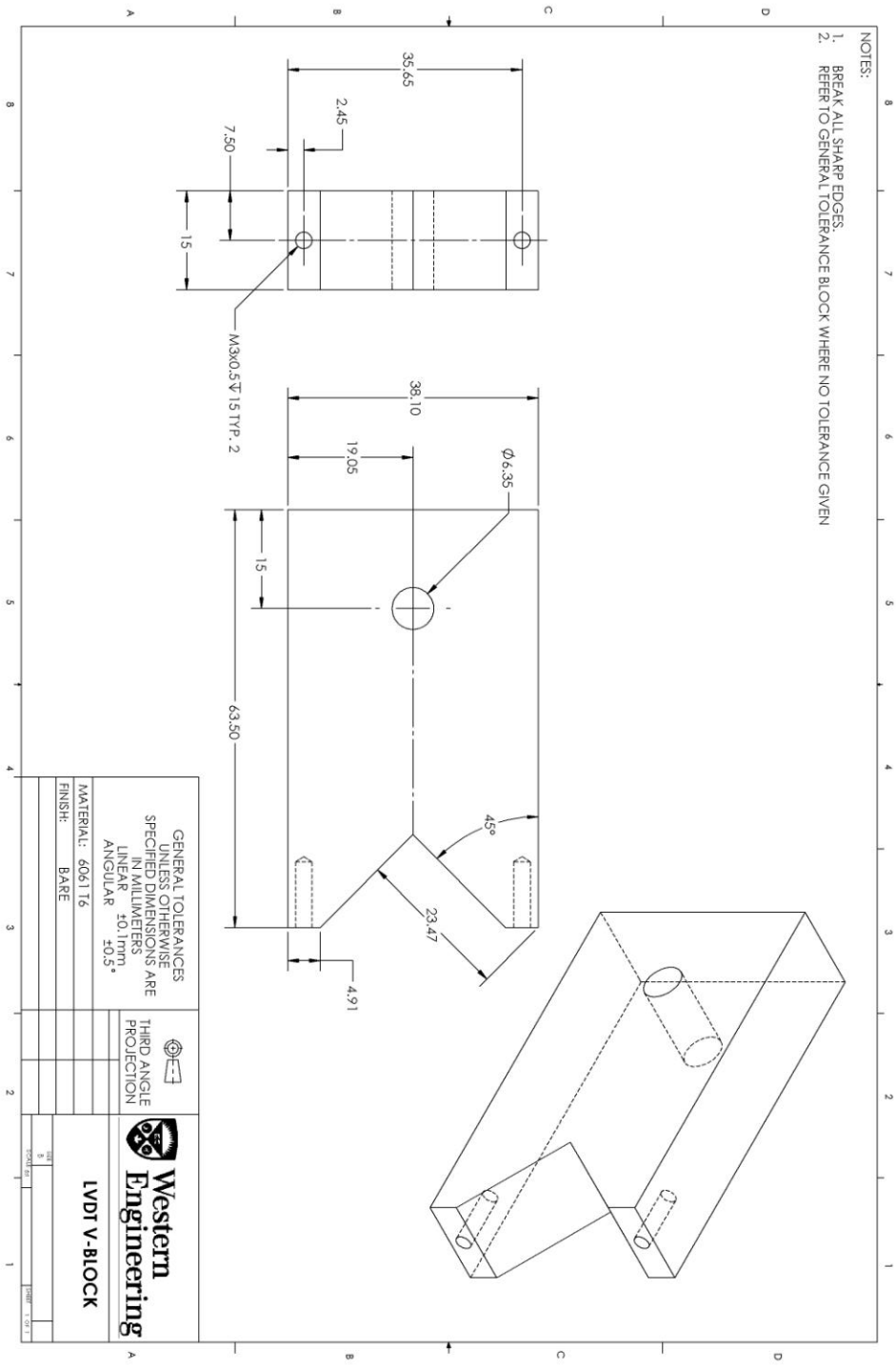


**Figure A. 9 LVDT V-block drawing.**

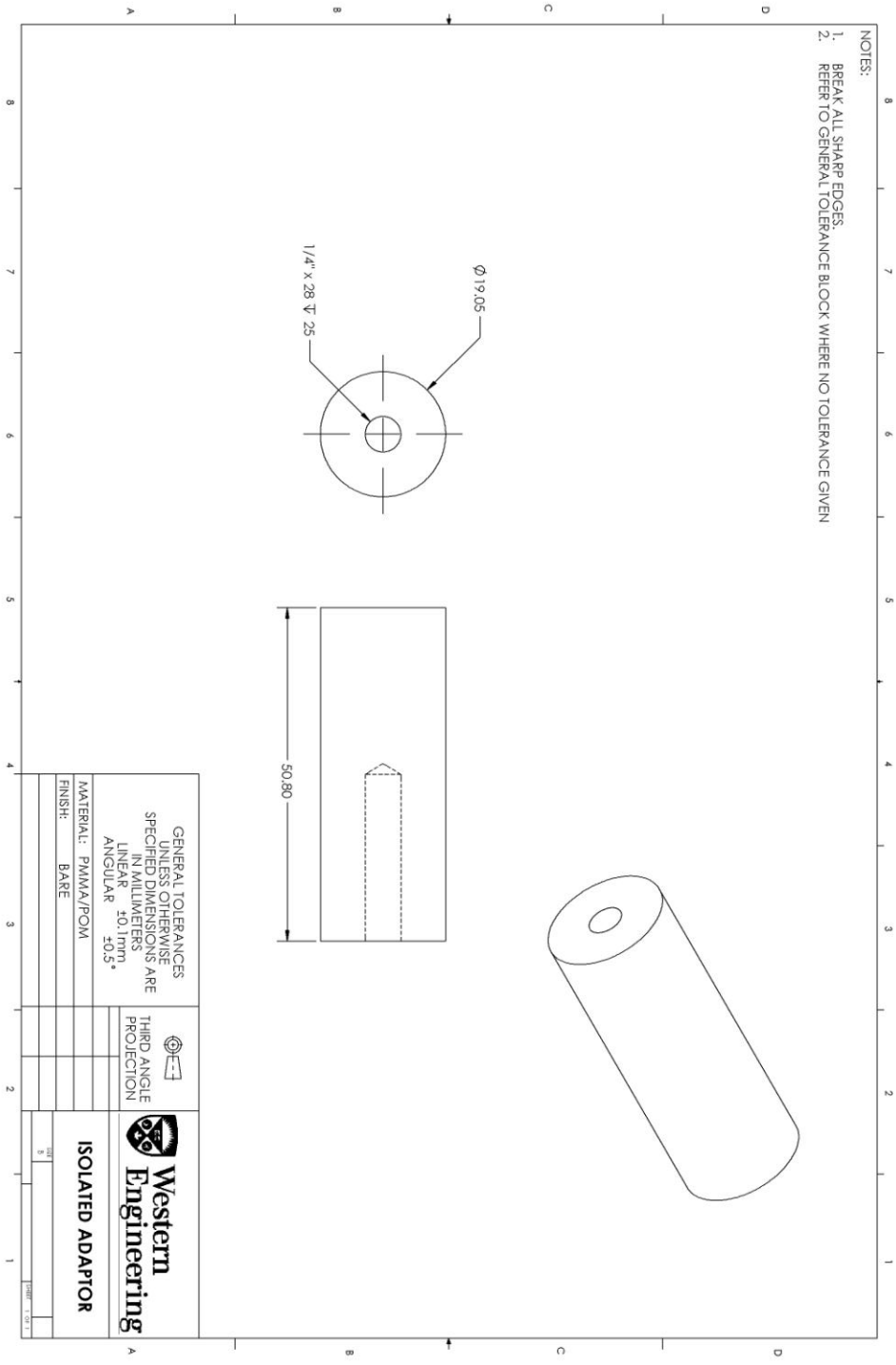


**Figure A. 10 Isolated adaptor drawing.**

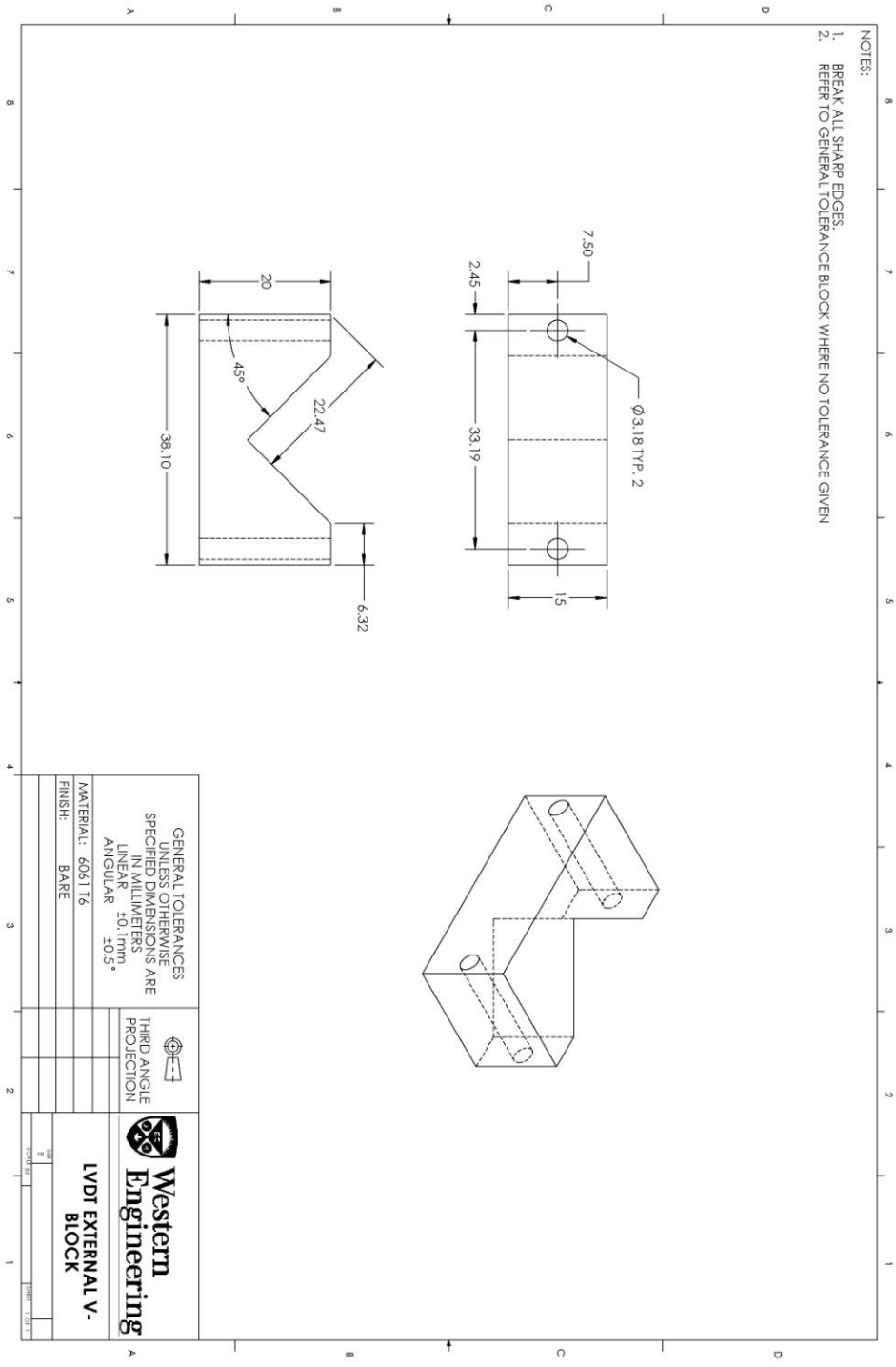


**Figure A. 11 LVDT external V-block drawing.**

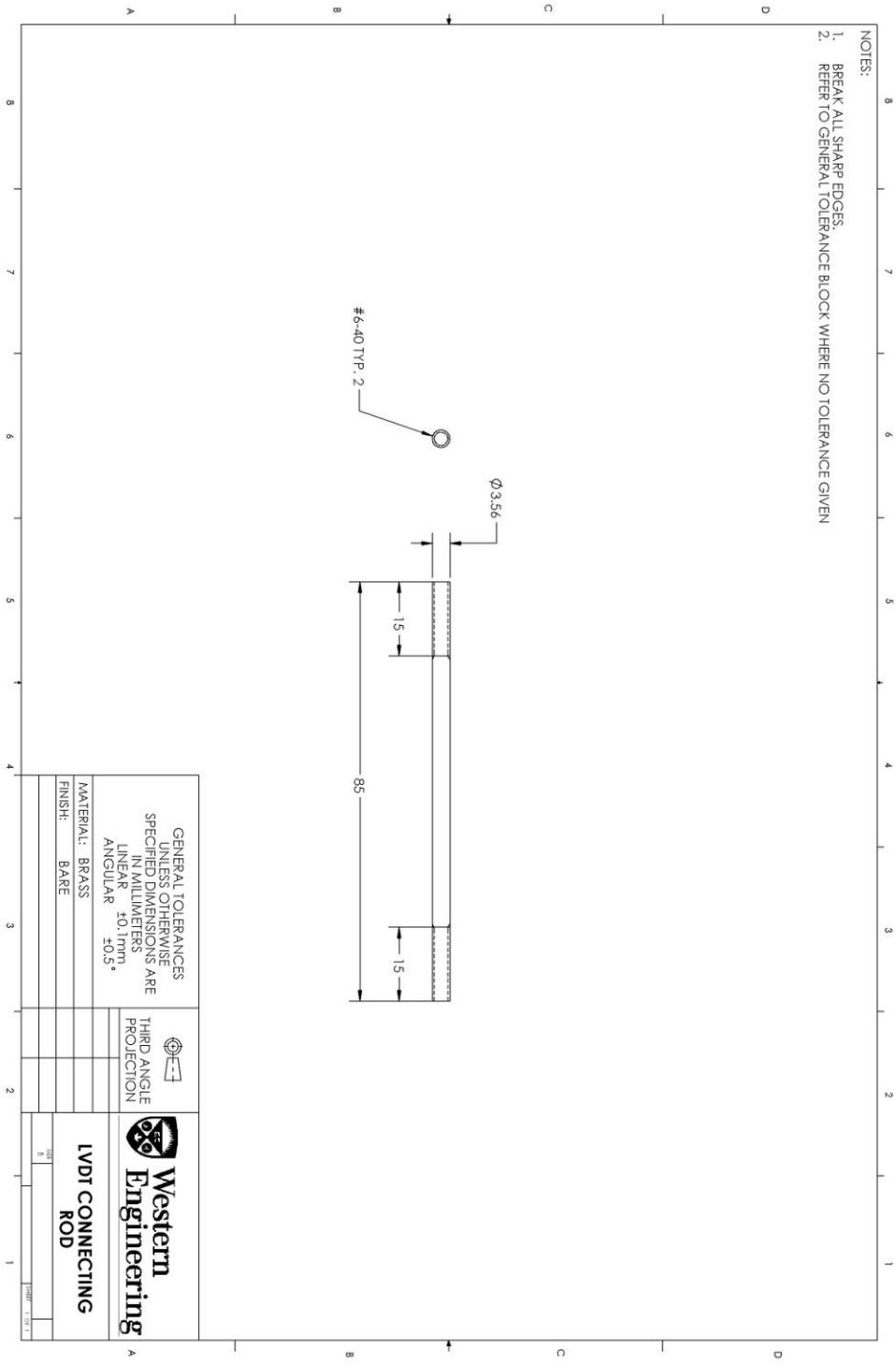


**Figure A. 12 LVDT connecting rod drawing.**

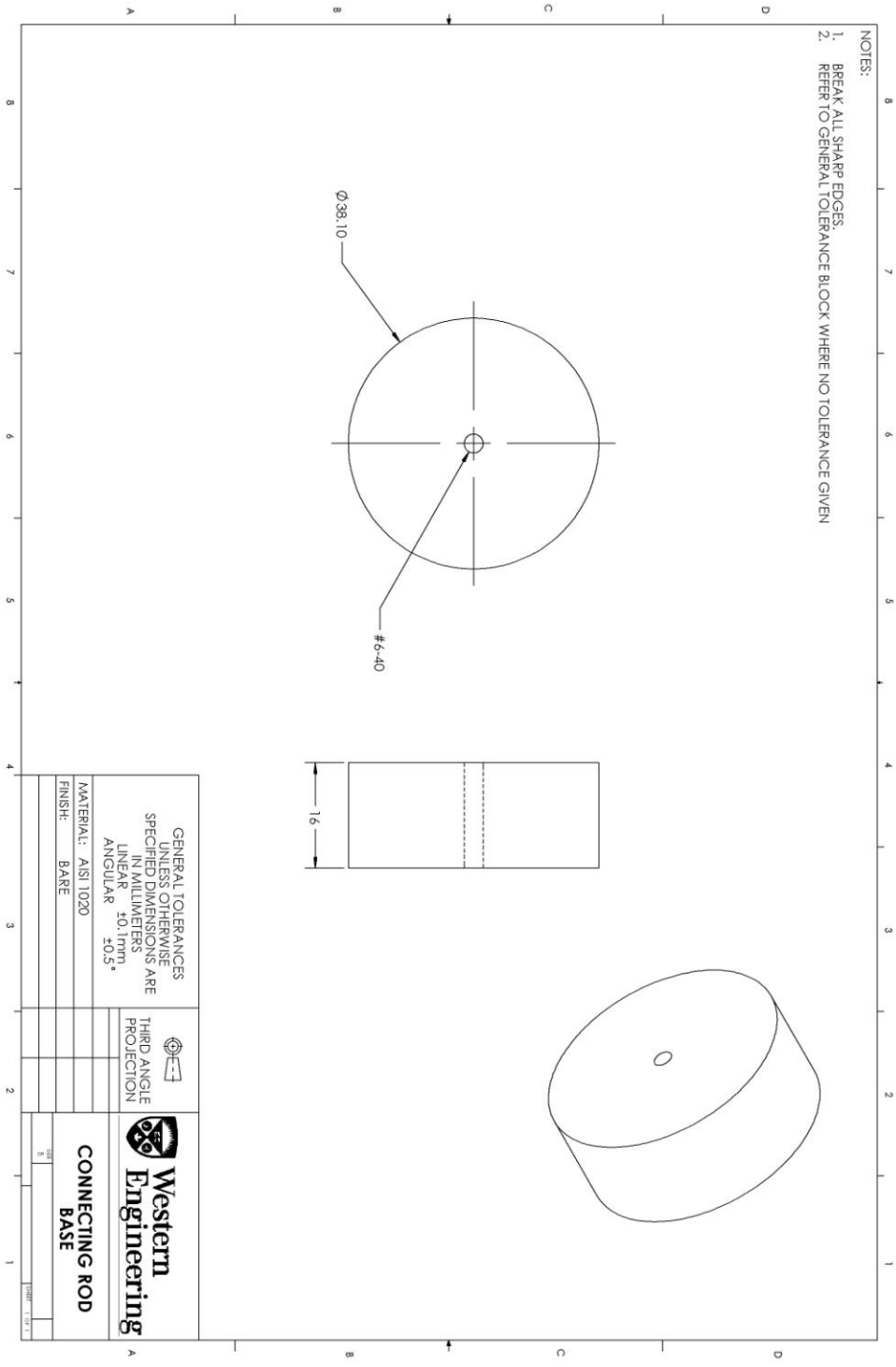


**Figure A. 13 Connecting rod base.**

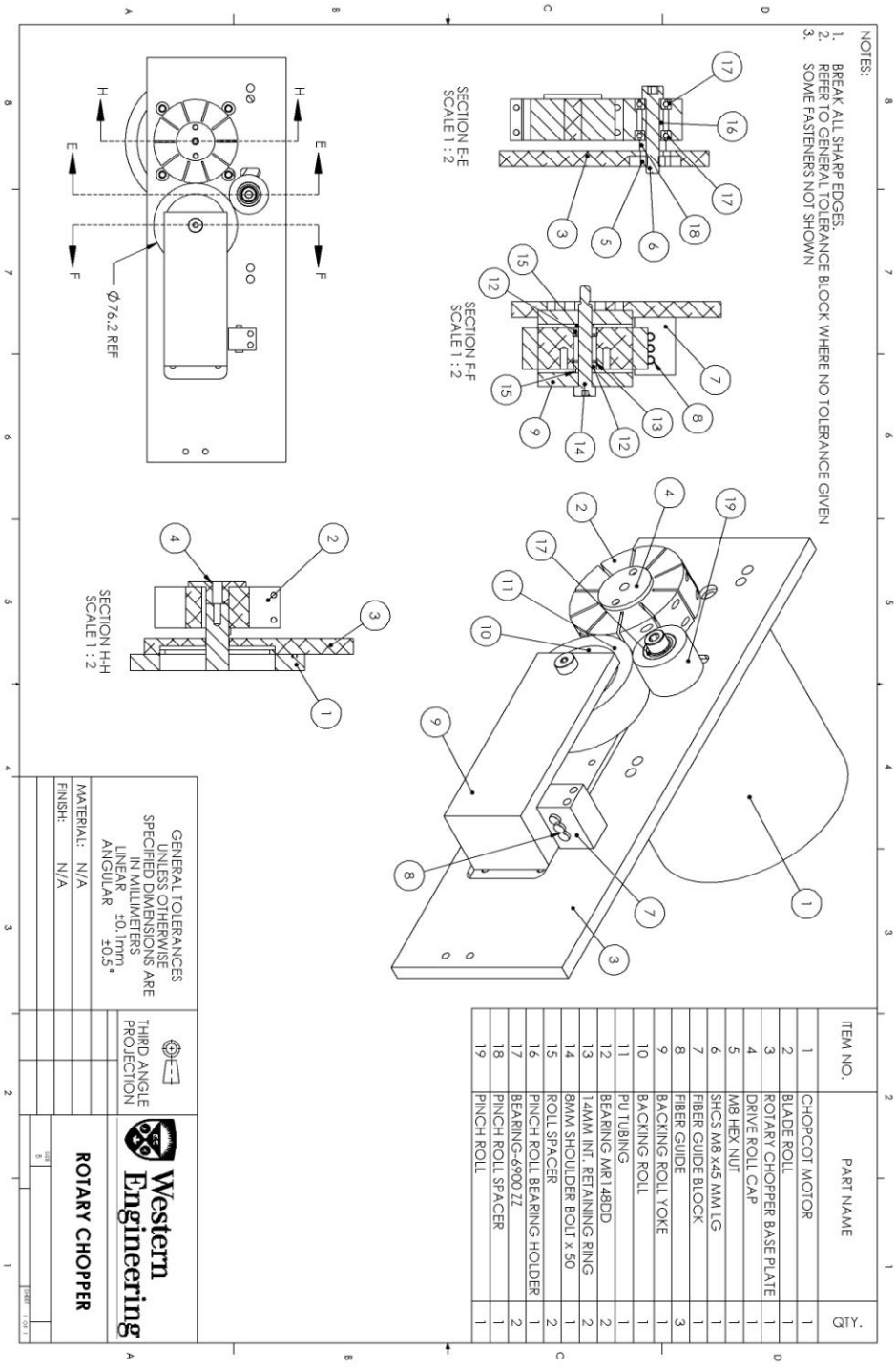


**Figure A. 14 Rotary chopper drawing.**

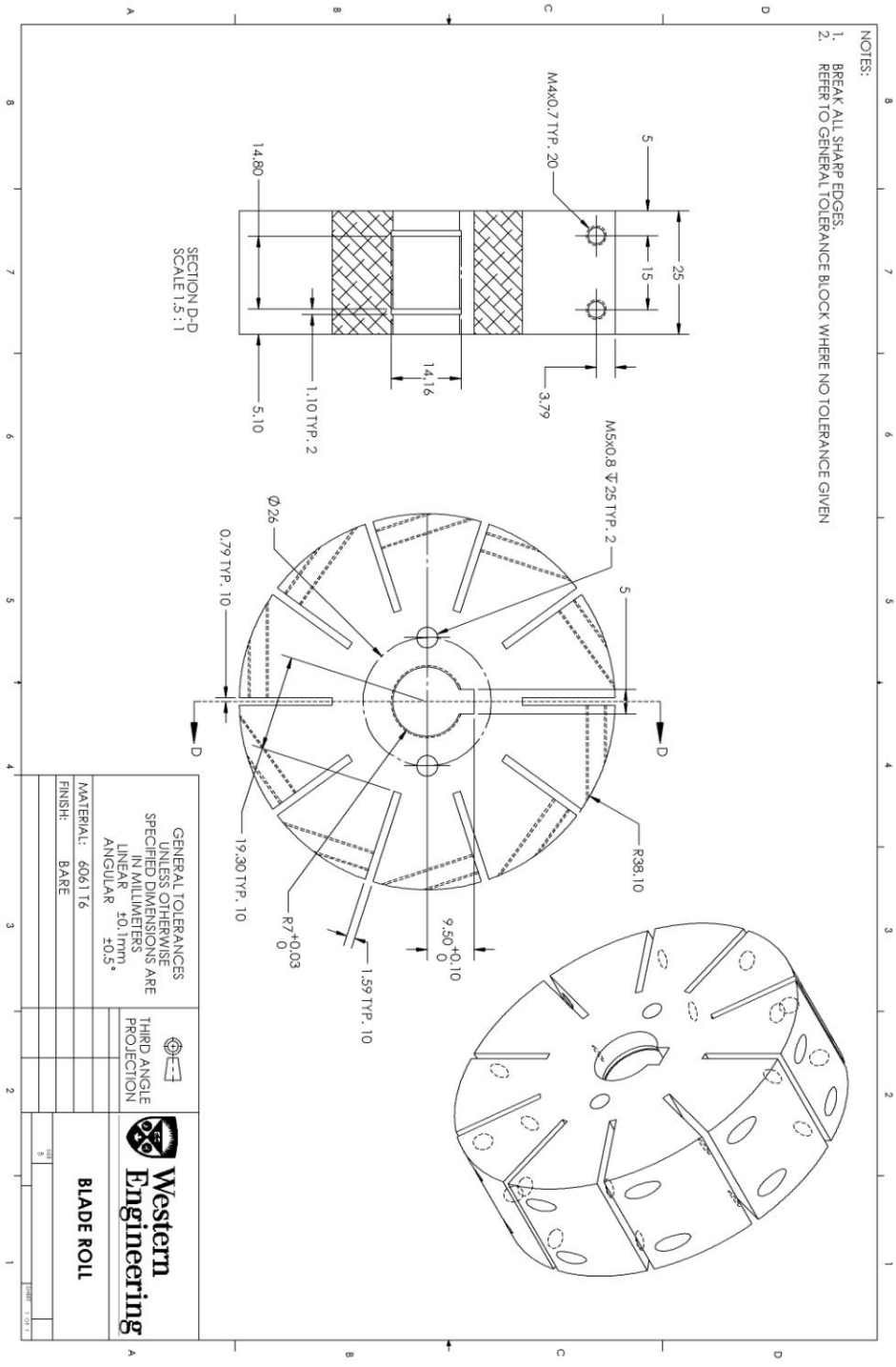


**Figure A. 15 Blade roll drawing.**

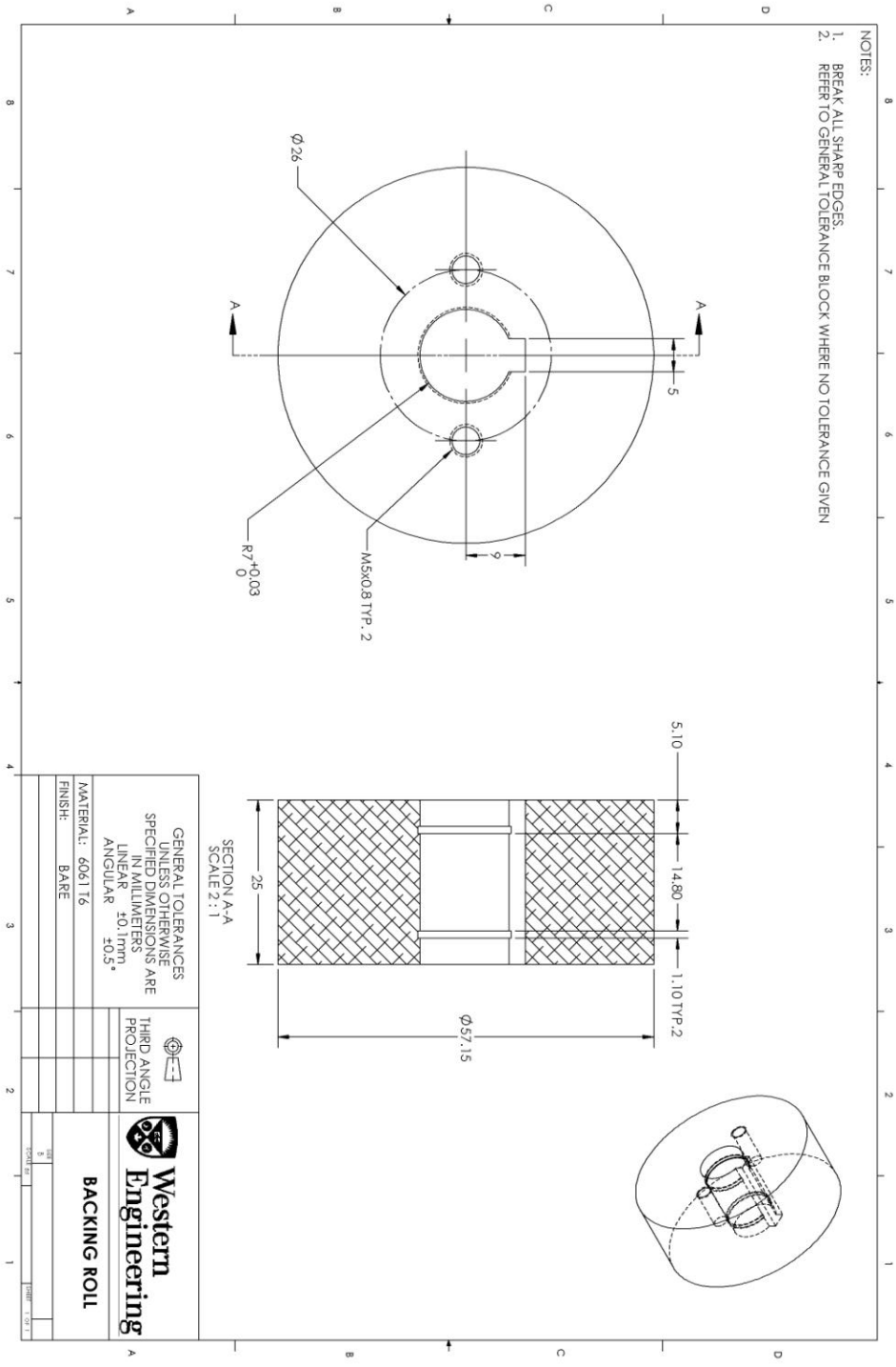


**Figure A. 16 Backing roll drawing.**

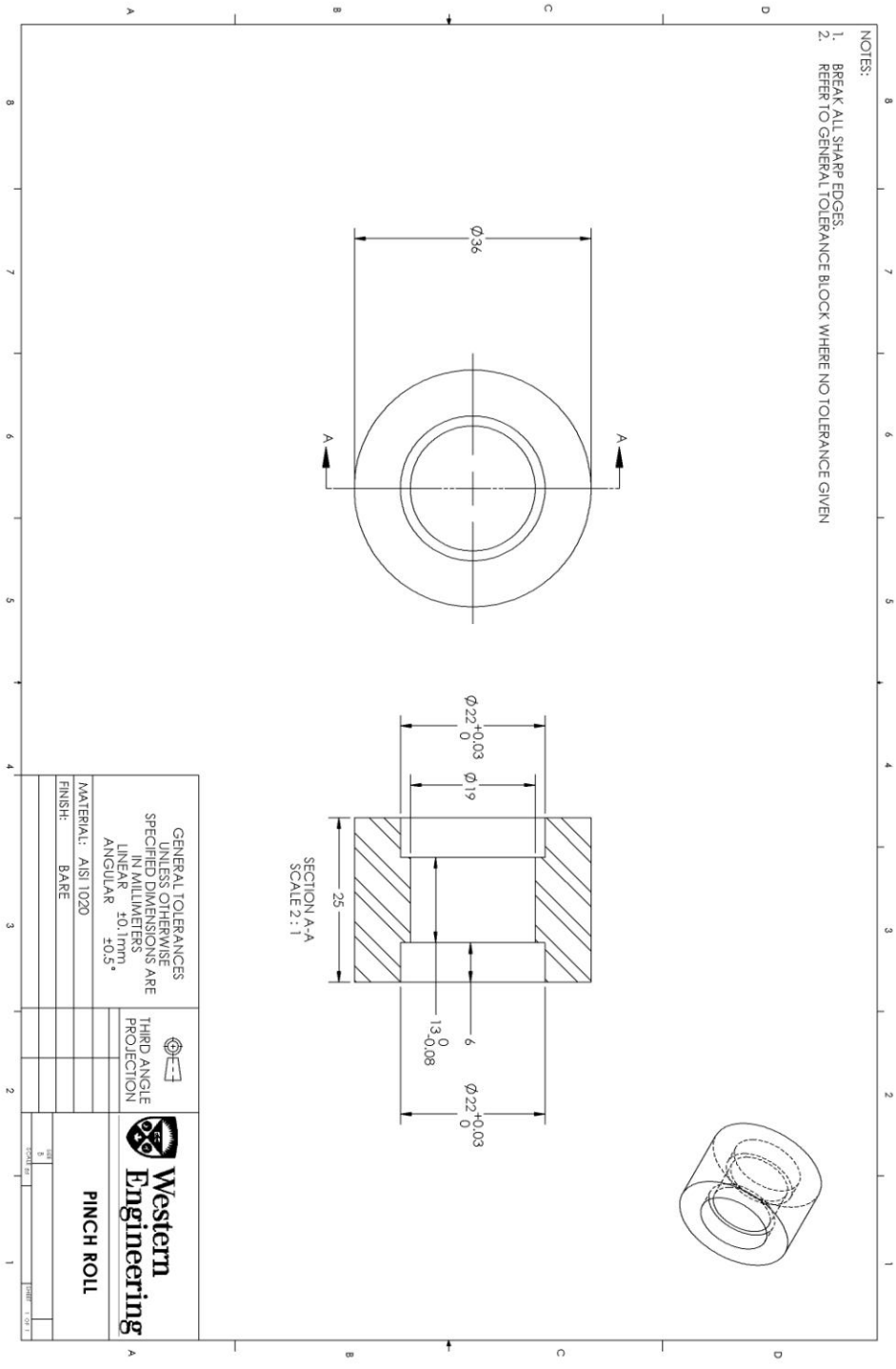


**Figure A. 17 Pinch roll drawing.**

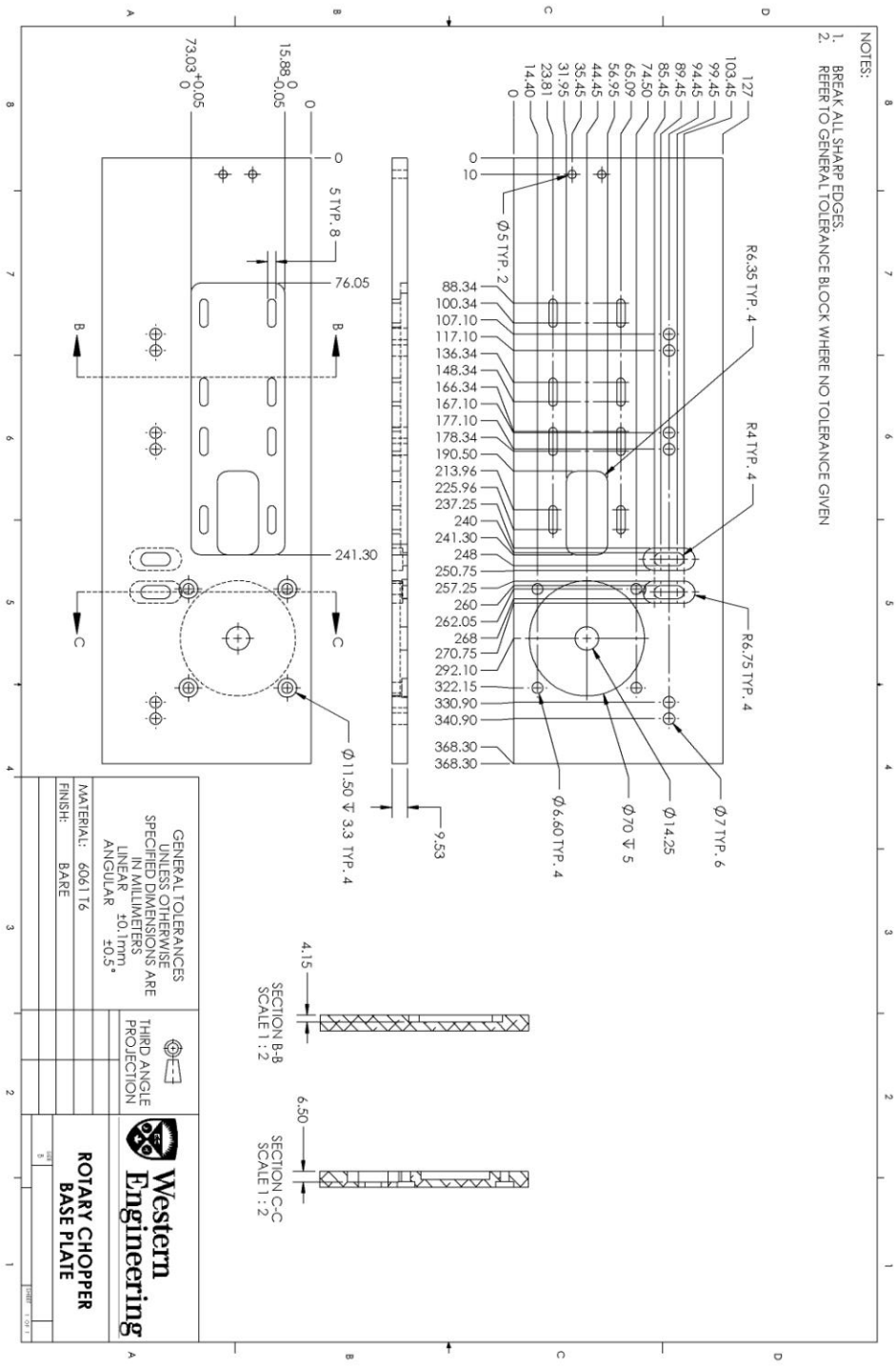


**Figure A. 18 Rotary chopper base plate drawing.**

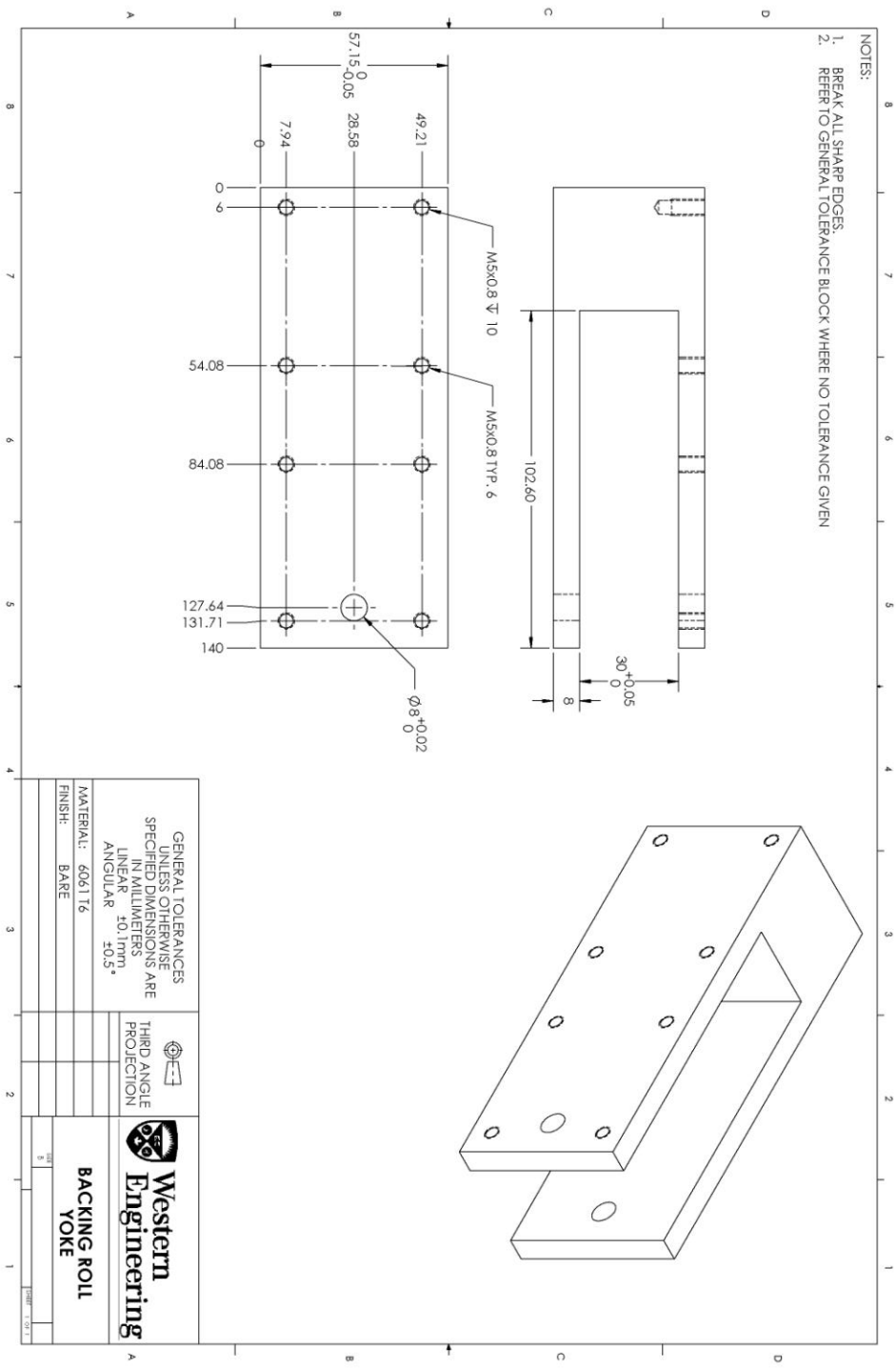


**Figure A. 19 Backing roll yoke drawing.**

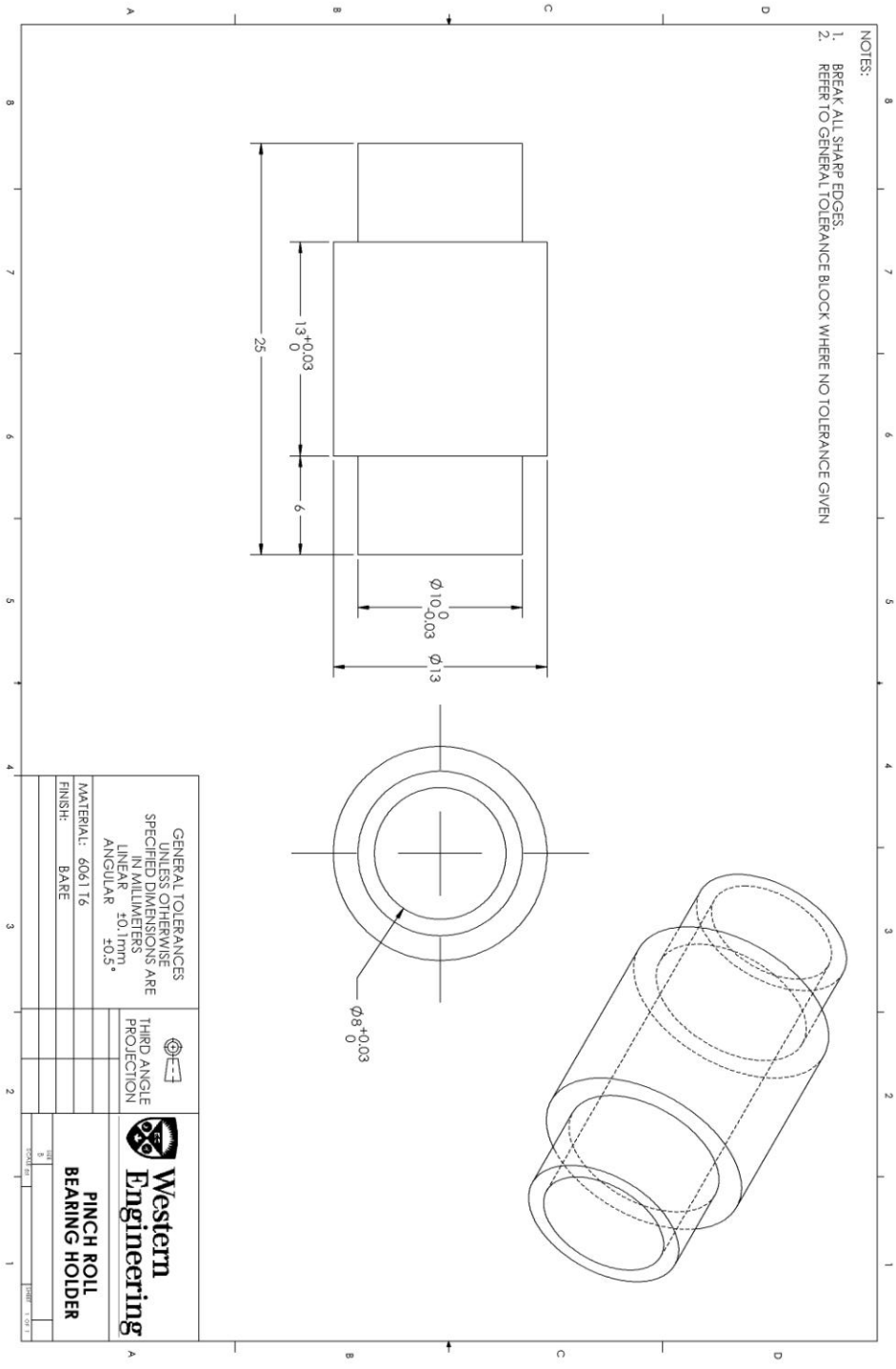


**Figure A. 20 Pinch roll bearing holder drawing.**

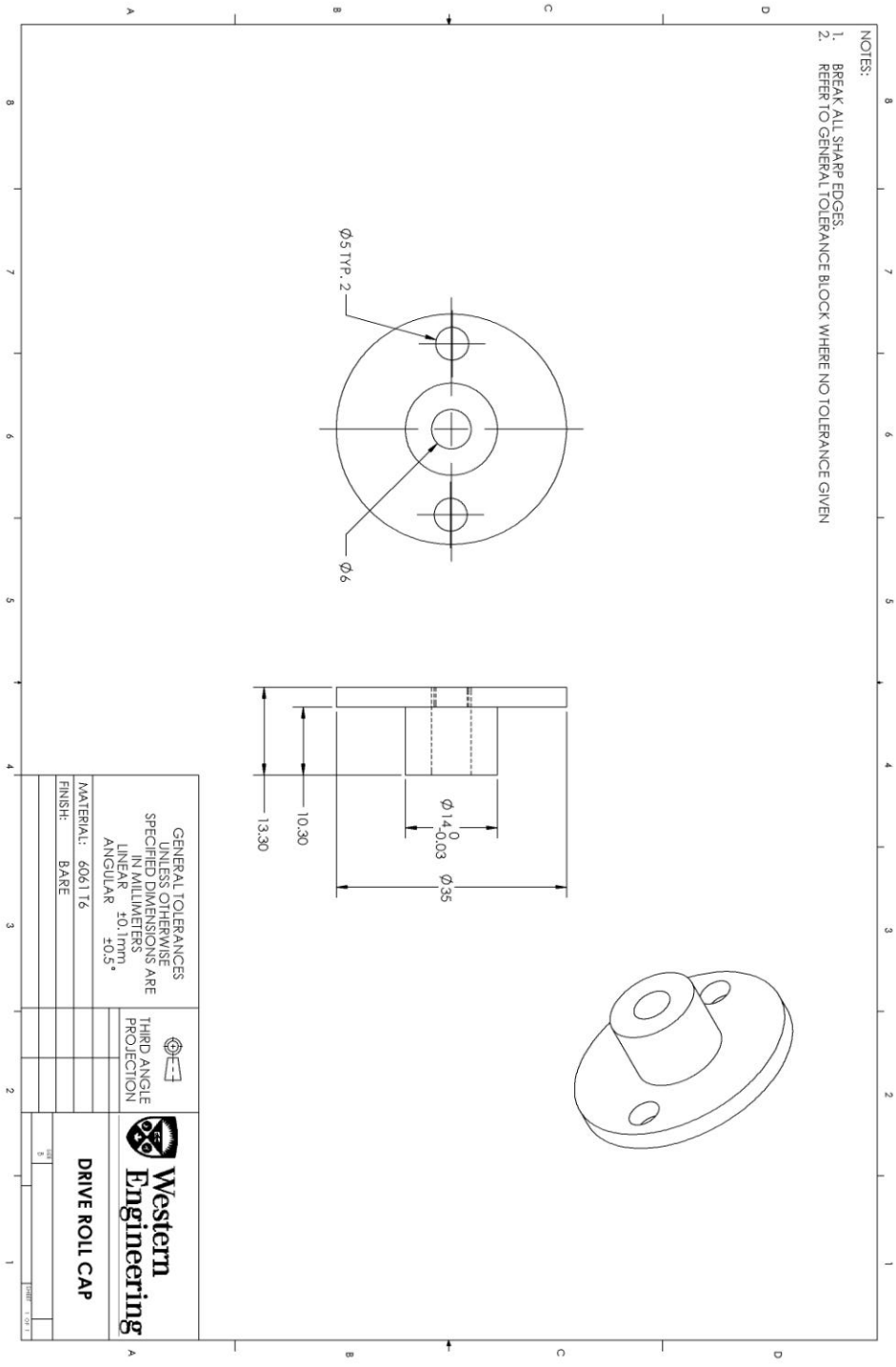


**Figure A. 21 Drive roll cap drawing.**

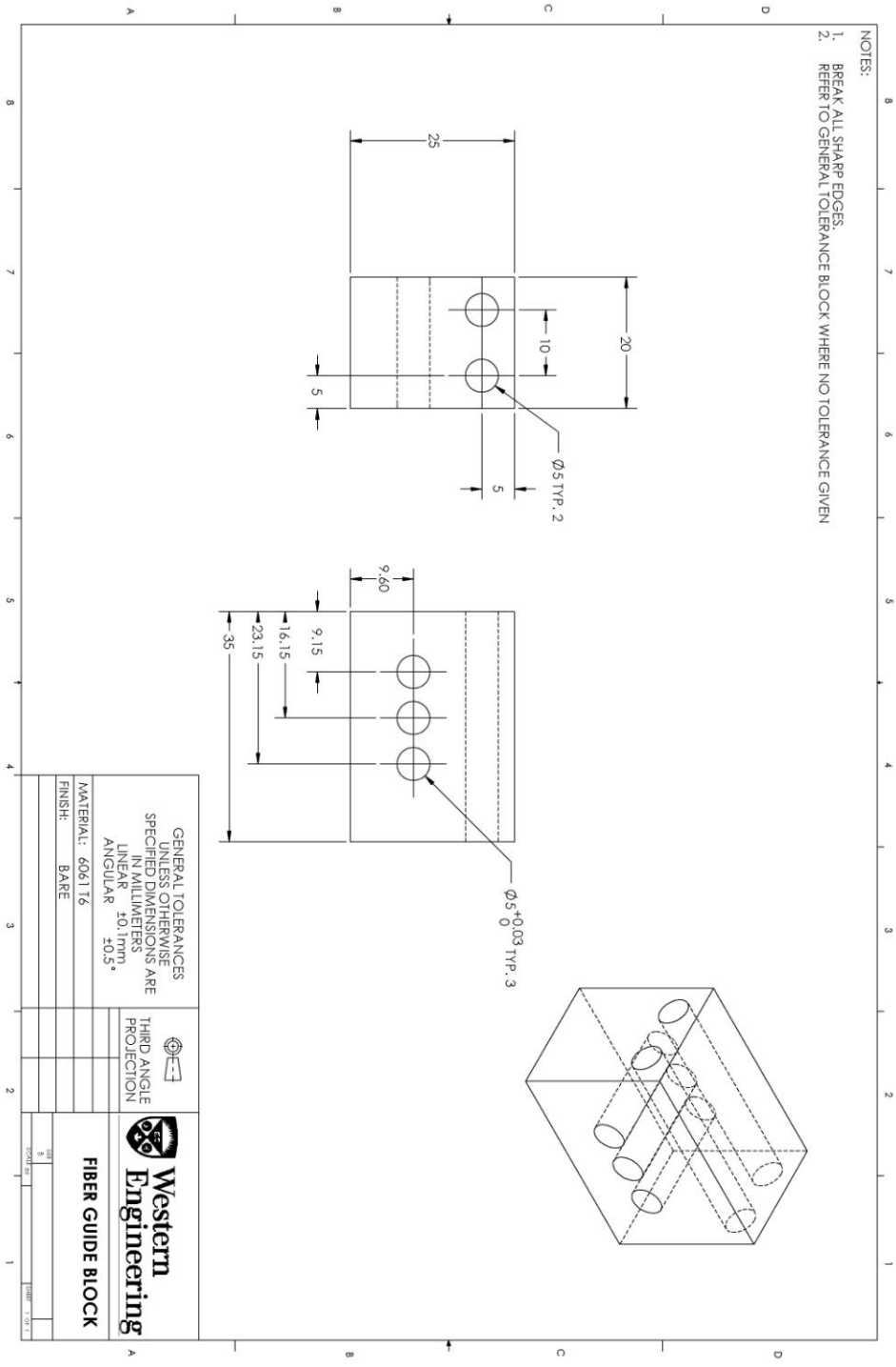


**Figure A. 22 Fiber guide block drawing.**

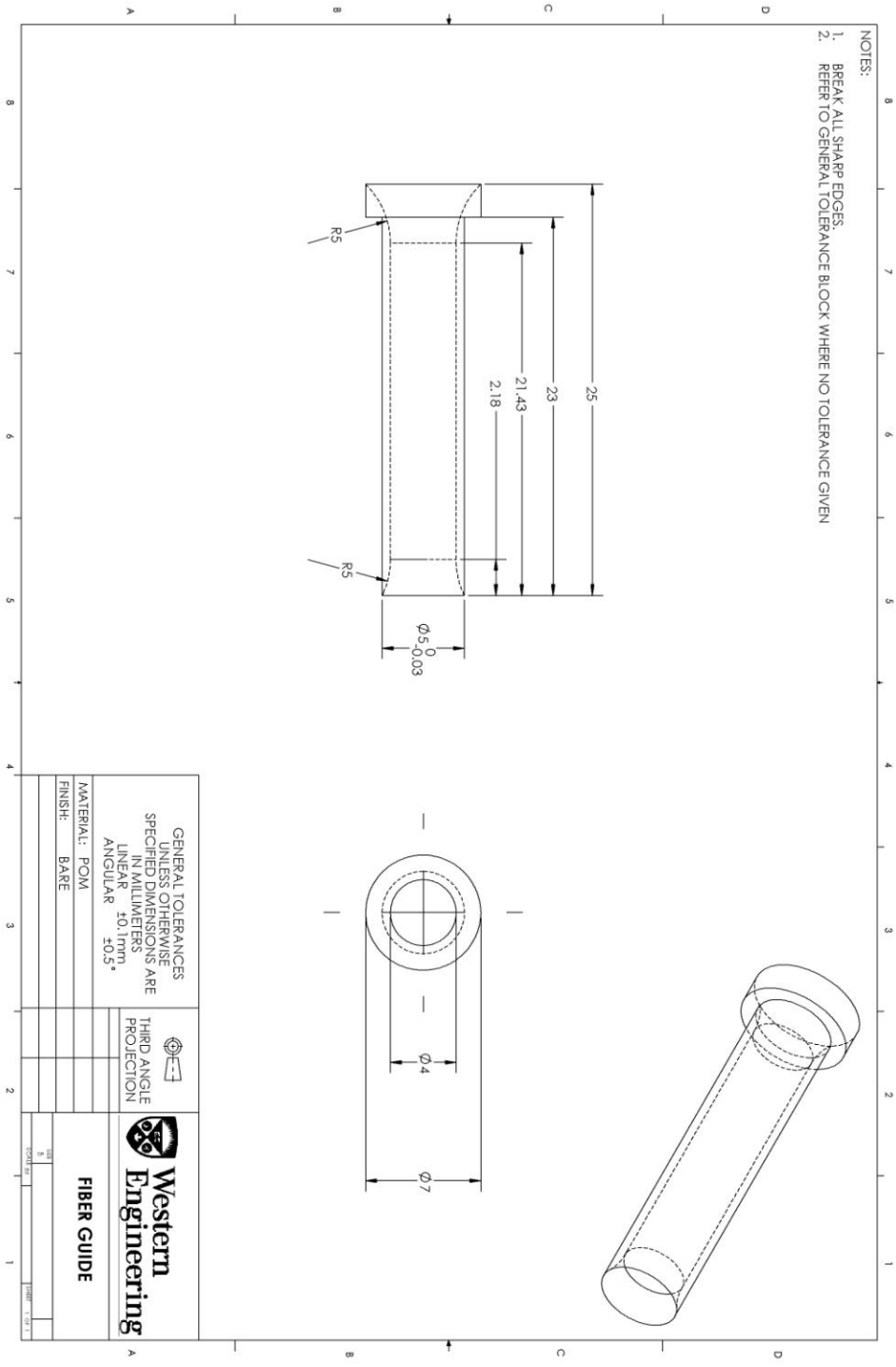


**Figure A. 23 Fiber guide drawing.**

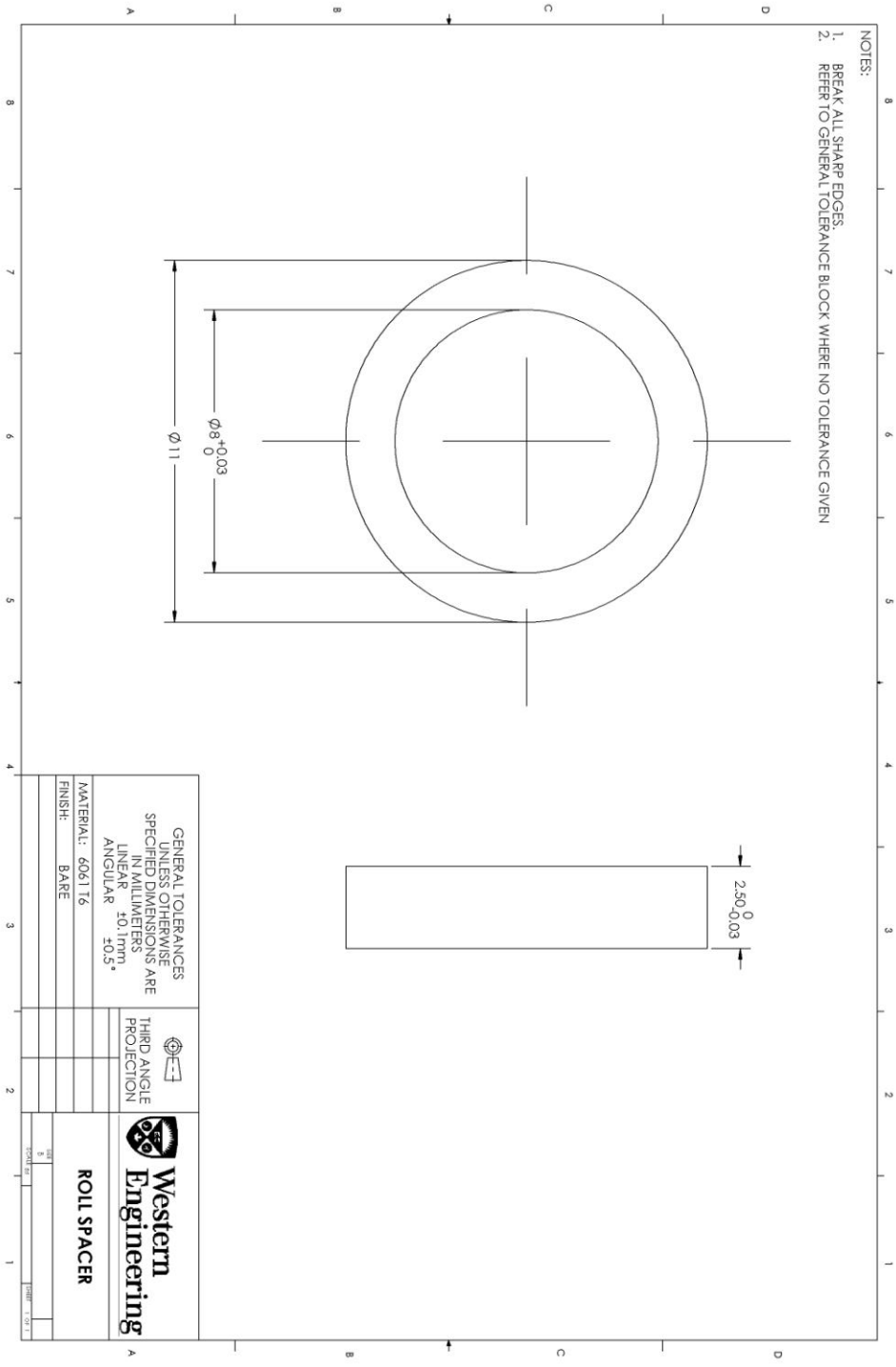


**Figure A. 24 Roll spacer drawing.**

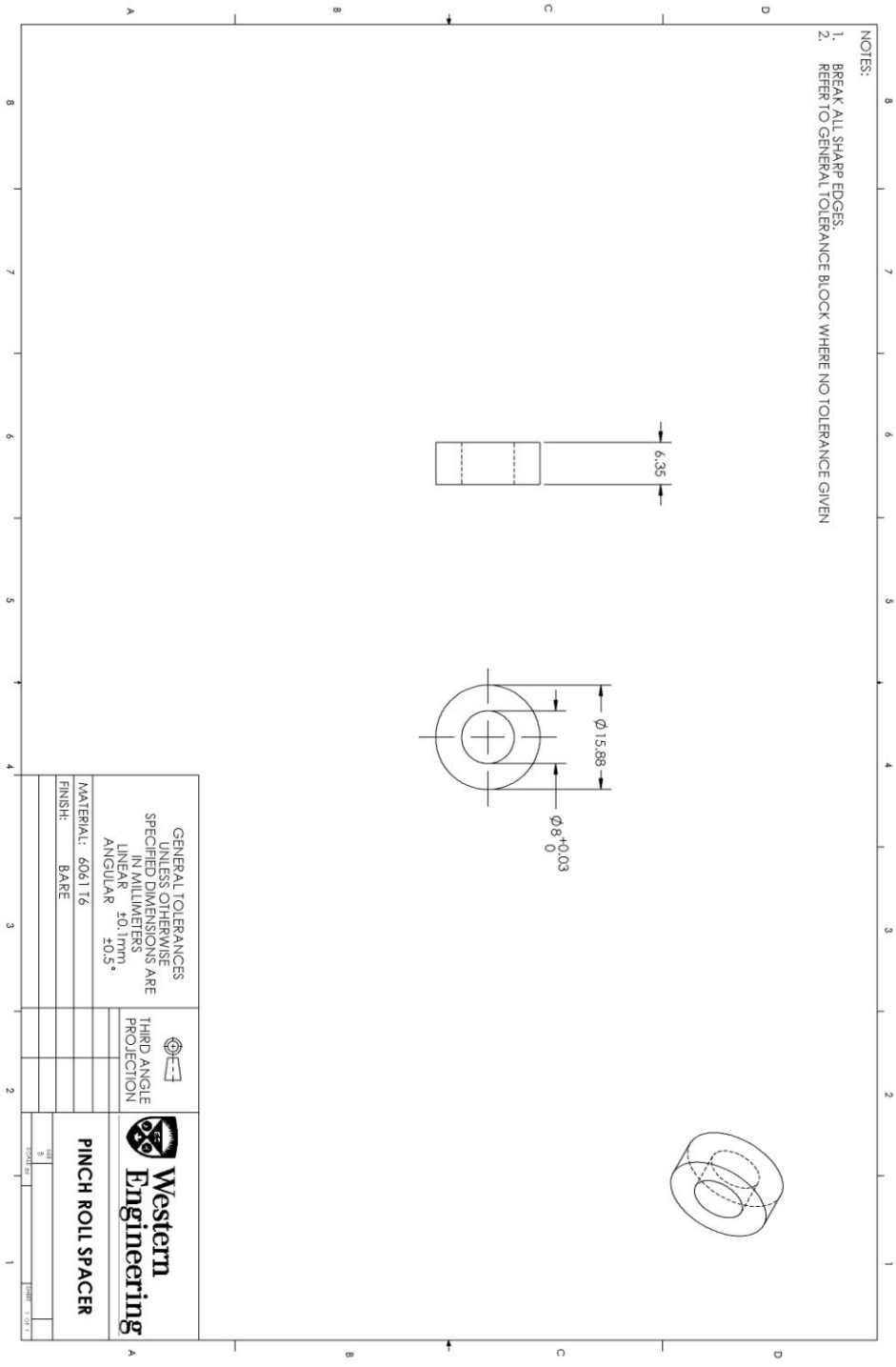


**Figure A. 25 Pinch roll spacer drawing.**

# Appendix B: Data Sheets

TECHNICAL DATA SHEET
No. CFA-005

**TORAYCA®**

## *T700S* DATA SHEET

Highest strength, standard modulus fiber available with excellent processing characteristics for filament winding and prepreg. This never twisted fiber is used in high tensile applications like pressure vessels, recreational, and industrial.

### FIBER PROPERTIES

| | | English | Metric | Test Method |
|---|---|---|---|---|
| Tensile Strength | | 711 ksi | 4,900 MPa | TY-030B-01 |
| Tensile Modulus | | 33.4 Msi | 230 GPa | TY-030B-01 |
| Strain | | 2.1 % | 2.1 % | TY-030B-01 |
| Density | | 0.065 lbs/in$^3$ | 1.80 g/cm$^3$ | TY-030B-02 |
| Filament Diameter | | 2.8E-04 in. | 7 µm | |
| Yield | 6K | 3,724 ft/lbs | 400 g/1000m | TY-030B-03 |
| | 12K | 1,862 ft/lbs | 800 g/1000m | TY-030B-03 |
| | 24K | 903 ft/lbs | 1,650 g/1000m | TY-030B-03 |
| Sizing Type & Amount | 50C | 1.0 % | | TY-030B-05 |
| | 60E | 0.3 % | | TY-030B-05 |
| | F0E | 0.7 % | | TY-030B-05 |
| | Twist | Never twisted | | |

### FUNCTIONAL PROPERTIES

| | |
|---|---|
| CTE | -0.38 $\alpha \cdot 10^{-6}/^{\circ}C$ |
| Specific Heat | 0.18 Cal/g·°C |
| Thermal Conductivity | 0.0224 Cal/cm·s·°C |
| Electric Resistivity | 1.6 x $10^{-3}$ Ω·cm |
| Chemical Composition: Carbon | 93 % |
| Na + K | <50 ppm |

### COMPOSITE PROPERTIES*

| | | | |
|---|---|---|---|
| Tensile Strength | 370 ksi | 2,550 MPa | ASTM D-3039 |
| Tensile Modulus | 20.0 Msi | 135 GPa | ASTM D-3039 |
| Tensile Strain | 1.7 % | 1.7 % | ASTM D-3039 |
| Compressive Strength | 215 ksi | 1,470 MPa | ASTM D-695 |
| Flexural Strength | 245 ksi | 1,670 MPa | ASTM D-790 |
| Flexural Modulus | 17.5 Msi | 120 GPa | ASTM D-790 |
| ILSS | 13 ksi | 9 kgf/mm$^2$ | ASTM D-2344 |
| 90° Tensile Strength | 10.0 ksi | 69 MPa | ASTM D-3039 |

* Toray 250°F Epoxy Resin. Normalized to 60% fiber volume.

**TORAY CARBON FIBERS AMERICA, INC.**

**Figure B. 1 Toray T700S carbon fiber data sheet.**

Johns Manville

- ☐ BMC
- ☐ LFT / GMT
- ☐ Pultrusion
- ■ SMC
- ☐ Extrusion compounding
- ☐ Carding / needling, air laid
- ☐ Others
- ☐ Filament winding
- ☐ Hand lay-up
- ☐ LCM
- ☐ Spray-up
- ☐ Textile

# *SMC Roving 272*

## Roving 272 for SMC- Class A

### Product description:

SMC Roving 272 is produced by assembling E glass fibers coated with a silane based sizing. Johns Manville technology enables the product to achieve outstanding **surface performance** in SMC Class A while exceeding **strength performance**. 272 Roving offers easy unwinding and excellent chopping characteristics and strand distribution. 272 has also been developed for **improved in-coloured SMC** parts, enabling SMC compounders and moulders to further develop new SMC moulded parts.

### Designation:

| JM designation | Glass type | Filament diameter [µm] | Roving bundle linear density (tex) | Sizing designation | Strand linear density (tex) |
|---|---|---|---|---|---|
| EC 13,5 2400 272 (80) | E | 13,5 | 2400 | 272 | 80 |
| EC 13,5 4800 272 (80) | E | 13,5 | 4800 | 272 | 80 |

### Technical data:

| | LOI content [%] | Moisture content maximum [%] | Stifness minimum [mm] | Sizing |
|---|---|---|---|---|
| All 272 types | 1.3 - 1.7 | 0.15 | 130 | Silane |

**Figure B. 2 Johns Manville SMC Roving 272 data sheet.**

# ALL STAINLESS STEEL "S" BEAM LOAD CELLS

## HIGH ACCURACY, ECONOMICAL PRICE

## STANDARD AND METRIC MODELS

***Tension/Compression***
***0-25 lb to 0-40,000 lb***
***0-10 kgf to 0-10,000 kgf***

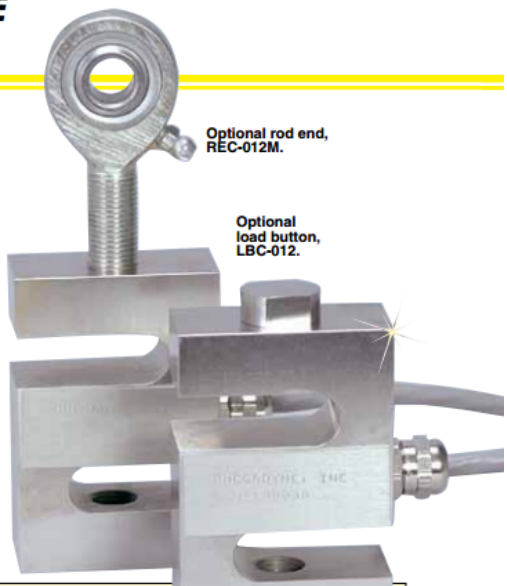


***LC101/LCM101 Series***
***LC111/LCM111 Series***

NIST RoHS
Standard

STANDARD
LC101-2K shown slightly smaller than actual size.

- **All Stainless Steel for Harsh Industrial Applications**
- **0.25% Interchangeability for Multiple Load Cell Applications**
- **5-Point Calibration Provided (in Tension)**

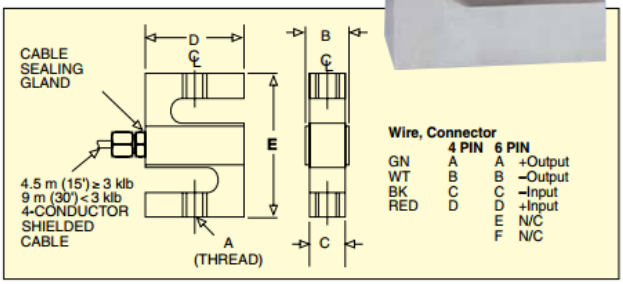


### SPECIFICATIONS

**Excitation:** 10 Vdc, 15 Vdc maximum
**Output:** 3 mV/V ±0.0075 mV/V
**Linearity:** ±0.03% FSO (0.1% 40 K)
**Hysteresis:** ±0.02% FSO (0.1% 40 K)
**Repeatability:** ±0.01% FSO (0.05% 40 K)
**Zero Balance:** ±1% FSO
**Operating Temp Range:**
-40 to 93°C (-40 to 200°F)
**Compensated Temp Range:**
17 to 71°C (60 to 160°F)
**Thermal Effects:**
**Zero:** 0.002% FSO/°C
**Span:** 0.002% FSO/°C
**Safe Overload:** 150% of capacity
**Ultimate Overload:** 300% of capacity
**Input Resistance:** 350 ±10 Ω
**Output Resistance:** 350 ±10 Ω
**Full Scale Deflection:** 0.010 to 0.020"
**Construction:** 17-4 PH stainless steel

**Electrical (LC101/LCM101) (4-Conductor Shielded Cable):**
**<100 kgf/250 lb:** 9 m (30') 24 AWG
**250 to 1000 kgf/250 to 2000 lb:** 9 m (30') 20 AWG
**≥1500 kgf/3000 lb:** 4.5 m (15') 20 AWG

**Mating Connector (LC111/LCM111):**
**≤100 kgf/200 lb:** PT06F8-4S, sold separately
**≥250 kgf/250 lb:** PT06F10-6S, sold separately

**Dimensions: mm (inch)**

| CAPACITY | A | B | C | D | E | WEIGHT kg (lb) |
|---|---|---|---|---|---|---|
| **lb** | | | | | | |
| 25 to 200 | ¼-28 | 19 (0.75) | 13 (0.50) | 38 (1.5) | 64 (2.5) | 0.45 (1.0) |
| 250 to 2.5K | ½-20 | 32 (1.25) | 25 (1.0) | 51 (2.0) | 76 (3.0) | 1.1 (2.5) |
| 3K to 5K | ⅝-18 | 32 (1.25) | 25 (1.0) | 51 (2.5) | 89 (3.5) | 1.6 (3.5) |
| 10K to 20K | 1-14 | 44 (1.75) | 38 (1.5) | 76 (3.0) | 108 (4.3) | 2.0 (4.5) |
| 25K to 30K | 1-14 | 57 (2.25) | 51 (2.0) | 102 (4.0) | 108 (4.3) | 4 (9) |
| 40K | 1¼-12 | 83 (3.25) | 76 (3.0) | 102 (4.0) | 140 (5.5) | 6 (13) |
| **kgf** | | | | | | |
| 10 to 100 | M6 x 1.00 | 19 (0.75) | 13 (0.50) | 38 (1.5) | 64 (2.5) | 0.45 (1.0) |
| 250 to 1000 | M12 x 1.75 | 32 (1.25) | 25 (1.0) | 51 (2.0) | 76 (3.0) | 1.1 (2.5) |
| 1500 to 2000 | M16 x 2.0 | 32 (1.25) | 25 (1.0) | 51 (2.5) | 89 (3.5) | 1.6 (3.5) |
| 5K to 10K | M24 x 2.00 | 44 (1.75) | 38 (1.5) | 76 (3.0) | 108 (4.3) | 2.0 (4.5) |

F-51

**Figure B. 3 Omega LC101 load cell data sheet**

measurement SPECIALTIES™

# HR Series – General Purpose LVDT

RoHS

- High Reliability
- Large core-to-bore clearance
- Operating temperature up to 220°C (option)
- Stroke ranges from ± 0.05 to ±10 inches
- AC operation from 400Hz to 5kHz
- Stainless steel housing
- Imperial or metric threaded core
- Many options and accessories

## DESCRIPTION

The **HR Series** general purpose LVDTs provide the optimum performance required for a majority of applications. The large 1/16 inch [1.6mm] bore-to-core radial clearance provides for ample installation misalignments and therefore reduces the application costs. Featuring a high output voltage and a broad operating frequency range, these versatile and highly reliable LVDTs deliver worry-free and precise position measurements.

Available in a variety of stroke ranges from ±0.05 to ±10 inches, the HR Series can be configured with a number of standard options including guided core, small diameter/low mass core and mild radiation resistance ($10^{12}$ NVT total integrated flux; $10^{7}$ rads Gamma). High temperature operation (+220ºC) and high pressure (vented case) versions are also available *(consult factory)*. The HR Series is compatible with the full line of Measurement Specialties LVDT signal conditioners.

Like in most of our LVDTs, the HR windings are vacuum impregnated with a specially formulated, high temperature, flexible resin, and the coil assembly is potted inside its housing with a two-component epoxy. This provides excellent protection against hostile environments such as high humidity, vibration and shock.

Measurement Specialties, Inc. (NASDAQ MEAS) offers many other types of sensors and signal conditioners. Data sheets can be downloaded from our web site at: http://www.meas-spec.com/datasheets.aspx

*MEAS acquired Schaevitz Sensors and the **Schaevitz™** trademark in 2000.*

## FEATURES

- 0.25% linearity (100% stroke)
- Large 1/16" core-to-bore clearance
- Shock and vibration tolerant
- Electromagnetic/electrostatic shielding
- Mild radiation resistance (optional)
- Calibration certificate supplied with each unit

## APPLICATIONS

- Process control
- Factory automation
- Materials testing
- Metrology
- Applications with large misalignments
- General industrial



**Figure B. 4 Measurement specialties HR Series data sheet.**

measurement SPECIALTIES™

# HR Series – General Purpose LVDT

## PERFORMANCE SPECIFICATIONS

| ELECTRICAL SPECIFICATIONS | | | | | | | | | | | | |
|---|---|---|---|---|---|---|---|---|---|---|---|---|
| **Parameter** | **HR 050** | **HR 100** | **HR 200** | **HR 300** | **HR 500** | **HR 1000** | **HR 2000** | **HR 3000** | **HR 4000** | **HR 5000** | **HR 7500** | **HR 10000** |
| Stroke range | ±0.05 [±1.27] | ±0.1 [±2.54] | ±0.2 [±5.08] | ±0.3 [±7.62] | ±0.5 [±12.7] | ±1 [±25.4] | ±2 [±50.8] | ±3 [±76.2] | ±4 [±101.6] | ±5 [±127] | ±7.5 [±190.5] | ±10 [±254] |
| Sensitivity V/V/inch [mV/V/mm] | 5.8 [228] | 4.2 [165] | 2.5 [98.4] | 1.3 [51.2] | 0.7 [27.6] | 0.39 [15.4] | 0.23 [9.1] | 0.25 [9.8] | 0.20 [7.9] | 0.14 [5.5] | 0.13 [5.1] | 0.07 [2.8] |
| Output at stroke ends, mV/V *(*)* | 290 | 420 | 500 | 390 | 350 | 390 | 460 | 750 | 800 | 700 | 975 | 700 |
| Phase shift | -1° | -5° | -4° | -11° | -1° | -3° | +5° | +11° | +1° | +3° | +1° | -5° |
| Input impedance (PRIMARY) | 430Ω | 1070Ω | 1150Ω | 1100Ω | 460Ω | 460Ω | 330Ω | 315Ω | 275Ω | 310Ω | 260Ω | 550Ω |
| Output impedance (SECONDARY) | 4000Ω | 5000Ω | 4000Ω | 2700Ω | 375Ω | 320Ω | 300Ω | 830Ω | 400Ω | 400Ω | 905Ω | 750Ω |
| Non-linearity | % of FR | | | | | | | | | | | |
| @ 50% stroke | 0.10 | 0.10 | 0.10 | 0.10 | 0.15 | 0.15 | 0.15 | 0.15 | 0.15 | 0.15 | / | 0.15 |
| **@100% stroke** (maximum) | **0.25** | **0.25** | **0.25** | **0.25** | **0.25** | **0.25** | **0.25** | **0.25** | **0.25** | **0.25** | **0.25** | **0.25** |
| @125% stroke | 0.25 | 0.25 | 0.25 | 0.35 | 0.35 | 1.00 | 0 .50 *(**)* | 0 .50 *(**)* | 0 .50 *(**)* | 1.00 *(**)* | / | 1.00 *(**)* |
| @150% stroke | 0.50 | 0.50 | 0.50 | 0.50 | 0.75 | 1.30 *(**)* | 1.00 *(**)* | 1.00 *(**)* | 1.00 *(**)* | / | / | / |
| Input voltage | 3 VRMS sine wave | | | | | | | | | | | |
| Input frequency | 400Hz to 5kHz | | | | | | | | | | | |
| Test frequency | 2.5kHz | | | | | | | | | | | |
| Null voltage | 0.5% of FRO, maximum | | | | | | | | | | | |

| ENVIRONMENTAL SPECIFICATIONS & MATERIALS | |
|---|---|
| Operating temperature | -65°F to +300°F [-55°C to 150°C] |
| Shock survival | 1,000 g (11ms half-sine) |
| Vibration tolerance | 20 g up to 2KHz |
| Housing material | AISI 400 Series stainless steel |
| Electrical connection | Six lead-wires, 28 AWG stranded Copper, PTFE insulated, 1 foot [30cm] long |

*Notes:*

*Dimensions are in inch [mm]*

*All values are nominal unless otherwise noted*

*Electrical specifications are for the test frequency indicated in the table*

*FR: Full Range is the stroke range, end to end; FR=2xS for ±S stroke range*

*FRO (Full Range Output): Algebraic difference in outputs measured at the ends of the range*

*(*) Unit for output at stroke ends is millivolt per volt of excitation (input voltage)*

*(**) Requires special reduced core length*

measurement SPECIALTIES™

# HR Series – General Purpose LVDT

## MECHANICAL SPECIFICATIONS

| | HR 050 | HR 100 | HR 200 | HR 300 | HR 500 | HR 1000 | HR 2000 | HR 3000 | HR 4000 | HR 5000 | HR 7500 | HR 10000 |
|---|---|---|---|---|---|---|---|---|---|---|---|---|
| Body length "A" | 1.13 [28.7] | 1.81 [46.0] | 2.50 [63.5] | 3.22 [81.8] | 5.50 [139.7] | 6.63 [168.4] | 10.00 [254] | 12.82 [325.6] | 15.64 [397.3] | 17.88 [454.2] | 24.09 [611.9] | 30.85 [783.6] |
| Core length "B" | 0.80 [20.3] | 1.3 [33.0] | 1.65 [41.9] | 1.95 [49.5] | 3.45 [87.6] | 4.00 [101.6] | 5.30 [134.6] | 5.60 [142.2] | 7.00 [177.8] | 7.00 [177.8] | 7.00 [177.8] | 8.50 [215.9] |
| Body weight, oz [g] | 1.13 [32] | 1.69 [48] | 2.12 [60] | 2.72 [77] | 3.85 [109] | 4.45 [126] | 5.93 [168] | 7.94 [225] | 10.41 [295] | 11.99 [340] | 16.16 [458] | 20.46 [580] |
| Core weight, oz [g] | 0.14 [4] | 0.21 [6] | 0.28 [8] | 0.35 [10] | 0.64 [18] | 0.74 [21] | 0.95 [27] | 0.99 [28] | 1.27 [36] | 1.27 [36] | 1.27 [36] | 1.52 [43] |

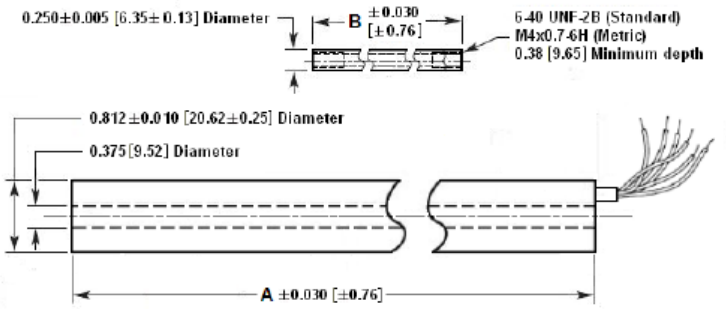


*Dimensions are in inch [mm]*

## WIRING INFORMATION

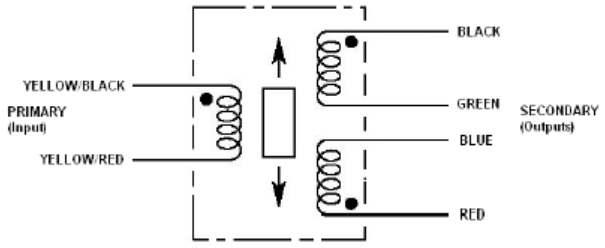


*Connect blue (BLU) to green (GRN) for differential output*

# HR Series – General Purpose LVDT

## ORDERING INFORMATION

| Description | Model | Part Number |
|---|---|---|
| ±0.05 inch LVDT | HR 050 | 02560389-000 |
| ±0.1 inch LVDT | HR 100 | 02560390-000 |
| ±0.2 inch LVDT | HR 200 | 02560391-000 |
| ±0.3inch LVDT | HR 300 | 02560392-000 |
| ±0.5 inch LVDT | HR 500 | 02560394-000 |
| ±1 inch LVDT | HR 1000 | 02560395-000 |

| Description | Model | Part Number |
|---|---|---|
| ±2 inch LVDT | HR 2000 | 02560396-000 |
| ±3 inch LVDT | HR 3000 | 02560398-000 |
| ±4 inch LVDT | HR 4000 | 02560399-000 |
| ±5 inch LVDT | HR 5000 | 02560400-000 |
| ±7.5 inch LVDT | HR 7500 | 02561011-000 |
| ±10 inch LVDT | HR 10000 | 02560401-000 |

| OPTIONS | | |
|---|---|---|
| 5.0 kHz calibration | HR 050, 100, 200 and 500 only | xxxxxxxx-002 |
| Metric threaded core | All | xxxxxxxx-006 |
| Guided core | All | xxxxxxxx-010 |
| Small-diameter/low-mass core *(consult factory for mass and dimensions)* | Consult factory | xxxxxxxx-020 |
| Mild radiation resistance | All | xxxxxxxx-080 |

*Note: Add multiple option dash numbers together to determine proper ordering suffix*
*Example: HR 1000, ±1 inch, with 5 kHz calibration and mild radiation resistance, P/N 02560395-082*

| ACCESSORIES | |
|---|---|
| Core connecting rod, 6 inches long, 6-40 threads | 05282947-006 |
| Core connecting rod, 12 inches long, 6-40 threads | 05282947-012 |
| Core connecting rod, 24 inches long, 6-40 threads | 05282947-024 |
| Core connecting rod, 36 inches long, 6-40 threads | 05282947-036 |
| Core connecting rod, 6 inches long, M4x0.7 metric threads | 05282978-006 |
| Core connecting rod, 12 inches long, M4x0.7 metric threads | 05282978-012 |
| Mounting block | 04560952-000 |

*Refer to our "Accessories for LVDTs" data sheet for our LVDT signal conditioning instrumentation and other accessories.*

## TECHNICAL CONTACT INFORMATION


| NORTH AMERICA | EUROPE | ASIA |
|---|---|---|
| Measurement Specialties, Inc.<br>1000 Lucas Way<br>Hampton, VA 23666<br>United States<br>Phone: +1-800-745-8008<br>Fax: +1-757-766-4297<br>Email: sales@meas-spec.com<br>Web: www.meas-spec.com | MEAS Deutschland GmbH<br>Hauert 13<br>D-44227 Dortmund<br>Germany<br>Phone: +49-(0)231-9740-0<br>Fax: +49-(0)231-9740-20<br>Email: info.de@meas-spec.com<br>Web: www.meas-spec.com | Measurement Specialties China Ltd.<br>No. 26, Langshan Road<br>High-tech Park (North)<br>Nanshan District, Shenzhen 518057<br>China<br>Phone: +86-755-33305088<br>Fax: +86-755-33305099<br>Email: info.cn@meas-spec.com<br>Web: www.meas-spec.com |

# UCM FOR INDUCTIVE TRANSDUCERS

## PERFORMANCE
## ELECTRICAL

### Power requirement

| | | |
|---|---|---|
| **Supply voltage range** | **Vdc** | 10 to 30 unregulated (limited to 13.5 minimum on certain ranges – see output options table) |
| **Supply current** | **mA** | 10 maximum (plus transducer current). Additional 9mA with **VM** card fitted, additional 2.6mA (plus output current) with **CM** card fitted or additional 3mA with **PWM** card fitted |
| **Reverse polarity protection** | | Yes |
| **Misconnection** | | Any terminal can be connected to ground without damage. Any terminal (except transducer primary excitation output) can be connected to positive supply without damage. |

### Transducer Excitation

| | | |
|---|---|---|
| **Options** | | Module is designed to operate 4, 5 or 6 wire differential LVDTs, ratiometric LVDTs and 3 wire inductive half bridge transducers (or RVDT equivalents). Can also be configured to work with potentiometers |
| **Primary voltage** | **Vrms** | 1 or 3 (link selectable) |
| **Primary frequency** | **Hz** | 2.5k, 5k or 10k (link selectable) |
| **Primary impedance** | **Ω** | >50 @ 1Vrms or >150 @ 3Vrms |

### Signal Input (Transducer sensitivity range)

| | | |
|---|---|---|
| **Voltage range** | **mVrms** | 60 to 5000 |
| **Primary/secondary phase shift** | ° | <±45 in differential mode. No restriction in ratiometric mode |
| **Circuit loading on transducer secondary coils** | **Ω** | >70k any connection |

### Signal Output – UCM only

| | | |
|---|---|---|
| **Output voltage range** | **Vdc** | 0.5 to 4.5 |
| **Output current - sourcing** | **mA** | <1 |
| **Output current - sinking** | **µA** | <20 |
| **Output impedance** | **Ω** | <1 |
| **Output load** | **Ω** | >5k resistive to 0V line (when **CM** module is fitted, should be between 20Ω and 400Ω for best linearity) |
| **Line regulation** | | <0.001% span/Volt |
| **Temperature stability** | **ppm/°C** | <200 |
| **Power on settlement time** | **mS** | <100 to within 0.25% of final reading |
| **Non-linearity (circuit only)** | **%** | <±0.01 full stroke |
| **Output filter** | | 3 pole low pass |
| **Frequency response** | **Hz** | 250 (-3dB) |
| **Output ripple and noise** | **mVrms** | <3 |
| **Output adjustment range** | | |
| **Zero** | | Electrical null may be set anywhere within the output range |
| **Gain (span)** | | Coarse adjustment by links, fine adjustment by potentiometer |
| **Gain/Zero interaction** | | Non interactive if zero adjusted first |

### Signal Output – option cards

| | | |
|---|---|---|
| **VM card** | **Vdc** | 0 to 5 & -5 to 0, 0 to 10 & -10 to 0, ±2.5, ±5, ±7.5, ±10 |
| **CM card** | **mA** | 4 to 20 |
| **PWM card** | | TTL level compatible signal with a 10 - 90% duty cycle. User selectable frequencies of 100, 130, 310 and 1000Hz. Logic signals: LOW <0.4Vdc HIGH 4.5 ±0.5Vdc |
| **Synchronisation** | | Up to 50 modules can be synchronised in one network |
| **LVDT/RVDT cable length** | | 25m maximum (best linearity is achieved with lowest acceptable input frequency when using longer cables) |

**Figure B. 5 Penny and Giles UCM data sheet.**

## OUTPUT OPTIONS

| Output option | Supply voltage range Vdc Single or (Dual) supply | UCM | UCM with VM card | UCM with CM card | UCM with PWM card |
|---|---|---|---|---|---|
| 0.5 - 4.5Vdc | 10 - 30 or ± (10 - 30) | ✓ | N/A | N/A | N/A |
| 0 - 5Vdc | 10 - 30 or ± (10 - 30) | N/A | ✓ | N/A | N/A |
| 0 - 10Vdc | 13.5 - 30 or ± (13.5 - 30) | N/A | ✓ | N/A | N/A |
| ±2.5Vdc | 10 - 30 or ± (10 - 30) | N/A | ✓ | N/A | N/A |
| ±5Vdc | 10 - 30 or ± (10 - 30) | N/A | ✓ | N/A | N/A |
| ±7.5Vdc | 13.5 - 30 or ± (13.5 - 30) | N/A | ✓ | N/A | N/A |
| ±10Vdc | 13.5 - 30 or ± (13.5 - 30) | N/A | ✓ | N/A | N/A |
| 4 - 20mA | 10 - 30 or ± (10 - 30) | N/A | N/A | ✓ | N/A |
| PWM | 10 - 30 | N/A | N/A | N/A | ✓ |
| Slope reversal | | ✓ | ✓ | ✓ | ✓ |

## MECHANICAL

| | | |
|---|---|---|
| **Enclosure** | | Powder coated aluminium alloy |
| **Weight** | g | 320 maximum |
| **Mounting** | | Bulkhead mounting via M5 fixing holes |
| **Cable exit** | | Via glands – cable diameter must be between 3.0 and 8.0mm diameter to seal to IP68 |

## ENVIRONMENTAL

| | | |
|---|---|---|
| **Operational temperature range** | °C | -40 to +85 |
| **Storage temperature range** | °C | -40 to +100 |
| **Protection class** | | IP68 to 2m for 1 hour duration – subject to user cable diameters 3-8mm and securely locked in glands |
| **EMC Immunity level EN61000-4-2** | | >100 V/m with 1m maximum distance to sensor |

## DIMENSIONS

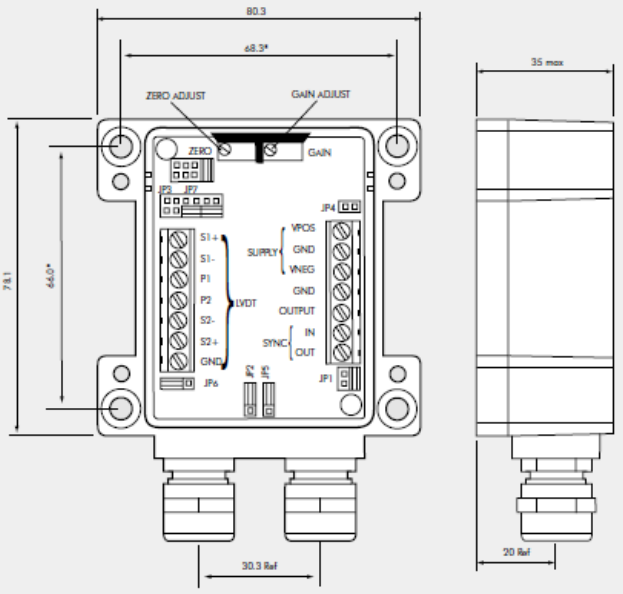


*Bulkhead fixing dimensions
Enclosure provided with four fixing holes to accept M5 screw x 28mm long minimum

**Cable glands** Cable must be between 3.0 and 8.0mm diameter to maintain IP68 rating of the enclosure. Ensure glands are fully tightened.

# Curriculum Vitae

| | |
|---|---|
| **Name:** | Michael Adamovsky |
| **Post-secondary Education and Degrees:** | Western University<br>London, Ontario, Canada<br>2003-2010 B.E.Sc |
| **Honours and Awards:** | OCE Discovery Student Connections Design Competition<br>Regional Winner, 2009<br><br>Scholarship of Distinction, Western University<br>2003 |
| **Related Work Experience** | Teaching Assistant<br>Western University<br>2013-2014 |

**Publications:**

Laschowski, B., Nolte, V., Adamovsky, M., & Alexander, R. (2015). The effects of oar-shaft stiffness and length on rowing biomechanics. Proc. IMechE, Part P: Journal of Sports Engineering & Technology.